Stator Inter-turn Fault Detection of Doubly-Fed Induction Generators Using Rotor Current and Search Coil Voltage Signature Analysis

By

Dhaval Shah

B.Eng., Nirma Institute of Technology, Gujarat University, India-2003

A Dissertation Submitted in Partial Fulfilment of the Requirements for the Degree of

MASTER OF APPLIED SCIENCE

In the Department of Electrical and Computer Engineering

University of Victoria

Supervisory Committee

Stator Inter-turn Fault Detection of Doubly-Fed Induction Generators Using Rotor Current and Search Coil Voltage Signature Analysis

By

Dhaval Shah

B.Eng., Nirma Institute of Technology, Gujarat University, India-2003

Supervisory Committee

Dr. Subhasis Nandi

Supervisor (Department of Electrical and Computer Engineering)

Dr. A.K.S. Bhat

Department Member (Department of Electrical and Computer Engineering)

Dr. Afzal Suleman

Outside Member (Department of Mechanical Engineering)

Dr. Michael McGuire

External Member (Department of Electrical and Computer Engineering)

Abstract

Supervisory Committee

Dr. Subhasis Nandi

Supervisor (Department of Electrical and Computer Engineering)

Dr. A.K.S. Bhat

Department Member (Department of Electrical and Computer Engineering)

Dr. Afzal Suleman

Outside Member (Department of Mechanical Engineering)

Dr. Michael McGuire

External Member (Department of Electrical and Computer Engineering)

Wind energy conversion is the fastest-growing source of renewable electric power generation in the world and it is expected to remain so for some time. Doubly Fed Induction Generators (DFIGs) hold more than 50% market share of wind power generators due to its unique benefits of low cost, control capability and scalability. Recent trend of DFIGs installed in wind power are within power range of 200KW-2MW and have stator windings rated at 690V, which are highly susceptible to inter-turn faults. This fault type account for more than 40% of the total failure causes of the generator. A reliable fault diagnostic system to detect this fault at incipient stage is highly in demand to prevent catastrophic failures and reduce preventive maintenance costs, since regular inspection is expensive and rewinding of generator takes time in period of days and costs nearly 20% of the original generator cost. Conventional techniques developed for detecting stator inter-turn faults in induction motor are not directly applicable for this machine partly due to difference in construction and their operating characteristics. Research for fault diagnosis in last 5 years has lead to variety of techniques, but none have proved to be feasible either due to need for dedicated sensors and high computing needs or they fail to account for operating conditions which lead to ambiguous fault triggering. This absence

of any proven technique to detect stator inter-turn faults in DFIG and the dire necessity for a fault diagnostic system to promote their reliability in wind power generation has motivated the research of this thesis.

A novel technique to detect stator inter-turn faults in a DFIG is proposed by analyzing rotor current and search coil voltage in this thesis. Our recent observations suggested that harmonics induced in the rotor circuit are very promising in detecting stator inter-turn faults in DFIGs. Hence, in this study, an in-depth investigation was conducted to determine the origin of various harmonic components in the rotor currents and their feasibility to detect inter-turn stator faults unambiguously. The theory is verified by modeling the DFIG and simulating various operating conditions of healthy state, severity of faults and unbalance loading conditions that cause ambiguity. Further to verify the concept, an experimental test-bed was created and tests were carried out on DFIG under varying speed operations, fault severity and loading conditions. The experimental results achieved from analyzing the frequency spectrum of rotor current and search coil voltage have been compared and discussed.

To verify feasibility of the proposed technique for detecting stator inter-turn faults and obtain results on speed sensitivity of fault detection, a prototype of DSP based Fault Diagnostic device was developed. Further discussion is made on challenges of realizing the proposed fault diagnostic technique in the industry and scope for further improvement.

The pursuit of research on this thesis topic, led to following publications:

1. D. Shah; S. Nandi; P. Neti, "Stator Inter-Turn Fault Detection of Doubly-Fed Induction Generators Using Rotor Current and Search coil Voltage Signature Analysis," *Conference Record of the IEEE Industry Applications Conference, 2007 42nd IAS Annual Meeting*, pp.1948-1953, 23-27 Sept. 2007.

2. D. Shah; S. Nandi, "Analytical Approach to Design of Slip-Controller for Constant Volts/Hz Scheme Induction Motor Drive Using Motor Name-plate Details," *Canadian Conference on Electrical and Computer Engineering. CCECE 2007*, pp.393-396, 22-26 April 2007.

Table of Contents

List of Tables

List of Figures

List of Abbreviations

AC	Alternating Current
COT	Continual On-line Training
DC	Direct Current
DFIG	Doubly Fed Induction Generator
DSP	Digital Signal Processor
DTC	Direct Torque Control
DFT	Discrete Fourier transform
EPVA	Extended Park's Vector Approach
FDS	Fault Diagnostic System
FEM	Finite Element Method
FFT	Fast Fourier Transform
FFNN	Feed Forward Neural Network
GMT	Global Minimum Training
HB	Healthy machine under Balanced supply
HU	Healthy machine under Unbalanced supply
ID	IDentification run, a pre-commissioning step for drives
MCSA	Motor Current Signature Analysis
MMF	Magneto Motive Force

MWFA	Modified Winding Function Approach
NN	Neural Network
PD	Partial Discharge
PF	Power Factor
PSD	Power Spectral Density
SM	Synchronous Machine
SC	Search Coil wound on rotor of DFIG
SRIM	Slip Ring Induction Machine
1T	Machine with 1-Turn fault under balanced load
2T	Machine with 2-Turn fault under balanced load
3T	Machine with 3-Turn fault under balanced load
4T	Machine with 4-Turn fault under balanced load
WECs	Wind Energy Conversion systems
WFA	Winding function approach
UPF	Unity power factor

List of Symbols

a	Stator phase-a
b	Stator phase-b
B_{ra}	Flux density with respect to rotor
B_{sa}	Flux density produced by the stator MMF, F_{sa}
c	Stator phase-c
f	Supply frequency
f_1	Fundamental frequency of stator voltage and current
f_2	Fundamental frequency of rotor voltage and current
F_{sa}	MMF produced by asymmetric stator winding
f_{st}	Frequency in a signal that is indicator of fault
$g^{-1}(\phi, \theta)$	Inverse air-gap function
I_+	Maximum value of current positive sequence
i_D	Direct-axis component from park's transform of current vector
I_f	Current in shorted-loop
I_l	Line current
I_{ph}	Phase current, where ph can be 'a','b','c','u','v','w'
i_Q	Quadrature-axis component from park's transform of current vector

J	Moment of inertia of the rotor
k	Order of space related harmonic
L_{12}	Mutual inductance between any two winding '1' & '2'
m	A number
n	Order of space related harmonic
$n_{a2}(\phi)$	Turns function of fault winding in phase-a
N_d	Number of shorted turns in stator phase-a winding
N_e	Number of turns removed from phase-u to create asymmetry
n_p	Number of layers of stator winding
$n_{ph}(\phi)$	Winding function of any phase, where ph can be 'a','b','c','u','v','w'
N_r	Number of conductor per phase per rotor slot
N_s	Number of conductor per phase per stator slot
$n_{u2}(\phi)$	Turns function of section removed from the rotor winding of phase-u to create asymmetry
p	Number of fundamental pole-pairs
P_0	Specific permeance function of the air-gap
P_e	Active power generated by stator of DFIG supplied to grid
P_{er}	Power drawn/fed by the rotor from/to the grid
P_f	Stator iron losses in DFIG
P_{js}	Stator power loss in DFIG
P_l	Mechanical power delivered by the turbine to the gear-box

P_m	Effective mechanical power input to the rotor of DFIG
P_r	Electrical power transferred from the rotor to stator of DFIG
s	Slip of the rotor with respect to stator.
T_e	Electromagnetic torque
T_l	Load torque
u	Rotor phase-u
v	Rotor phase-v
v_{gr}	Voltage per phase of the rotor
v_{gs}	Voltage per phase of the stator
V_{ph}	Voltage per phase, where ph can be 'a','b','c','u','v','w'
w	Rotor phase-w
x	$2\pi/3$
θ	Rotor position (mechanical radian)
μ_o	Permeability of the free space
ϕ	Space-angle (mechanical radian) with respect to stator frame of reference
ϕ'	Space-angle (mechanical radian) with respect to rotor frame of reference
φ_1	Arbitrary phase angle referenced to the stator
φ_2	Arbitrary phase angle referenced to the rotor
λ	Flux linkage

ω	Angular speed of the rotor
ω_1	Angular frequency of the stator voltage and current

Acknowledgments

I would like to acknowledge and extend my deep sense of gratitude to my supervisor Dr. Subhasis Nandi for his valuable time and constant guidance during the period of this thesis work. He has always encouraged for meeting high standards of quality and timely completion of this thesis, hence I am highly indebted to him.

I would like to thank all the members of my supervisory committee, Dr. A.K.S. Bhat, Dr. Michael McGuire and Dr. A. Suleman for their valuable time and their very beneficial comments and suggestions in my thesis preparation.

I would like to thank all my fellow graduate students and friends for their constant encouragements. My special thanks go to Mr. Rob Fichtner, Mr. Eric Laxdal and Mr. Kevin Jones from the Department of ECE; for their kind cooperation and help to setup arrangements to conduct many critical experiments.

I would like to thank my parents, who have devoted all they can do to support me in finishing this work and has been a constant source of encouragement.

Dedication

Dedicated to my beloved parents and my brother

Chapter 1

Introduction to Doubly Fed Induction Generators and Stator Fault Diagnosis

In this chapter, the use of Doubly Fed Induction Generator (DFIG) in wind power generation is introduced and the research from literature survey for stator inter-turn fault diagnosis of DFIG is discussed.

Wind energy conversion is the fastest-growing source of renewable electric power generation in the world and it is expected to remain so for some time. 20GW of new wind power generating units were installed during year 2007 as reported by Global Wind Energy Council. It is expected that by year 2012, the installed capacity will grow up to 240GW [1]. Figure 1.1 shows the statistics of past installation and predictions. During the last two decades wind turbines have been increased in size from 20kW to 2MW, while recent prototypes of 5MW turbines already operational [2]. The latest research on wind turbines focus on design for 12MW turbines [3]. Interest in research for harnessing wind energy for electric power generation is growing at an immense rate with emphasis on cost-effective utilization of this energy resource with quality and reliability of power supply.

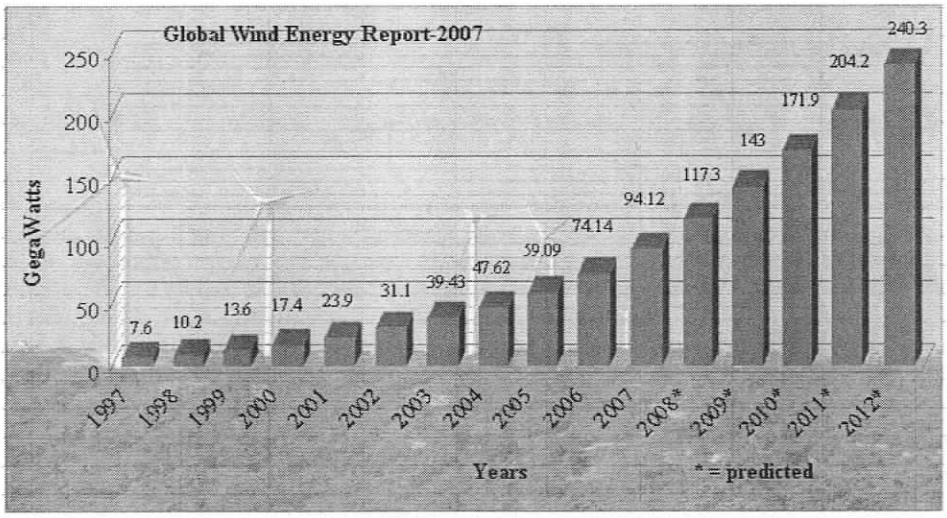

Figure 1.1 Installed Wind Power

A detailed survey of wind turbines, generator types, power electronics and configurations are discussed in [4-8]. All wind turbines installed to date can be grouped into two categories:

- Fixed-speed wind turbines
- Variable-speed wind turbines.

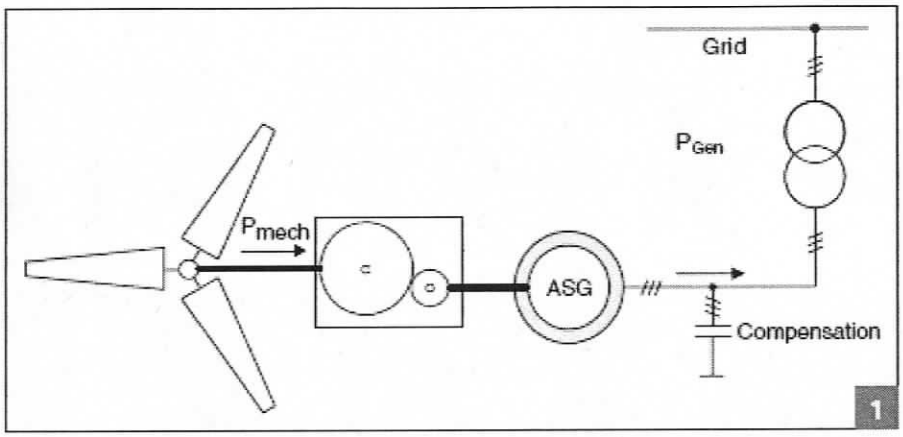

Figure 1.2 Fixed speed "Danish" concept

Many low-power wind turbines built to-date are fixed speed wind turbines which were constructed according to the "Danish concept" as shown in Figure 1.2. It uses a simple squirrel-cage induction machine directly connected to a three-phase power grid. The rotor of the wind turbine is coupled to the generator shaft with a fixed-ratio gearbox. Some induction generators use pole-adjusting winding configurations to enable operation at different synchronous speeds. However, at any given operating point, this Danish turbine basically has to operate at constant speed. The construction and performance of fixed-speed wind turbines very much depends on the characteristics of mechanical or electro-mechanical components, e.g., pitch control time constants, main breaker maximum switching rate, etc. The response time of some of these mechanical circuits may be in the range of tens of milliseconds. As a result, each time a gust of wind hits the turbine, a fast and strong variation of electrical output power can be observed. These load variations not only require a stiff power grid to enable stable operation, but also require a sturdy mechanical design to absorb high mechanical stresses. This

strategy leads to expensive mechanical construction, especially at high-rated power. They can be manufactured as one- or two-speed versions and they are suitable for low power ranges up to 2 MW.

The majority of modern megawatt wind turbines are variable-speed wind turbines equipped with a DFIG [4-8]. Because of its ability to provide variable speed operation and independent active and reactive power control in a cost effective way, the DFIG has been widely used. It holds the largest share in the world market share of wind turbine concepts since the year 2002. The most widely used configuration of wind energy conversion system using DFIG is shown in Figure 1.3 in which the generator is coupled to the power grid via a main transformer and rotor voltage and frequency is controlled from a converter [9].

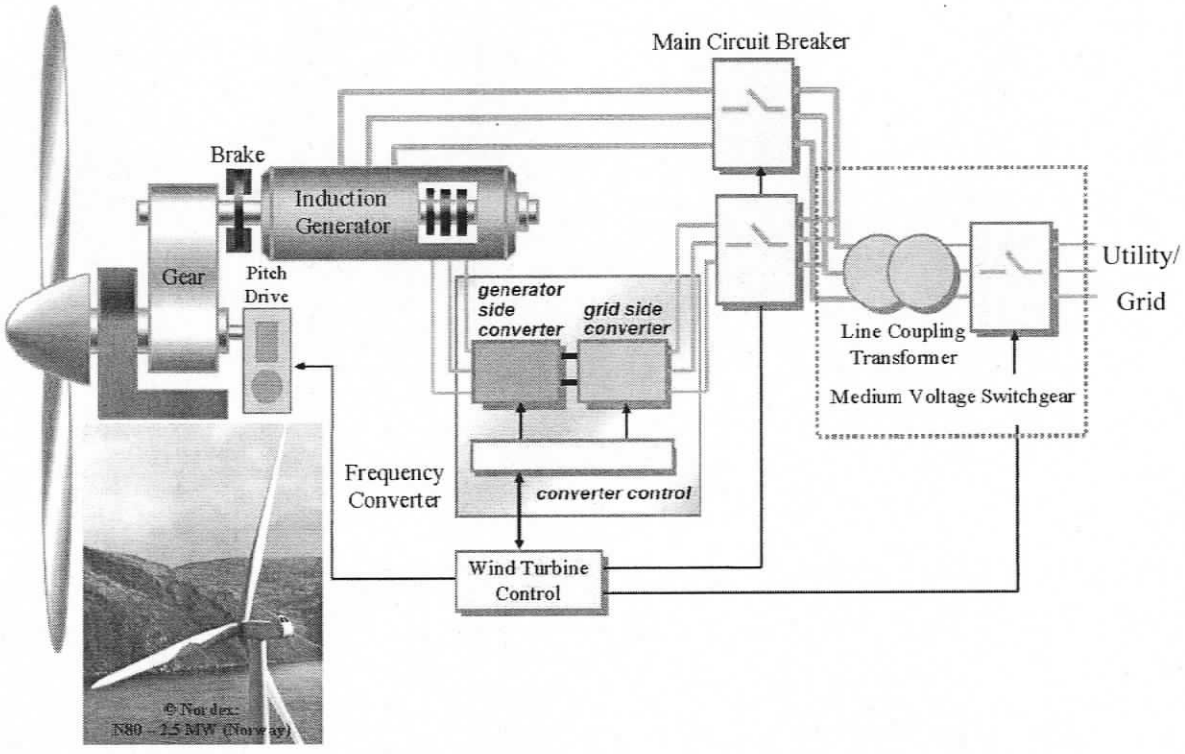

Figure 1.3 Most widely used Variable Speed Wind Turbine configuration (DFIG arrangement) [9]

1.1 Doubly Fed Induction Generators (DFIG) used in wind generation

The construction of DFIG is very similar to a wound rotor asynchronous machine. Variable speed operation is obtained by injecting a variable voltage into the rotor at slip frequency proportional to difference of synchronous speed and the speed of the generator shaft. The injected rotor voltages are obtained using two AC/DC Insulated Gate Bipolar Transistors (IGBTs) based voltage source converters (VSCs), linked by a DC bus; refer to Figure 1.3 for clarification. The converter ratings determine the variable speed range. The DFIG has two modes of operation depending on speed: a) Sub-Synchronous operation, b) Super-Synchronous operation. This difference in operating condition affects the slip of generator and induction of various harmonics in the stator and rotor circuit. Also, the power-flow of the DFIG operation differs, which is shown in Figure 1.4 and Figure 1.5.

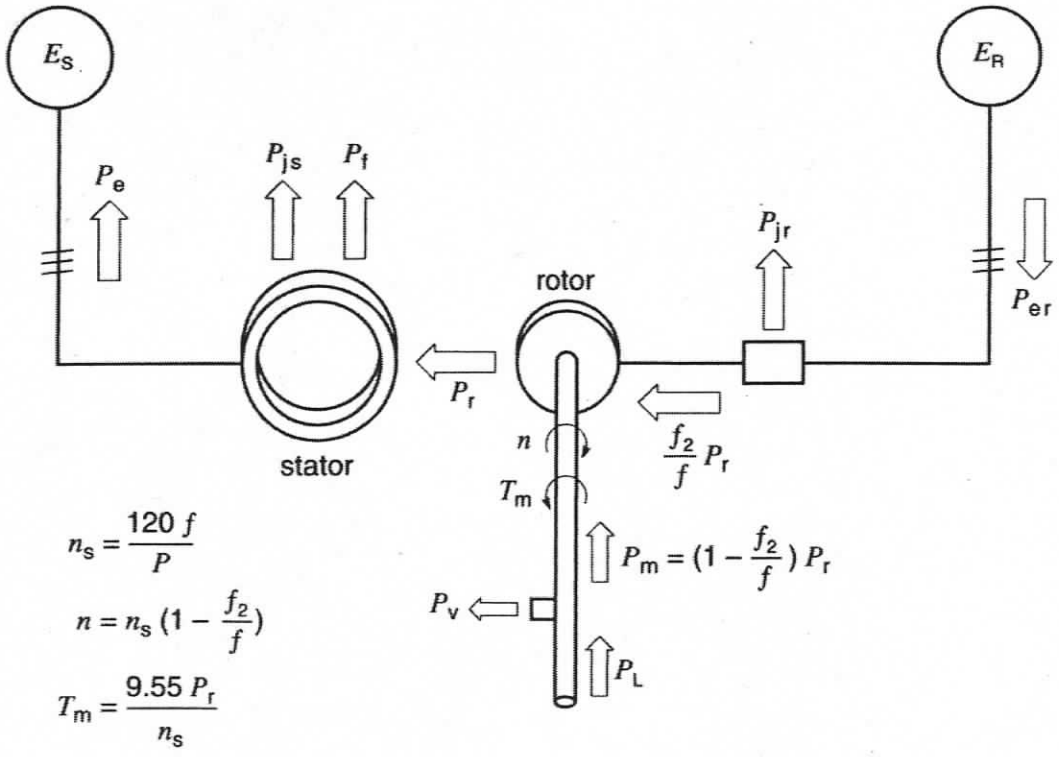

Figure 1.4 Power flow diagram of a doubly-fed wound-rotor induction generator operating in sub-synchronous mode [10]

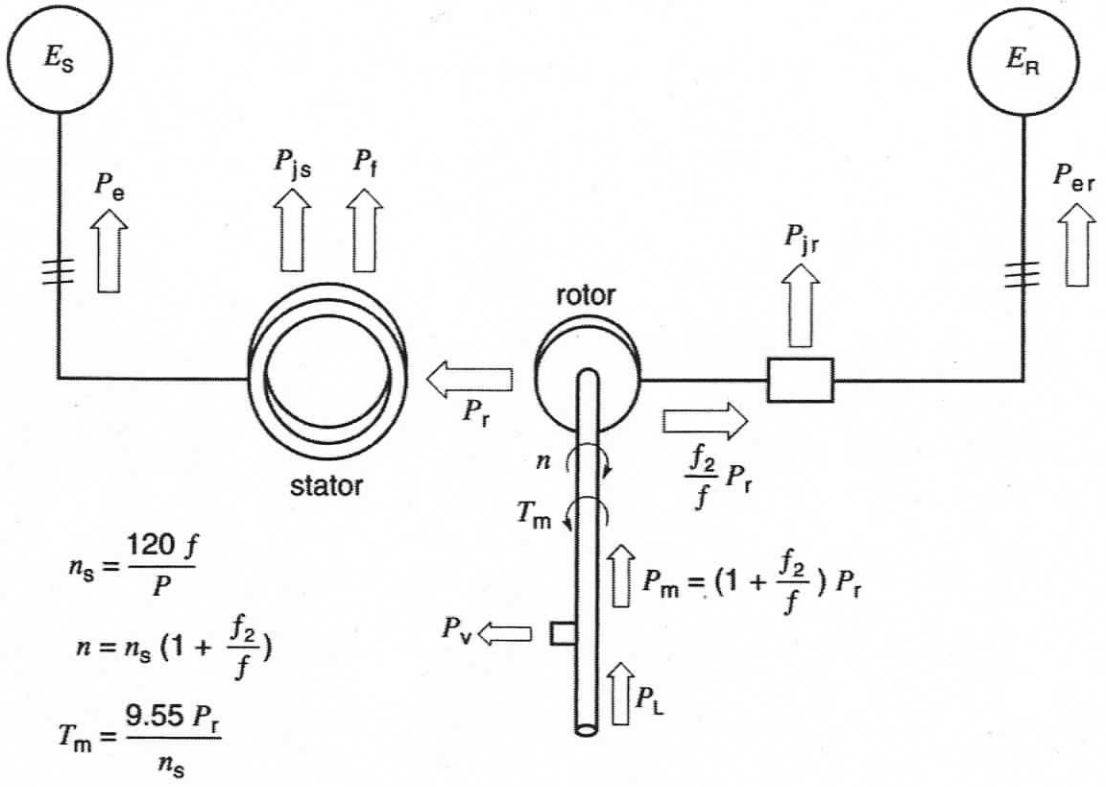

Figure 1.5 Power flow diagram of a doubly-fed wound-rotor induction generator operating in super-synchronous mode. [10]

In these figures, E_s is the 3-phase load/grid that receives the power from the generator at voltage frequency f. E_r is source that is connected to the rotor that feeds the power to rotor at voltage frequency f_2 when operating at sub-synchronous speed and when operating at super-synchronous speed, it extracts the power at voltage frequency f_2. P_1 is the mechanical power delivered by the turbine to the gear with a rotational speed n and torque T_m. After subtracting the gearbox power loss P_v the effective mechanical power input to the rotor is P_m. When DFIG is operating under sub-synchronous/super-synchronous mode, the rotor draws/injects power from/to the source E_R which is proportional to the variable slip frequency f_2 depending on n in order to keep the stator frequency constant. After subtracting the stator joule losses P_{js} and iron losses P_{js}, the resulting active power P_e is supplied to the E_s.

There are several variations in control scheme configurations used in DFIG, most of which are chosen based on the generator-turbine characteristics [11]. Typical type is DFIG with Static Kramer Drive shown in Figure 1.6 where the rotor is connected to an uncontrolled rectifier and the grid side converter is a VSI. This type of configuration restricts the DFIG operation to only super-synchronous mode. Most widely installed configuration is a DFIG with Back-to-Back Converters, Figure 1.7 in which operation is possible in either sub-synchronous or super-synchronous mode. It is possible to capture twice the energy rating of the DFIG using this configuration as shown by [12]. To achieve double energy capture, the DFIG is required to spin at twice the rated speed in super-synchronous mode. However due to turbine characteristics, most installations have a rotor side converter rated at 30% of DFIG power rating and this restriction limits the speed range. In certain installations DFIG can only operate under sub-synchronous speed due to turbine speed limitation [2] and a configuration shown in Figure 1.8 is used. This configuration has several cost benefits for high power rating installation; most importantly the grid side converter does not have to be bidirectional. The rating of the converter used in any configuration depends on the speed range of turbine. Hence a fault-diagnostic method should be capable to work on any DFIG, irrespective of its configuration.

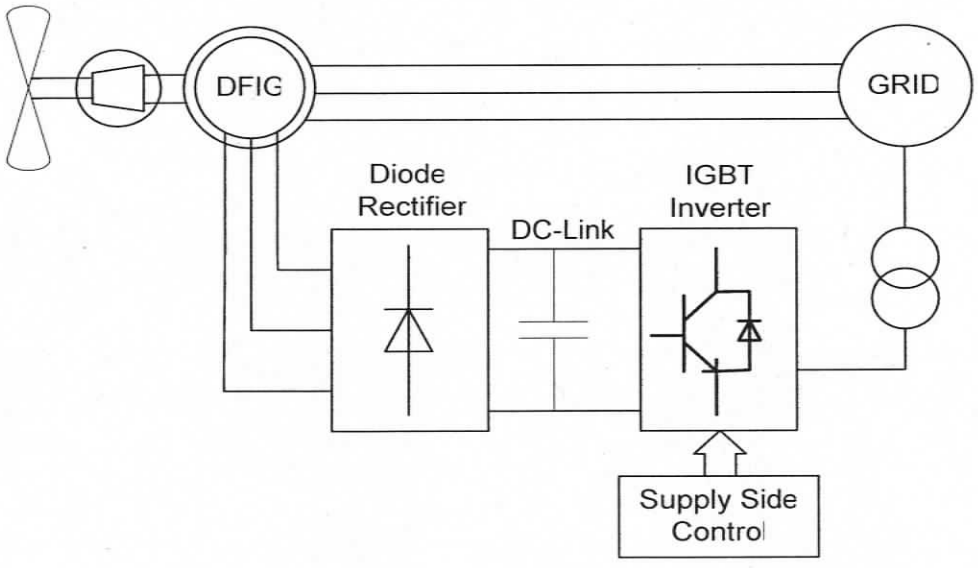

Figure 1.6 DFIG with Static Kramer Drive [11]

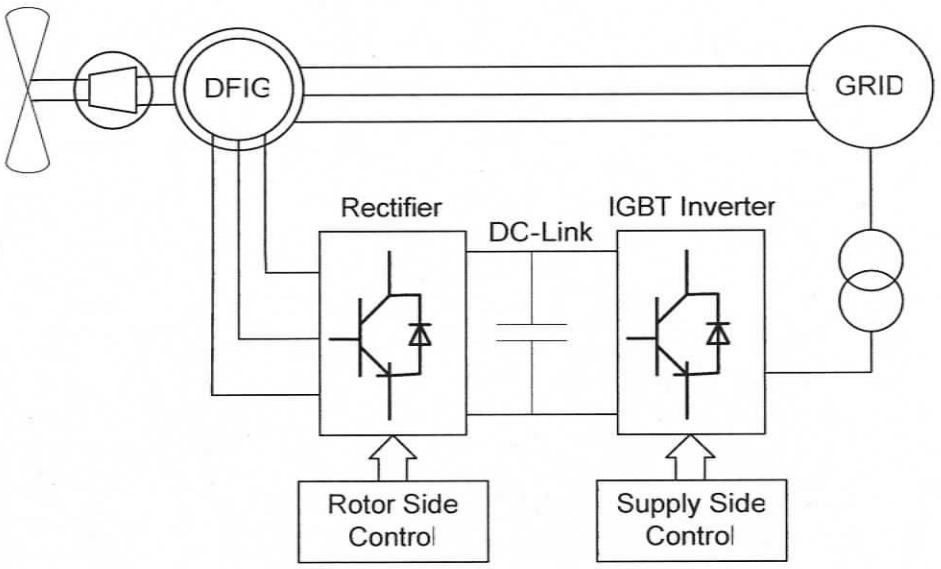

Figure 1.7 DFIG with Back-to-Back Converter [11]

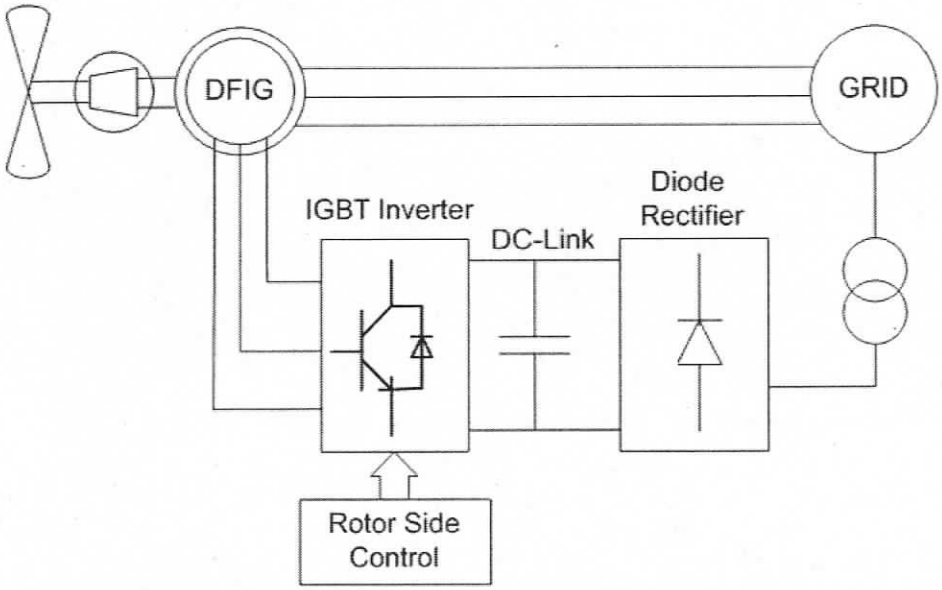

Figure 1.8 DFIG with Rotor Side Control for sub-synchronous operation

1.2 Need for On-line Fault Diagnosis of DFIG

Although modern wind turbines have reached high technical standards, there is still a strong potential for further development, especially with large, megawatt size machines. To make wind energy competitive with other power plants in the near future,

enhancements of availability, reliability and lifetime of the turbines will be required. Significant improvement in this field is possible from efficient maintenance and repair strategies on the basis of Condition Monitoring Systems (CMS) and Fault Diagnostic Systems (FDS). FDS is state of the art in many kinds of industrial processes, e.g. power station turbines, rotating machines, etc. early detection of incipient faults prevents major component failures and allows for efficient repair strategies.

The need for an accurate condition monitoring and fault detection method is high in demand to reduce the operation and maintenance cost of wind energy systems. For offshore wind, the costs for operation and maintenance are estimated in the order of 30 to 35 % of the costs of electricity. Roughly 25 to 35% of this cost is related to preventive maintenance and 65 to 75% to corrective maintenance [5]. The revenue losses for offshore wind turbines are estimated in the same order as the direct costs for repair whereas for onshore projects the revenue losses are negligible. Autonomous online condition monitoring systems with integrated fault detection algorithms allow early warnings of mechanical and electrical faults. These early warnings help in preventing major component failures which can be a very costly and in some cases can cause a serious safety hazard. Additionally, side effects on other components can be reduced significantly. Many faults can be detected while the defective component is still operational. Thus, necessary repair actions can be planned in time and need not be taken immediately. This is important especially for offshore Wind Energy Conversion systems (WECs), where bad weather conditions (storm, high waves, and icing conditions) can prevent any maintenance and repair actions for several weeks. If shorted turns in a stator coil can be diagnosed, a shutdown can be immediately executed using an autonomous system to prevent any equipment or personnel loss.

Like every electrical machine, wind generators are prone to electro-mechanical faults and require attention at the incipient stage of failure to avoid escalation of the fault to cause a breakdown or major damage. Incipient faults may occur in stator, rotor, bearings, air gap eccentricity, etc. Survey of Failures in Wind Power Systems reported in [6] suggests that generator failures take the longest duration to fix. Many sources have shown that bearing faults and stator insulation breakdown causes the majority of

induction machine failures [13, 14]. The present trend for high power DFIGs has stator windings at 690V [2]. The stator winding insulation degradation is one of the major causes (30-40%) of machine failure for stator windings of induction machines [15, 16]. Stator faults begin with the degradation of the insulation between turns and consequent inter-turn short circuit. It has been reported that inter-turn fault can seriously threaten the safety of operation of the machine by causing excessive heat to the shorted windings and stator core [17, 18]. Further, if the fault is not detected immediately, it ultimately leads to commonly known line to ground or line to line faults [18]. Often stator faults lead to fire, explosion in a very short period of time after initial failure [18, 19]. Thus with stator faults, the machine has to be stopped very quickly in a matter of one third of a second or even less in order to prevent any damage to other devices or even personnel [17-19]. Figure 1.7 shows a picture of a wind generator that went under a series of generator faults, starting with an oil leakage that degraded the insulation of stator windings, resulting into inter-turn short and escalating into fire and later an explosion [20].

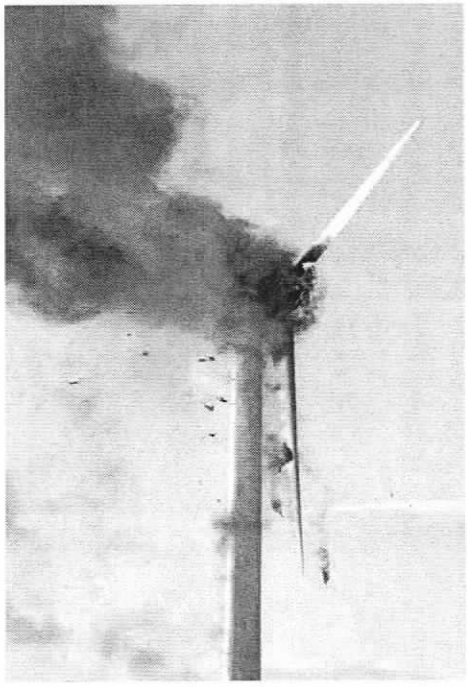

Figure 1.9 Wind turbine burning at the Nissan Motor Manufacturing (UK) Ltd (Sunderland, UK) after an oil leak [20]

1.2.1 Failure Mode Analysis:

Quantitative analyses of real wind turbine failure data have shown important features of failure rate values and trends [21]. Figure 1.10 shows failures number distribution for Swedish wind power plants that occurred between 2000 and 2004. Another study concerning Danish and German wind power plants [22] shows principal contributors to the higher German failure rate are the electrical control or system subassemblies (grid or electrical system, yaw system and mechanical or pitch control system) rather than mechanical subassemblies such as the gearbox. Figure 1.11 shows the failure rate in the two power plants during the period 1994-2004.

Of all the electrical faults: Generator, control system, sensors, electric system; the faults in generator are most time consuming to fix and also cannot be provided with a back-up protection as is possible with sensors or a control board. Increasing insulation thickness is not a panacea, since what causes fault is the insulation puncture caused due to generator operation at peak of its thermal rating or high dv/dt and moisture. Though increasing insulation can prolong the life of windings before an actual fault occurs; there is a limit to such increase.

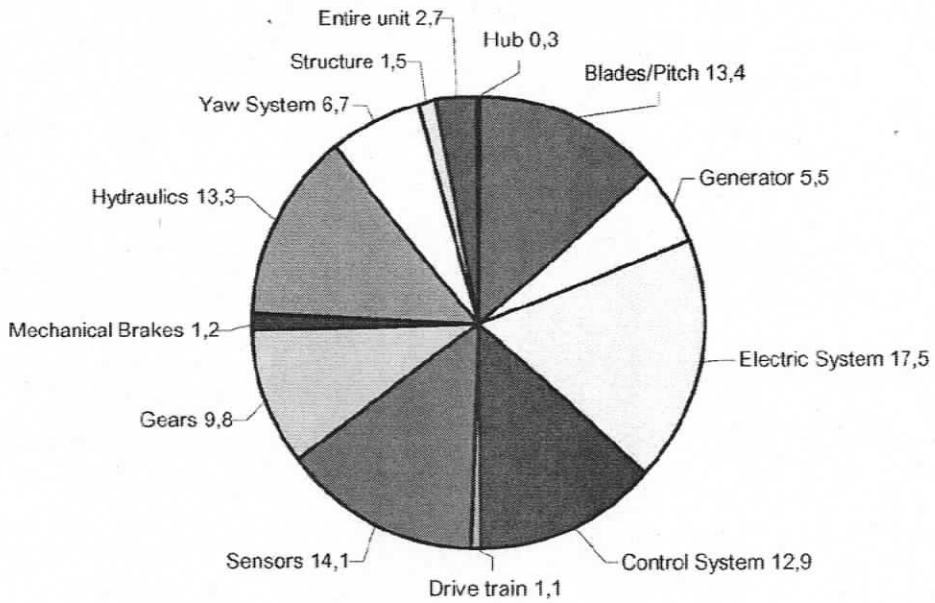

Figure 1.10 Failure number distribution [%] for Swedish wind power plants [21]

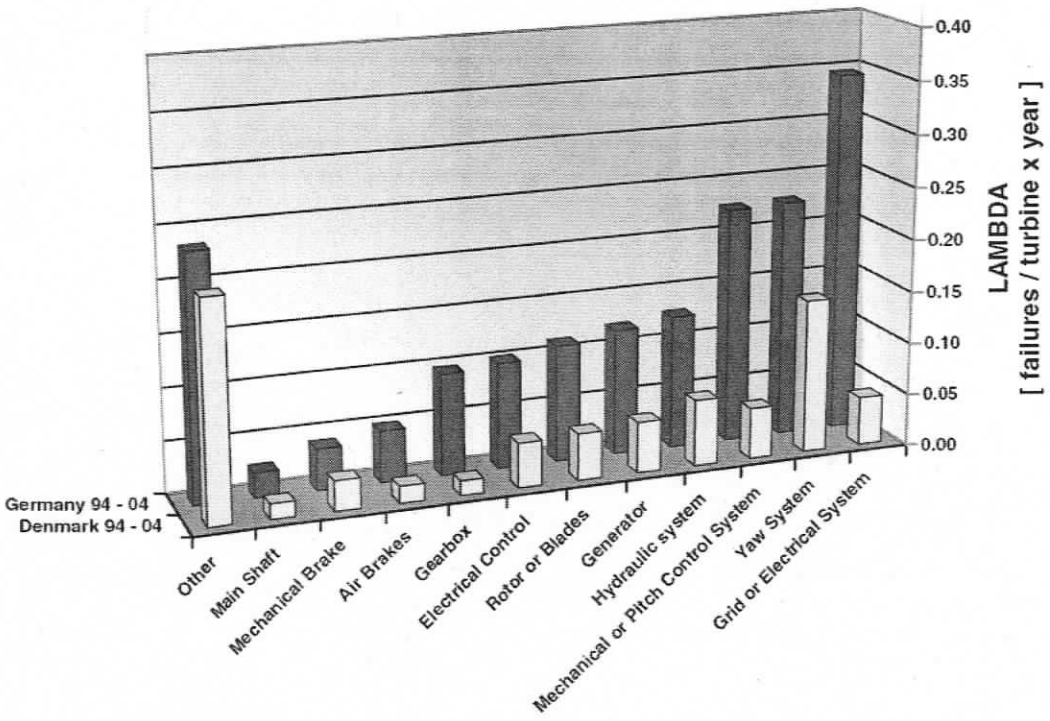

Figure 1.11 Failures rate for Danish and German wind power plants [22]

As seen from the analysis, there are several possibilities to cause a failure in the WECs, however electrical faults account for more than 50% of all faults. The mechanical faults causing failure are not a topic of discussion and hence excluded from the remainder of the thesis. The failures arising due to malfunction by electrical sensors (14.1%) and control system (12.9%) have a very simple prevention remedy. Installing back-up extra sensors and control system constitute little additional cost; cost of less than 1% of the cost of the entire wind plant. The Electric System faults (17.5%) can be decreased by installing special power relays based on the type of grid connectivity of the generator. However, for generator faults (5.5%), a failure preventive system of a back-up generator is an exorbitantly expensive idea. Hence, continuous condition monitoring and a reliable fault diagnostic system capable of detecting faults at an incipient stage is the only reasonable alternative.

1.3 Stator Inter-turn Faults

Causes of stator-inter turn fault in large AC machines such as the DFIG are discussed in great detail in [23]. The organic materials used for insulation in electric machines are subjected to deterioration from a combination of thermal overloading and cycling, transient voltage stresses on the insulating material, mechanical stresses, and contaminations. Among the possible causes, thermal stresses are the main reason for the degradation of the stator winding insulations [23, 15]. Generally, thermal stresses on the stator winding insulations are categorized into three types: aging, overloading, and cycling. Even the best insulation will fail quickly if operated above its temperature limit. As a rule of thumb, the life of insulation is reduced by 50% for every 10 degree increase above the stator winding temperature limit. Because of the high-cost and difficulty of installing thermal sensors, thermal protection relies on fuses and thermal/electronic overload relays, which have provided low-cost thermal protection for many years. However, these devices are tripped based on a crude temperature estimate due to the mismatch between the thermal characteristics of the motor and the thermal element employed in these devices (bimetals or eutectic melting alloys) [24]. The stator winding faults can be classified as follows [16]:

1. Turn to turn shorts within a coil
2. Short between coils of the same phase
3. Phase to phase short, machine fails and protection equipment disconnects supply.
4. Phase to earth short, machine otor fails and protection equipment disconnects supply.
5. Open circuit in one phase (single-phasing) - motor may continue to operate depending on the load condition (e.g. at no-load or light load running) and protection equipment.

Type 2 to 5 faults always start as type-1 fault. Thus pre-warning of motor failure such as in type 2 to 5 above can only be achieved if shorted turns within a coil (e.g. one or two shorted turns) can be initially diagnosed via an on-line diagnostic technique. Ideally, this requires continuous online monitoring to diagnose the fault of type-1. There is also the question of how long does it take for shorted turns within a coil to develop into a phase-to-phase or phase-to-earth fault and motor failure in low voltage machines. This question has not been resolved and will be a function of many variables and will in fact be unique to each motor [16]. It is however perceived that detection in less than one third of a second is most desirable [17].

Among the five failure modes, turn-to-turn faults have been considered the most challenging one since the other types of failures are usually the consequence of turn faults [25]. Furthermore, turn faults are very difficult to detect at their initial stages. Basically the development of inter-turn fault within a stator winding is due to the insulation failure. A variety of factors have been found to contribute to the failure of insulation. Some of them are listed below [26]:

- High temperatures of stator core or winding;
- Slack core lamination, slot wedges, and joints;
- Loose bracing for end winding;
- Contamination due to oil, moisture;
- Electrical discharges;
- Leakage in cooling systems.

An explicit description upon how inter-turn short circuit developed within stator winding of an induction machine will be given next. First as background information, some fundamental definitions are reviewed.

- A turn consists of two conductors connected to one end by an end connector.

- A coil is formed by connecting several turns in series.
- A winding is fabricated by connecting several coils in series.

The configuration of turn, coil and winding are shown as Figure 1.12 [27], where S implies start and F finish.

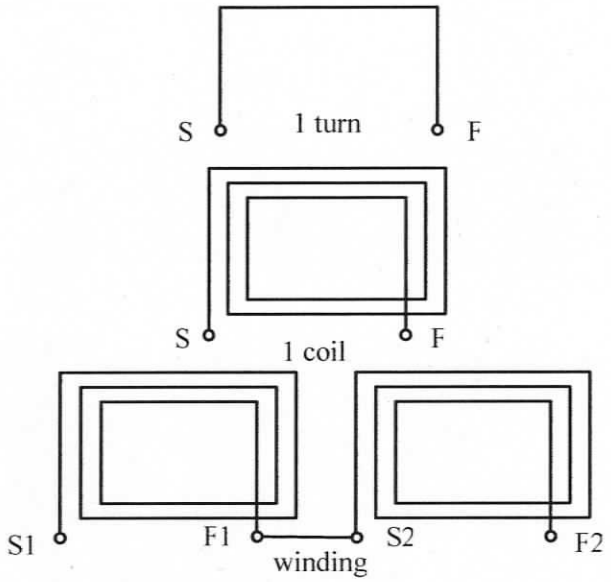

Figure 1.12 Configurations of turn-coil and winding structure [27]

In a practical machine, a phase winding is formed by packing multiple numbers of conductors in stator slots and connected via end winding in a systematic manner. These conductors are covered with a thin layer of insulation to provide isolation between conductors as well end windings. Internal short circuit of different turns can thus be prevented by the insulation layer on these conductors. The cross section of one stator slot as well all conductors included is shown in Figure 1.13 [28].

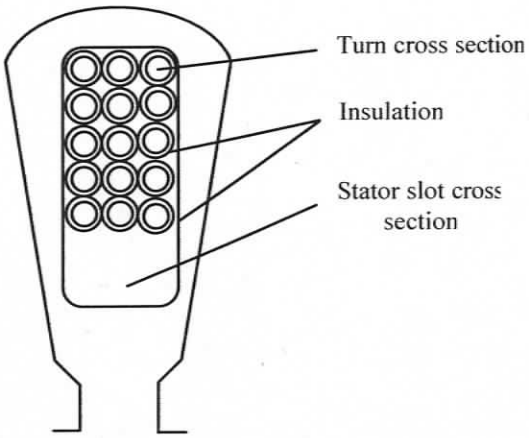

Figure 1.13 Stator slot cross section with a particular number of conductors included [28]

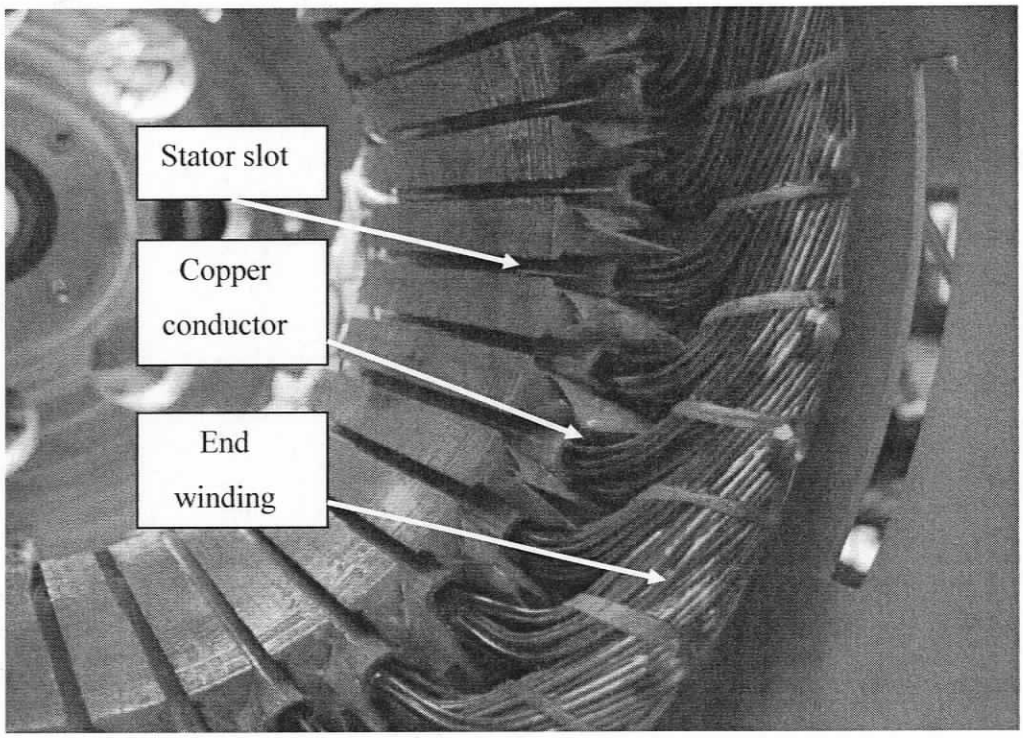

Figure 1.14 Stator winding of an induction machine [29]

A picture of actual stator winding together with end winding is shown in Figure 1.14. From Figure 1.13 and Figure 1.14 one can see that all the conductors in one stator slot are put together intimately. Suppose due to some reasons mentioned earlier, the insulation between two turns fail. This will result in the direct electric contact between these two turns. Figure 1.14 also shows that it is possible for inter-turn short circuit to develop in end winding portion [29]. In either case, a shorted turn loop which includes

one or several turns will be generated in the stator winding [30, 31]. In order to visualize the shorted turn loop created in the stator winding, a faulty loop including several number of turns developed within a three phase system is shown in Figure 1.15. In Figure 1.15, 'I_a', 'I_b' and 'I_c' are three phase currents, 'I_f' is the faulty current which is circulating within the faulty loop. Due to the short circuit, the magnitude of this current is going to reach a very high level (almost on the order of twice the short circuit current of the motor [17]) and a large amount of heat will thus be generated [17, 30].

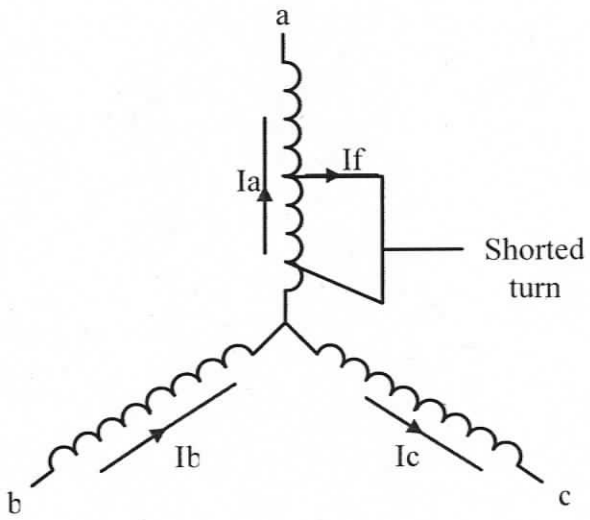

Figure 1.15 Inter turn short circuit on star connected induction machine phase-A

Also from Figure 1.15 one can see that due to existence of faulty loop, the balance of the 3-phase system has been broken. As the results, 3-phase unbalanced currents will be established accordingly [19, 31].

Excellent examples of typical failures in random wound, low voltage induction motors are shown in reference [16], and the reader is referred to that paper for full details of the causes and failures of LV stator windings.

1.4 Literature Survey on Stator Inter-turn Fault Diagnosis of DFIG

Literature survey of faults in induction machines suggest that, up to 30-40% of faults are inter-turn stator faults [15]. Hence, exclusive attentions has been paid by various researchers to find out the cause of inter-turn fault and pursue decisively its prediction. There are many techniques and tools available, which are used to monitor the condition of induction machines. Some of the technologies used for monitoring include sensors, which may measure speed, output torque, vibrations, temperature, flux densities, etc. These sensors together with different detection algorithms and techniques allow for efficient monitoring of the machine conditions. The most popular methods of induction machine condition monitoring utilize the steady-state spectral components of the stator quantities. These stator spectral components can include voltage, current and power and are used to detect turn faults, broken rotor bars, bearing failures, air gap eccentricities. Presently, many techniques that are based on steady-state analysis are being applied to wind generators.

Fault diagnostic methods for induction motors has been highly researched and commercial systems for diagnosis of mechanical problems such as broken rotor bars using Motor Current Signature Analysis (MCSA) and bearing faults using vibration analysis are currently available [32, 33]. Fault diagnosis for induction generators, especially DFIG has been little explored. Induction motor fault diagnosis methods cannot be directly applied to induction generator, especially for electrical faults like stator winding inter-turn faults. In the case of DFIG, the value of operating parameters like power flow, slip speed, excitation voltage of generator are very different than conventional induction motor and hence the magnetic field of machine is changed in a different way by the inter-turn faults in the generator compared to the motor. However, there has been work conducted in last five years and a literature survey was conducted to explore the developed methods. The study revealed that existing techniques use either invasive flux or vibration sensors based analysis or MCSA of stator current. However, the proposed methods have short-comings such as the need for sophisticated tools,

excessive computation power, have ambiguous detection for operations under unbalanced load condition or else they are based only on experimental and empirical observations without clear theoretical basis.

There are several techniques for determining the health of DFIG. They can be classified under invasive, non-invasive, steady-state or transient techniques [33]. The following techniques are reviewed to determine their feasibility and limitations to detect inter-turn stator faults in DFIG.

1.4.1 Current and Impedance Negative-Sequence Component Signature Analysis

The inter-turn short circuit produces an asymmetry of the stator winding. For this reason the negative-sequence components of currents, voltages or impedance show a change of their values when a fault occurs [34]. Hence, most of the turn-fault detection techniques are based on the detection of changes in the negative-sequence components.

The monitoring of the current negative-sequence component is easy as it is calculated from the measurements of the line currents. Inherent machine asymmetries, unbalanced stator voltage voltages and mismatched instrumentation gains produce a similar effect. These factors have to be taken into account in the fault detection strategy. Nevertheless, in [17] the negative sequence current component due to inherent machine asymmetries and the asymmetry of the sensors is calculated and subtracted so that the fault alone can be monitored. This value depends on the load. For this reason it must be calculated and stored as a function of load, which complicates the method.

Effective negative sequence impedance has proven to be a valid stator fault indicator for AC machines [35, 36]. The scheme is able to give a clear fault signature under most stator inter-turn fault conditions but may fail in detecting extremely low-level of faults (1-2 turn fault), especially under supply unbalance. Voltage mismatch detectors were then developed in [37] to overcome this drawback. Compared with negative sequence impedance, voltage mismatch detectors have better performance in detecting extremely small stator winding deterioration. However, as has been pointed

out by the authors, voltage mismatch detectors are more difficult to apply as a training period is needed in order to develop the impedance parameters.

In the method proposed in [38], a feed-forward neural network (FFNN) is proposed for the diagnosis. Simulation data is used to train the neural network. The supply voltage is supposed to be symmetric. As the model does not consider the real-life asymmetries, the results obtained are not reliable.

In another case [39], the diagnostic approach is based on a FFNN, but in this case the asymmetries are taken into account. The Neural Network (NN) is trained with the sequence-components of the voltage and the positive-sequence component of the current to estimate the negative-sequence component of the current. In the monitoring phase this estimated value is compared with the measured value. A deviation will be an indication of fault. The FFNN is trained off-line over the entire range of operation conditions expected. This scheme, known as global minimum training (GMT) is not suitable for practical implementation, as it requires considerable data memory and computation. For this reason a continual on-line training (COT) algorithm was proposed [40]. This algorithm has lower computation and data storage requirements, but if the fault develops slowly, it is not detected reliably.

These techniques have to overcome difficulties due to the effects of stator unbalances, sensor asymmetries and machine inherent asymmetries in the negative-sequence components.

1.4.2 Axial flux Signature Analysis

It has been shown that axial flux monitoring can detect inter-turn short circuits [41-45]. The perfect electrical machine does not produce any axial flux because the currents flowing in the end windings of both the rotor and stator circuits are perfectly balanced. However, there are always small asymmetries in metal core and windings due to the material and geometric aspects (mainly end windings) of a machine. This results in every machine producing a small, but measurable axial leakage flux. Both stator and rotor windings produce axial leakage flux that are a result of the winding currents.

Hence, the axial leakage flux spectral content may be related directly to the harmonic components present in the winding currents. These harmonic components depend on the harmonic components of the air gap flux. A stator inter-turn short circuit changes the distribution of the MMF in the air gap because of the current that circulates through the short-circuited turns. The MMF distribution due to the inter-turn short circuit induces the following new frequencies in the axial leakage flux [32, 46],

$$f_{st} = \left[\frac{n}{p}(1-s) \pm k\right] \cdot f_1 \tag{1.1}$$

where f_1 is the fundamental frequency of the supply, k = 1, 3, 5... is the supply voltage harmonic order, p is the number of pole pairs, s is the slip and n is an integer n = 1, 2, 3...

If flux sensors are placed around the air gap of the machine, it will have induced in it a voltage which can be related to the axial flux. The main drawback is that the flux sensors are invasive to the motor's environment. Furthermore, results have shown that components in the axial flux that are indicative of shorted turns are also very loading dependent [32]. This causes a problem for reliable diagnosis. Also, this method will give ambiguous results during an unbalanced load condition on the generator phases, which causes alteration in axial flux and the fault frequency being monitored will have to be chosen appropriately.

1.4.3 Extended Park's Vector Approach (EPVA)

The EPVA is a relatively new diagnostic technique, which has been successfully applied in the steady-state diagnosis of rotor faults, inter-turn stator faults, unbalanced supply voltage and mechanical load-misalignment. This technique is based on the Park's Vector Approach.

The instantaneous line current of the stator are transformed into the Parks vector using (1.2). The park-vector's components are shown in (1.3). A perfectly healthy and balanced machine theoretically shows a perfect circle where the instantaneous park's

vector modulus given by $\sqrt{i_D{}^2 + i_Q{}^2}$ is constant as shown in Figure 1.16. An unbalance due to turn faults results in an elliptic representation of the Park's Vector as shown in Figure 1.17. The magnitude of the Park's Vector will contain a frequency that is twice the fundamental frequency. The amplitude of this double frequency component is proportional to the degree of unbalance. In the case of a real healthy machine there will always be a small degree of unbalance. A severity factor is described as the ratio of the magnitude of the twice-fundamental frequency to the constant component in the magnitude of the Park's Vector's modulus can be introduced to quantify the fault. In this case a FFT is applied to the magnitude of the Park's Vector to determine the amplitude of the spectral components needed [44].

$$\begin{bmatrix} i_D \\ i_Q \end{bmatrix} = \begin{bmatrix} \sqrt{\frac{2}{3}} i_a & \frac{-1}{\sqrt{6}} i_b & \frac{-1}{\sqrt{6}} i_c \\ 0 & \frac{1}{\sqrt{2}} i_b & \frac{-1}{\sqrt{2}} i_c \end{bmatrix} \tag{1.2}$$

$$i_D = \frac{\sqrt{6}}{2} I_+ Sin(\omega_1 t), i_Q = \frac{\sqrt{6}}{2} I_+ Sin\left(\omega_1 t - \frac{\pi}{2}\right) \tag{1.3}$$

where, i_+ is the maximum value of the positive sequence current component, ω_1 is the angular supply frequency and t is the time variable.

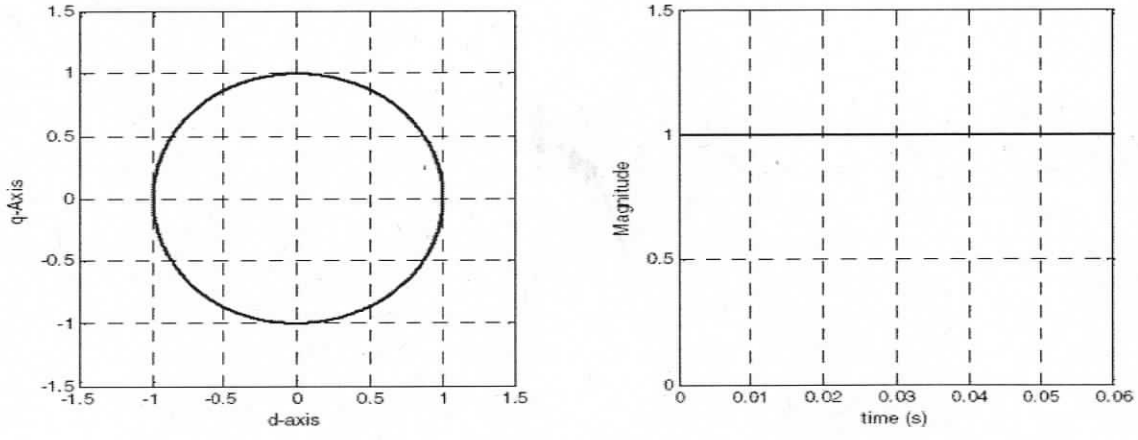

Figure 1.16 The Park's Vector (left) and magnitude (right) for a healthy machine operating in steady state [32].

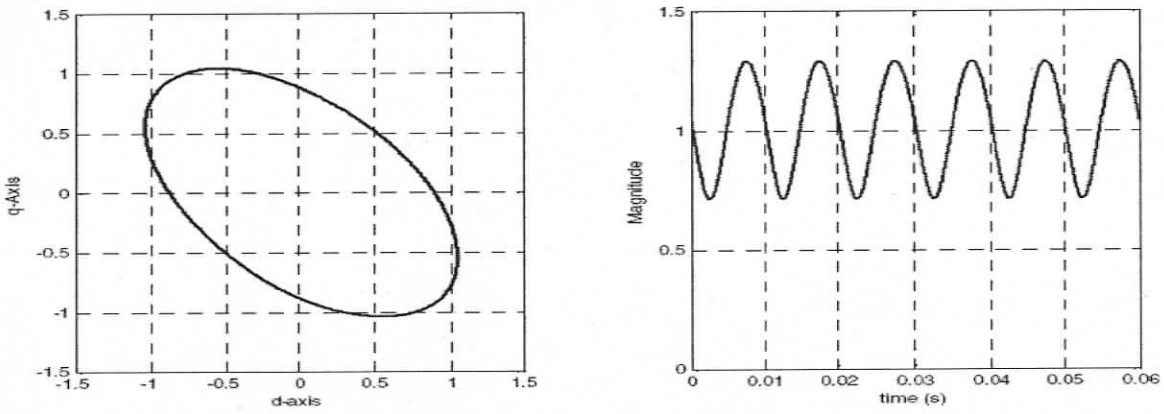

Figure 1.17 The Park's Vector (left) and magnitude (right) for a damaged machine operating in steady state [32].

This method of detection works well if the machines being diagnosed operate only in steady state. The behaviour of DFIGs is however transient. In a set of experiments the speed of a 4-pole machine under test was varied [32] from 1170 rpm to 1900 rpm (sub-synchronous to super-synchronous) as shown in Figure 1.18. Observing the Park's vector of the healthy machine in Figure 1.18 (b), shows that it is not at constant amplitude. In fact the amplitude spirals in and then out as time progresses. This obviously complicates the expression for the severity factor since the dc component is not a constant. The amplitude of the twice fundamental frequency component changes and therefore the use of Fourier analysis in case of DFIG is questionable.

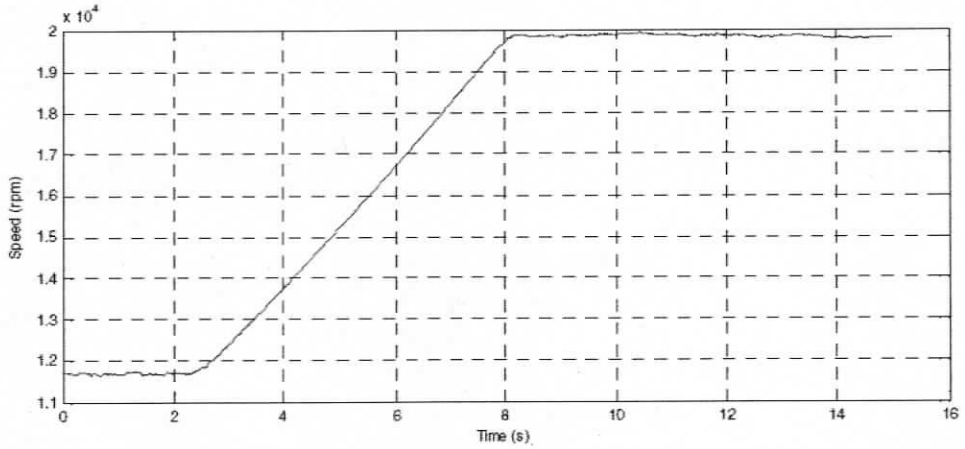

(a)

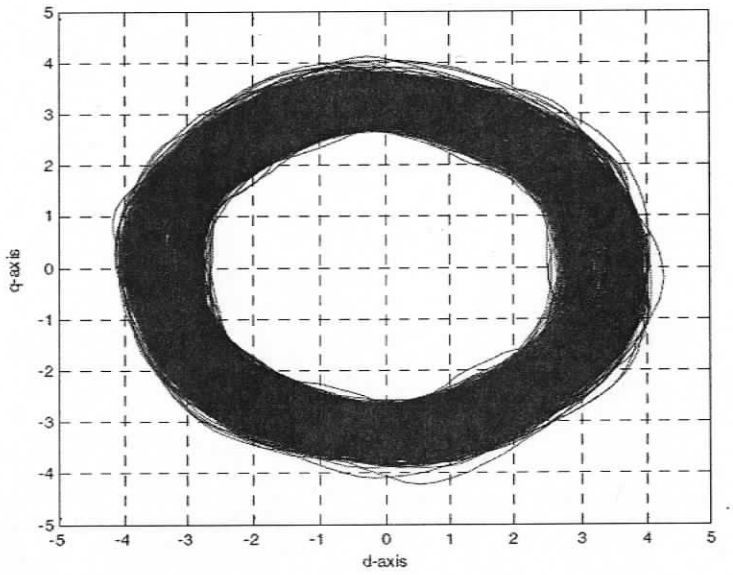

(b)

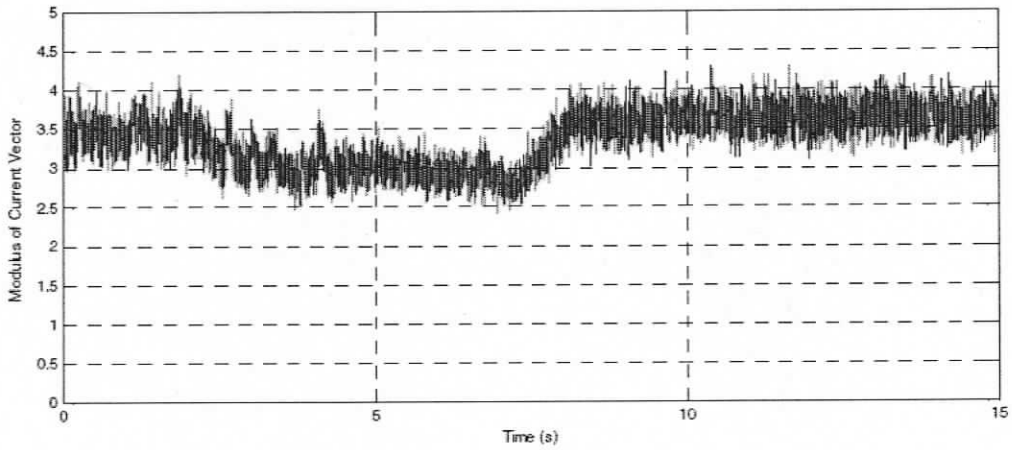

(c)

Figure 1.18 Park's Vector analysis when DFIG is under speed transient(a) speed profile of undamaged machine, (b) Park's Vector of an undamaged machine, (c) magnitude of Park's Vector [32].

1.4.4 Wavelet analysis

In recent years wavelet analysis has been applied to many areas of signal processing and induction motor fault diagnosis [32, 46, 47]. The way wavelet analysis localize signal's information in the time frequency plane makes it especially suitable for the analysis of non stationary signals and a good alternative to traditional Short Term Fourier Transform (STFT) analysis [46].

This technique relies on the detection algorithm which is a combination of the Extended Park's Vector, wavelet analysis and statistics [32]. It has a benefit that, it is not affected by changes in the speed of the machine which is crucial when applied to wind generators. This technique focuses mainly on the fault detection in state of speed being transient at a rate such that steady-state analysis could not be applied. However, this method does not account for a situation when the three phases of the generator are having any unbalance loading, which could trigger a false alarm.

1.4.5 Partial Discharge Methods

Most of the asynchronous generators for DFIG generation are medium voltage machines, rated at 690V [2, 7, 26, 32]. The voltage level of the machine is a factor that determines the diagnostic strategy. The diagnosis is much easier in the case that partial discharges are present in the insulation. But this phenomenon only appears when the voltage level is above 4 kV. In the case that the generator voltage is above 4 kV, partial discharge monitoring can identify insulation degradation prior to complete breakdown. The technique is widely applied in industry. For the generators with voltage below 4 kV, the diagnosis is based on the detection of inter-turn short circuits by other techniques.

1.4.6 Motor Current Signature Analysis (MCSA)

MCSA involves machine condition monitoring utilizing mostly steady-state spectral components of stator currents. These spectral components have been prove accurately to detect broken rotor bars, bearing failures, air gap eccentricity etc. with proven accuracy [13, 19, 48, 49]. Other quantities such as induced voltage and power can also be used for fault detection. However, the accuracy of these techniques depend on the loading of the machine, the signal to noise ratio of the spectral components being examined and the ability to maintain a constant speed to facilitate detection [32]. For detecting stator inter-turn faults, the principle of the Motor Current Signature Analysis is to identify the stator current spectral components that are characteristic of inter-turn stator faults exclusively and check for any abnormal deviation from the expected values.

Figure 1.19 shows an example of MCSA applied to detect broken rotor bars in squirrel cage induction motor by monitoring the spectrum of stator current for a particular frequency [50]. In the figure shown the frequency monitored is ± $2sf_1$. Detecting a rise of such a frequency component with respect to the fundamental triggers the fault alarm.

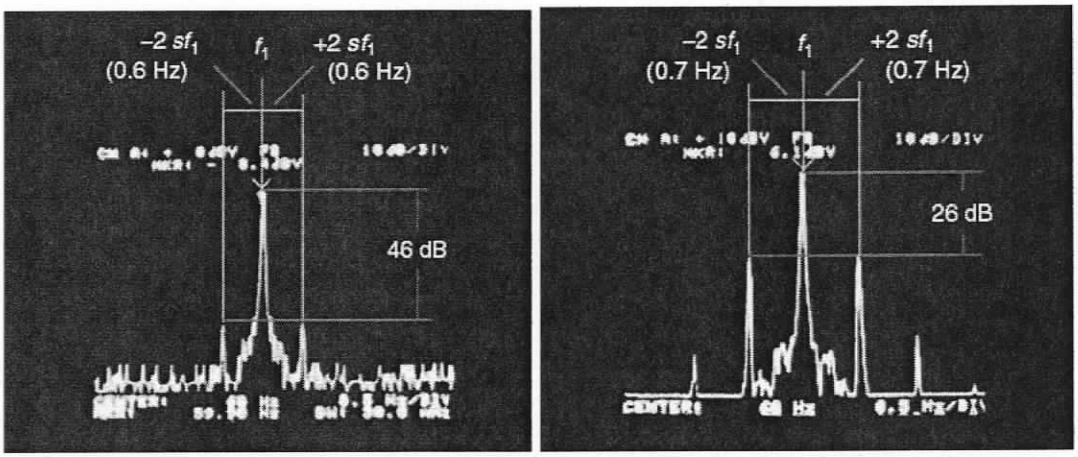

Figure 1.19 MCSA for broken rotor bar detection in squirrel cage motors a) spectrum of stator current for healthy rotor condition, b) spectrum of stator current under unhealthy rotor (broken bars) condition [50]

A literature survey [16, 51] revealed that couple of attempts have been made to find the unique frequency that is exclusively an indicator of stator inter-turn fault. Further detailed analysis revealed that either, these techniques failed under voltage supply unbalance of the machine [52] or were based on empirical observation and no mathematical proof was provided [16]. According to [51], a typical harmonic component that will be exclusively induced in rotor during a turn fault is at the monitoring frequency:

$$f_{st} = (2 - s) \cdot f_1 \tag{1.4}$$

Thus for s = 0.25, the fault frequency to monitor will be, (2-0.25)*60 = 105 Hz. However this frequency also gets affected due to any load unbalance or rotor winding asymmetry, which is proved in detail in section 2.2. This would lead to ambiguity in fault detection. According to [16] which also uses equation (1.1), fails to provide any mathematical proof of selecting a particular fault frequency. Instead based on series of experiments conducted over different machines and operating condition, it derives an

empirically observed frequency that increases in power level under fault. Also, the influence of unbalance loading of the generator on the fault frequency was not examined.

Moreover, using MCSA for fault diagnosis has a challenge; the inter-turn fault frequency components are dependent upon slip. During transient conditions there is a change in speed and hence the slip. The frequency components are therefore continuously changing and identifying these frequencies requires signal processing to be based on shortest duration of data sampled.

Although considerable research has been carried out, there is no agreement on the best method to detect inter-turn short circuit. To summarize the literature survey, it can be said that though majority of the diagnostic techniques falls into category of non-invasive approach (except the axial-flux analysis) they are not suitable in implementation of existing installations. The proposed techniques of Park, Extended-Park techniques all fail to function under certain operating conditions. The proposed MCSA techniques are ambiguous or based on observations not clearly substantiated by theory. The most promising method, the negative-sequence fault detection method requires complicated training and computational procedures.

1.5 Motivation and Objectives of Present Work

From the above facts, it can be clearly felt that the existing techniques of condition monitoring cannot reliably detect the DFIG stator inter-turn faults. This is because of the fact that one or more of the unbalance loading, time harmonics, internal asymmetry and changes in operating point of the machine could cause ambiguity in the detection. Some of the better methods need special devices like axial flux sensor or need high computations and memory or are ambiguous to detect the turn-to-turn faults or have limitations as they are not proven with analytical theory. Hence this research area needs special attention.

In this work, an attempt has been made to develop diagnostic technique that is capable of detecting the incipient stages of stator inter-turn faults in DFIG machines. Also it has been aimed to minimize the influence of load unbalance, time harmonics and

internal asymmetry of the machines on the diagnostic results. A detailed mathematical proof is provided to justify that the technique used is minimally influenced by unbalanced loading, time harmonics or internal asymmetry.

Finally, it has been intended to devise a simple and fast diagnostic tool by making use of the computational capabilities of a DSP to generate a trip signal in the event of a fault. The motivation of this thesis is to develop a technique which is not invasive and relies on hardware (sensors, DSP) used for driving the machine to perform the fault-diagnosis and detect up to one turn fault in most cases.

1.6 Thesis Outline

The thesis has been structured as follows. In Chapter 1, a general discussion on the use of DFIG and need for on-line fault diagnosis is made. Further, causes of stator inter-turn faults have been explored and the importance of decisively detecting inter-turn fault have been explained. Finally, a literature survey of some prevalent inter-turn faults diagnosing methodologies has been listed and discussed. The short-comings of previous research have also been discussed briefly.

In Chapter 2, detailed mathematical derivations, analysis and simulation results are used to prove the concept that stator inter-turn faults can be unambiguously and successfully detected by monitoring the rotor current spectrum.

In Chapter 3, experimental results are used to justify the proposed concept based on results from actual operating conditions of a machine for varying speed and load under different severity of faults. A detailed discussion is provided to help understand the test-setup that was created to acquire the experimental results. Also, an alternative method of observing voltage induced in a search coil is described and results are discussed.

To determine the feasibility of the proposed method, a prototype was created. Its detailed design and operation results are discussed in Chapter 4. Results from the fault

detection system are discussed to help understand the advantages and limitations of the proposed concept.

Based on the learning from the implementation and results from experiments, recommendations are made as a future scope for conducting further research on the proposed method of Fault Diagnostic System (FDS) for DFIG. The contributions by this research work and conclusions are described in Chapter 5.

Chapter 2

Analysis of Harmonics in Rotor Current of DFIG Suitable for Detecting Stator Inter-turn Faults

In this chapter, detailed mathematical derivations, analysis and simulation results are used to prove the concept that stator inter-turn faults can be unambiguously and successfully detected by monitoring the rotor current spectrum.

2.1 Mechanism of Induction of Various Harmonic Components in Rotor Current under Stator Fault

The way an ac electric motor is wound makes it behave like an antenna. It means that in a specific type of winding a particular time harmonic will be induced if and only if any pole pair (or mode) number associated with it matches that of the voltage inducing flux wave [53]. It is well known that due to manufacturing imperfections and the non-homogeneity of iron, every electric machine will possess asymmetries to a certain extent. When there is any asymmetry arising due to fault, eccentricity or unbalanced supply voltage, the consequent magnetic field distortion gives rise to new components in the stator and in the rotor spectrum that are directly caused by the fault. This also leads to torque oscillations and subsequent speed oscillations can further induce harmonic components both on stator and rotor. When an asymmetry of any type exists on the stator side, the negative sequence component at frequency –f in the stator causes a counter-rotating magnetic field. This produces a harmonic component in the rotor at frequency $(2-s)\cdot f_1$ and gives rise to electromagnetic and mechanical interaction between stator and rotor [51] as represented in Figure 2.1. As a consequence of this interaction, the following rotor current components appear.

$$f_{ksa} = (2k \pm s)\cdot f_1 \tag{2.1}$$

Where $k = 1, 2, 3...$, s is the slip and f_l is the fundamental frequency of the stator.

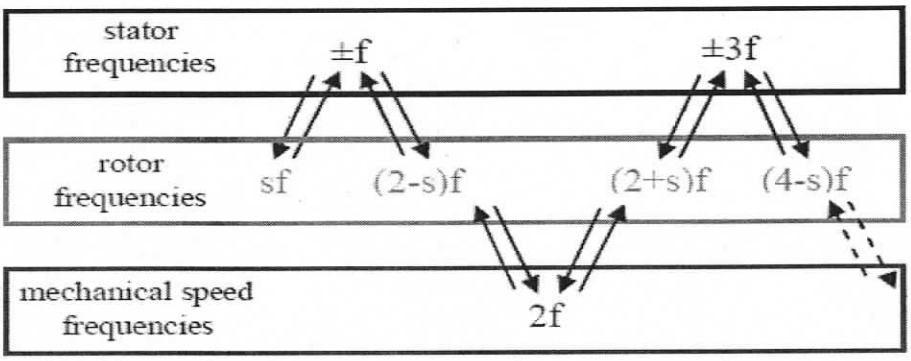

Figure 2.1 Frequency propagation for a stator fault[51]

However, the above theory does not differentiate between the effect of asymmetry caused by unbalanced loading and inter-turn fault. Also it fails to account for all stator space harmonics and time harmonics and asymmetries of the rotor winding. Hence a more detailed explanation is required which is provided in next section to understand the reason of harmonics observed in the rotor circuit. The objective of reliable fault-detection is to find the rotor circuit current components through MCSA that are function of shorted turns in stator winding only and not due to any other problem of load unbalance or winding imperfections.

2.2 Mathematical Proof for Various Harmonic Components Induced in Rotor Circuit

2.2.1 Time harmonics in rotor current due to stator space harmonics and time harmonics in stator current due to rotor space harmonics, under ideal conditions

In a wound rotor machine, with regular three phase integral slot winding both on stator and rotor, any time harmonic in stator will get induced in rotor and vice-versa as a different time harmonic, modulated by the effect of space harmonics. In [53], equations are derived to compute the harmonics induced in stator and rotor currents due to space and time harmonics for a wound rotor machine under ideal conditions, i.e. when there is no asymmetry in stator and rotor arising due to a fault or unbalance loading on the stator.

Only space harmonics arising due to non-sinusoidal distribution of the stator and rotor windings were considered. The frequencies induced in rotor due to space and fundamental time harmonics in stator is given by expression in curly brackets of (2.2) and frequencies induced in stator due to space and fundamental time harmonics in rotor are given by expression in curly brackets of (2.3)

$$B_{rs} = B_{m1}\cos\left(np\phi' + \left\{np\omega t \pm \omega_1 t\right\} + \varphi_1\right) \tag{2.2}$$

$$B_{sr} = B_{m2}\cos\left(np\phi + \left\{-np\omega t \pm \omega_r t\right\} + \varphi_2\right) \tag{2.3}$$

where n = 1, 6m $\pm$ 1 (m = 1,2,3…) is the order of the space harmonic, $\omega_1 = 2\pi f_1$, f_1 is the fundamental frequency of the stator voltage, The '+' sign comes before ω_1 when magnetic field is reverse rotating and '-' sign when field is forward rotating, while in (2.3) the '+' sign comes before forward rotating field and '-' sign when field is reverse rotating. $\omega = (1-s)\cdot {}^{\omega_1}\!/_{p}$ is the rotor speed in rad/sec and φ_1, φ_2 are arbitrary phase angles referred to stator and rotor respectively. p is the number of pole pairs and 's' is the slip. $\omega_r = 2\pi f_r$, f_r is the fundamental frequency of the rotor voltage. ϕ is the angle in stator co-ordinates; whereas ϕ' is the angle in rotor co-ordinates. Also $\phi' = \phi + \omega t$.

Hence under ideal operating conditions, with no unbalance load on the stator or inter-turn fault and no rotor asymmetry, for f_1 = 60Hz, and slip = 0.25 the harmonics induced in the rotor current can be calculated using (2.2), for n = 5, 7:

for n = 5, reverse rotating field, $\{5\cdot(1-0.25)\cdot 60 + (60)\} = 285\text{Hz}$

for n = 7, reverse rotating field $\{7\cdot(1-0.25)\cdot 60 - (60)\} = 255\text{Hz}$

Similarly, the harmonics induced in stator current due to time harmonics in rotor current and rotor space harmonics can be calculated using (2.3), for n = 5, 7:

for n = 5, forward rotating field, $\{5\cdot(1-0.25)\cdot 60 - (15)\} = 210\text{Hz}$

for $n = 7$, forward rotating field $\{7 \cdot (1-0.25) \cdot 60 + (15)\} = 330\text{Hz}$

This analysis is validated using simulation results in section 2.4. To maintain congruency in the explanation of the theory, the operating condition of DFIG running at a sub-synchronous speed of slip = 0.25 and a generating stator voltage at frequency f_1 = 60Hz is used for further discussion.

2.2.2 Time harmonics in current when stator is connected to unbalance load

Load unbalance in the stator phases causes negative sequence currents, which causes reverse rotating magnetic fields. The frequency of this reverse rotating magnetic field is same as that of fundamental frequency, but rotating in opposite direction. Hence this reverse rotating magnetic field at -60Hz interferes with fundamental frequency of 60Hz and will induce harmonic frequencies in rotor which can be calculated using (2.2):

for $n = 1$, reverse rotating field, $\{1 \cdot (1-0.25) \cdot (60) + (-60)\} = 105\text{Hz}$

for $n = 5$, forward rotating field, $\{5 \cdot (1-0.25) \cdot (60) + (-60)\} = 165\text{Hz}$

for $n = 7$, reverse rotating field, $\{7 \cdot (1-0.25) \cdot (60) - (-60)\} = 375\text{Hz}$

2.2.3 Time harmonics in rotor current due to inter-turn fault in stator winding

During an inter-turn fault the stator has a shorted loop (can thus be treated as a single-phase winding) carrying current at a supply frequency that generates two counter-rotating MMF waves [43]. The MMF produced by the asymmetric stator carrying 3-phase balanced voltage can be given as:

$$F_{sa} = A_{sa} cos(k\phi \pm \omega_1 t + \varphi_1) \tag{2.4}$$

where $k = 1, 2, 3..$ the order of space harmonic, $\omega_1 = 2\pi f_1$, f_1 is the fundamental frequency of the stator voltage and φ_1 is an arbitrary phase angle. Considering the

specific permeance function (P_0) the flux density produced by this MMF, with respect to stator, can be given as:

$$B_{sa} = A_{sa} P_0 cos(k\phi \pm \omega_1 t + \varphi_1) \tag{2.5}$$

With respect to rotor, this flux density is given as:

$$B_{ra} = A_{sa} P_0 cos(k\phi' + k\omega t \pm \omega_1 t + \varphi_2) \tag{2.6}$$

Following (2.3), now substituting $\omega = (1-s)\cdot {}^{\omega_1}\!/_{p}$ in (2.7), we have

$$B_{ra} = A_{sa} P_0 cos\left(k\phi' + \left\{ \frac{k}{p}(1-s) \pm 1 \right\} \omega_1 t + \varphi_2 \right) \tag{2.7}$$

The frequencies that will be induced in the rotor circuit due to a fault in stator winding when DFIG is running at s = 0.25, f_1 = 60Hz and different values of k, is expressed in Table 2.1 using the equation in curly brackets of (2.7). As seen from Table 2.1, several frequencies could be induced as a result of the fault. The time harmonics in current of stator winding also induce harmonics in the current of rotor winding due to load unbalance and other mechanical faults. The objective is to find the frequency, which is most affected by the fault and is not influenced by the unbalanced load on the generator.

Table 2.1 Frequencies induced in rotor current due to turn-fault in stator winding, slip = 0.25, f_1 = 60Hz

k	1	2	3	4	5	6	7	8	9
Freq.	82.5	105	127.5	150	172.5	195	217.5	240	262.5
(Hz)	-37.5	-15	7.5	30	52.5	75	97.5	120	142.5
k	10	11	12	13	14	15	16	17	18
Freq.	285	307.5	330	352.5	375	397.5	420	442.5	465
(Hz)	165	187.5	210	232.5	255	277.5	300	322.5	345

2.2.4 Time harmonics in rotor current due to stator and rotor asymmetry

There always exists an asymmetry to a certain extent in the rotor windings of any practical induction machine. The frequency which is selected to be monitored for fault diagnosis should not be affected due to asymmetry of rotor winding. Whenever there is an asymmetry in the windings, it gives rise to time harmonics related to triplen(3^{rd} order) space harmonics. i.e. for $n = 3$ and $f_1 = 60$Hz, using (2.2) suggests following frequencies to be induced in rotor current, even under with healthy machine and balanced load:

for $n = 3$, reverse rotating field, $\{3 \cdot (1-0.25) \cdot 60 - (60)\} = 75\text{Hz}$

The harmonics induced in stator current for n = 3, using (2.3) can be given by:

for $n = 3$, forward rotating field, $\{3 \cdot (1-0.25) \cdot 60 + (15)\} = 150\text{Hz}$

The asymmetry also causes a reverse rotating magnetic field at frequency -15Hz which induces 30Hz harmonics in stator phase current, given by (2.3) for $n = 1$,

for $n = 1$, reverse rotating field, $\{1 \cdot (1-0.25) \cdot 60 + (-15)\} = 30\text{Hz}$

This 30Hz harmonics subsequently induces the following harmonics in the rotor, given by (2.2),

for $n = 3$, reverse rotating field, $\{3 \cdot (1-0.25) \cdot 60 - (30)\} = 105\text{Hz}$

However, in a perfectly balanced machine (that only exists in theory), these effects are cancelled out.

Based on the above theory and analysis and from Table 2.1, all the frequencies associated with even values of k that are multiple of 1, 3, 5...etc. are found to be influenced by either unbalanced load on the stator or rotor asymmetry, or exist due to space harmonics even under ideal condition. Hence, if any frequency is selected for fault diagnosis from the Table 2.1 that corresponds to these values of k, the results are

ambiguous. From the remaining set of frequencies, frequencies associated with odd values of k as will be shown later; tend to be influenced due to stator inter-turn fault. The above theory will now be verified via simulation of DFIG models to explore which frequencies provide the best indication for the inter-turn stator fault.

2.3 Modelling of DFIG under Healthy, Unbalanced and Stator inter-turn fault conditions

In order to carry out a detailed simulation study, different models of the DFIG have been considered. Following are the six different cases considered for this study:

Case A: DFIG with symmetric rotor winding, connected to balanced load

Case B: DFIG with symmetric rotor winding, connected to 10% unbalanced load on one phase

Case C: DFIG with asymmetric rotor winding, connected to balanced load

Case D: DFIG with asymmetric rotor winding, connected to 10% unbalanced load on one phase

Case E: DFIG with symmetric rotor winding, subjected to 4-turn fault

Case F: DFIG with asymmetric rotor winding, subjected to 4-turn fault

The equations used for modelling of these six cases are listed in Appendix-A. The purpose of creating these models is to understand how unbalanced load, rotor asymmetry and inter-turn fault individually affect the harmonics in rotor current. Winding Function Approach [54] was used to model the DFIG. The process involved:

- Determining the turns function for stator and rotor phases of healthy machine.
- Determining the position dependent inductance (self, mutual) for stator and rotor phases.

- Determining the position dependent derivative of inductances for stator and rotor phases.
- Stator and rotor currents are obtained using coupled circuit equations solved dynamically with computed position information fed back.
- Machine is modelled in steady-state with constant speed, assuming $T_e = T_l$
- Resistive load was connected to the stator and a 15Hz 3-phase source is used for energizing the rotor.

For simulating cases of DFIG with inter-turn fault and rotor winding asymmetry, the above steps were repeated for faulty turn and asymmetry causing turn. The DFIG chosen for simulation has parameters similar to the motor that will be used for experiments. The simulation was carried out in MATLAB and results from the simulation are discussed in the following section.

2.4 Simulation Results for Healthy, Faulty and Supply Unbalance Conditions

A thorough simulation study was carried out using the six different models of the machine as mentioned in the earlier section. Based on the analysis of harmonics that will be induced in rotor phase current and stator phase current under different operating conditions are verified in following sections. Power Spectral Density (PSD) function was used to analyze the existence of harmonics in the stator and the rotor phase currents. A complex PSD was done on the vector sum of stator phase currents and rotor phase currents to understand which harmonics are associated to forward and reverse rotating fields. The complex PSD provides information about the sign associated with a time frequency component [29]

Case A: DFIG is modelled with symmetric rotor and connected to a balanced load. According to the previous analysis done in section 2.2.1, the harmonics of 255Hz

and 285 Hz are observed in the frequency spectrum of rotor phase current shown in Figure 2.2. While, the harmonics of 210Hz and 330Hz are observed in frequency spectrum of stator phase current shown in Figure 2.3. The complex PSD of rotor current vector in Figure 2.4 reveals 255Hz harmonic in negative, which indicates that, the MMF caused due to 7^{th} stator space harmonic is rotating reverse with respect to magnetic field of rotor's fundamental frequency in rotor reference frame. The 285Hz harmonic is positive caused due to 5^{th} stator space harmonic. Hence the corresponding MMF is rotating forward with respect to magnetic field due of rotor's fundamental MMF harmonics. Similarly in Figure 2.5, the 210Hz and 330Hz harmonics are caused due to MMF of 5^{th} and 7^{th} rotor space harmonics and the corresponding MMFs are rotating in forward direction respectively with reference to stator fundamental MMF harmonics.

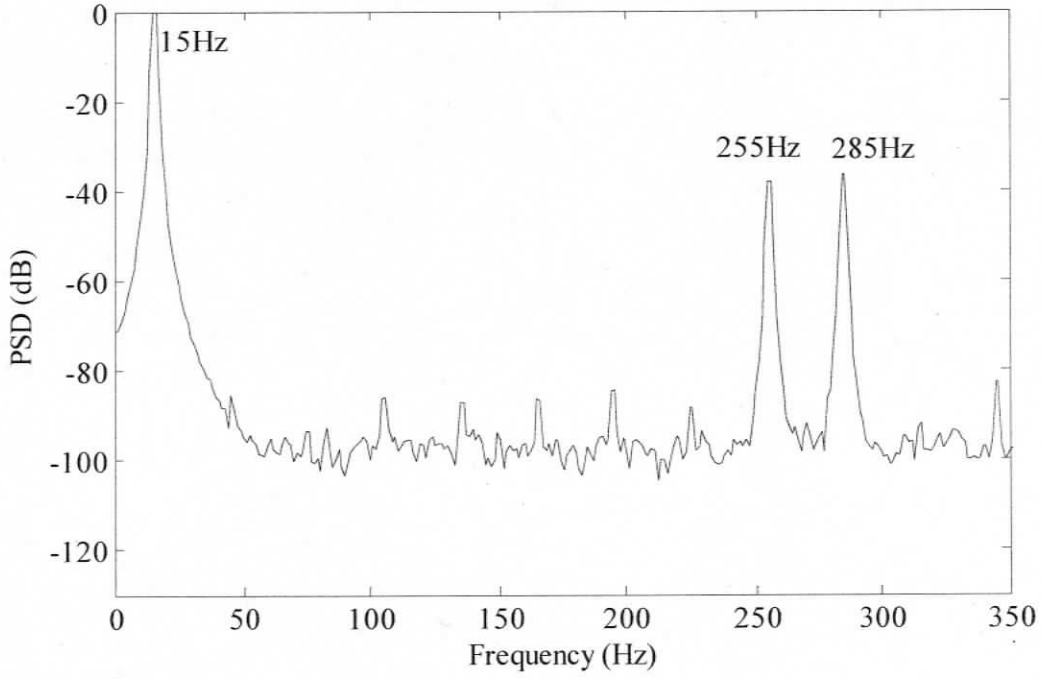

Figure 2.2 PSD of rotor phase current, DFIG modelled with symmetric rotor, connected to a balanced load, operating at slip = 0.25, full-load

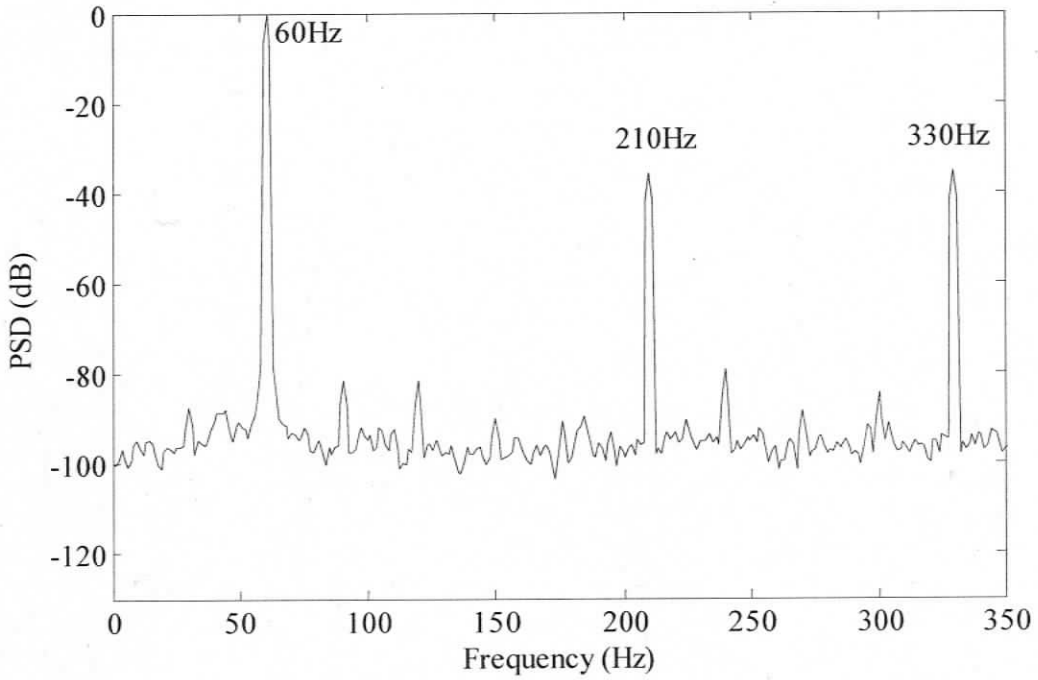

Figure 2.3 PSD of stator phase current, DFIG modelled with symmetric rotor, connected to a balanced load, operating at slip = 0.25, full-load

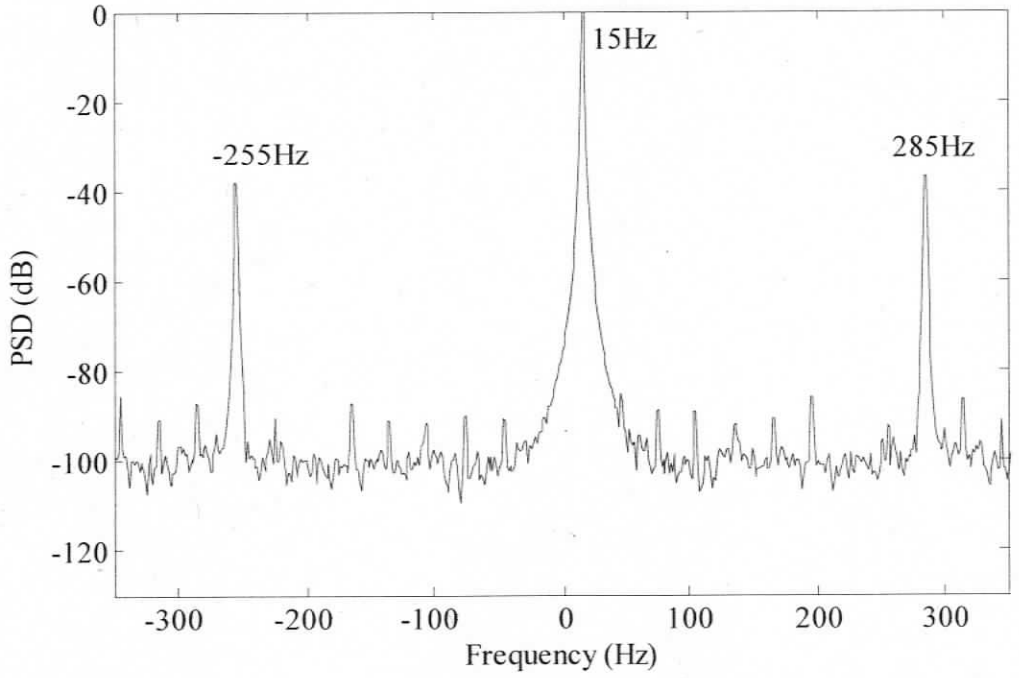

Figure 2.4 Complex PSD of rotor current vector, DFIG modelled with symmetric rotor, connected to a balanced load, operating at slip = 0.25, full-load

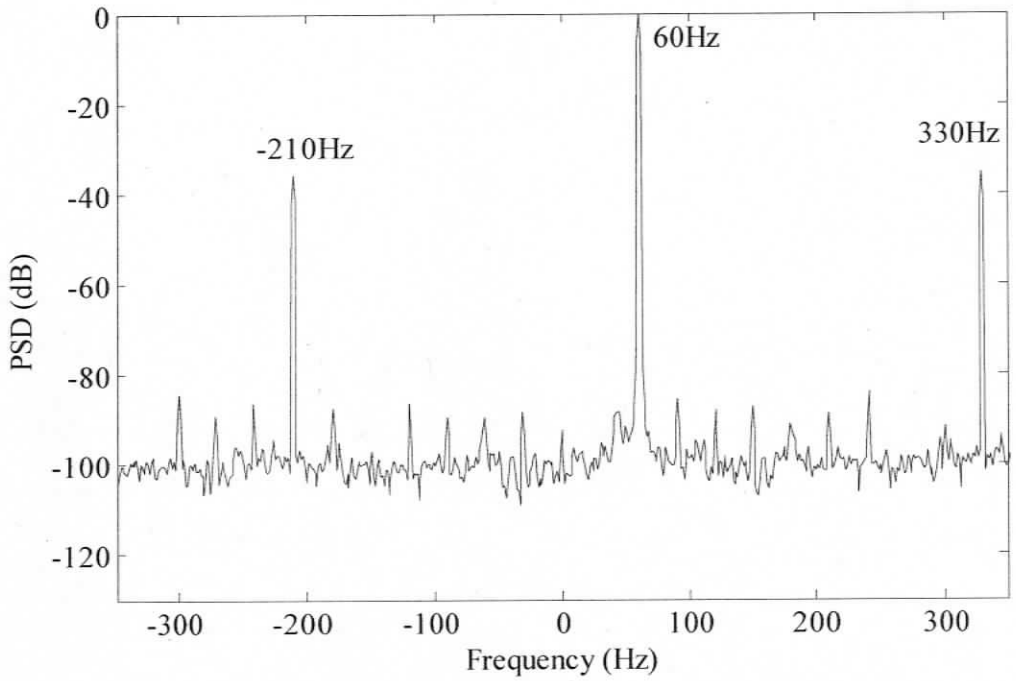

Figure 2.5 Complex PSD of stator current vector, DFIG modelled with symmetric rotor, connected to a balanced load, operating at slip = 0.25, full-load

Case B: DFIG is modelled with symmetric rotor and connected to an un-balanced load of 10% on phase-a. As discussed in section 2.2.2, unbalanced load on the stator generates negeative sequence current and a reverse rotating magnetic field at frequency same as fundamental. This can be observed in Figure 2.6 which shows -60Hz harmonic induced in stator current due to load unbalance. The -60Hz harmonic links with fundamental space harmonic to cause a 105Hz harmonic component and with a 5^{th} order stator space harmonic to cause 165Hz harmonic in the rotor current shown in Figure 2.7. Also, the rotor 5^{th} and 7^{th} space hamronic links with this 105Hz component to cause 210Hz and 330Hz harmonics in the stator current, observed in the positive and negative halves respectively in Figure 2.6.

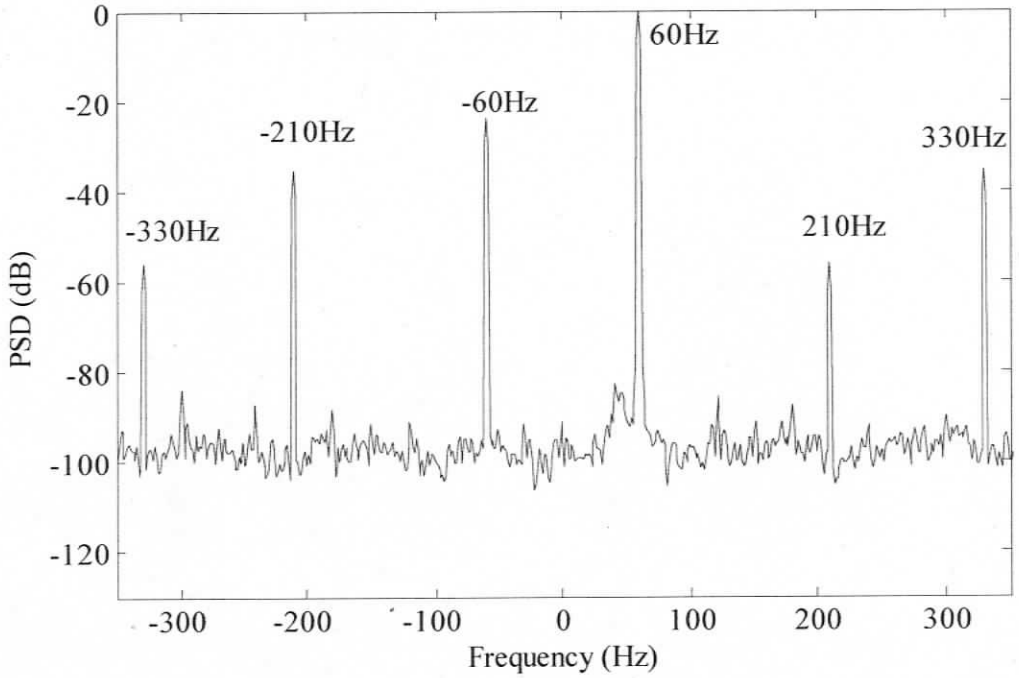

Figure 2.6 Complex PSD of stator current vector, DFIG modelled with symmetric rotor, connected to an unbalanced load of 10% on phase-a, operating at slip = 0.25, full-load

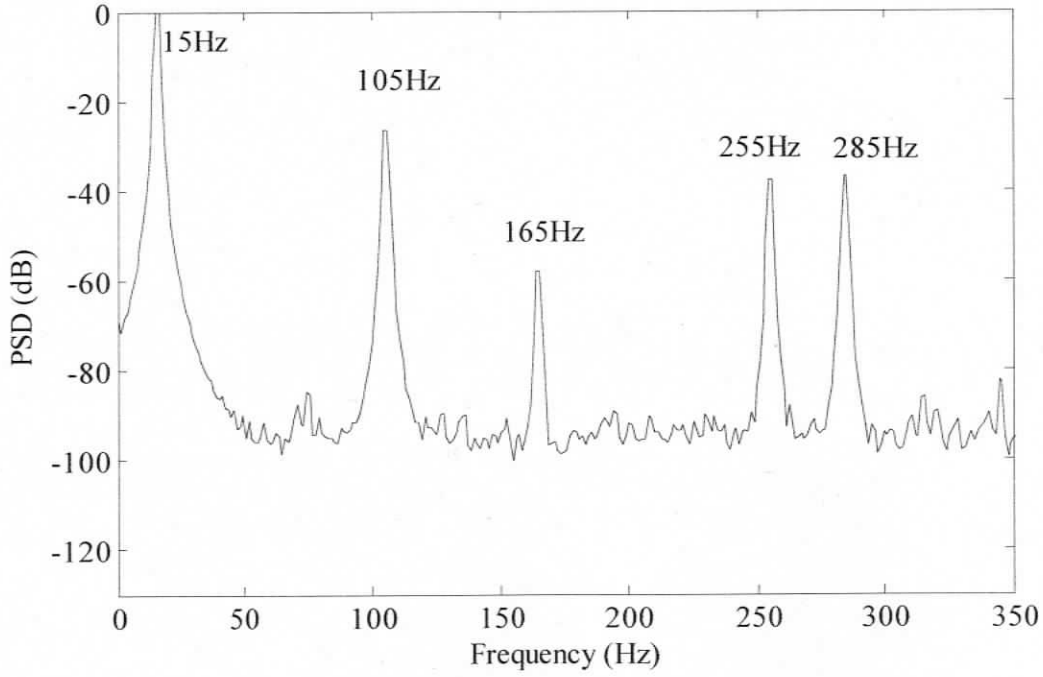

Figure 2.7 PSD of rotor phase current, DFIG modelled with symmetric rotor, connected to an un-balanced load of 10% on phase-a, operating at slip = 0.25, full-load

Case C: DFIG is modelled with rotor asymmetry and connected to a balanced load. As discussed in section 2.2, the asymmetry in rotor winding, leads to a reverse rotating field of -15Hz which is observed in the complex PSD of rotor current vector in Figure 2.8. This reverse rotating field of -15 Hz induces a 30Hz harmonic in the stator current observed in Figure 2.9. This 30Hz interference causes 105 Hz harmonic in the rotor current observed in Figure 2.10. This is because rotor asymmetry makes time harmonics associated with trpilen space harmonics non zero. Similarly, the 3rd space harmonic of the stator in association with the 60Hz time harmonic induces the 75Hz harmonic in the rotor current, which can be seen in the negative half of rotor current vector PSD in Figure 2.8.

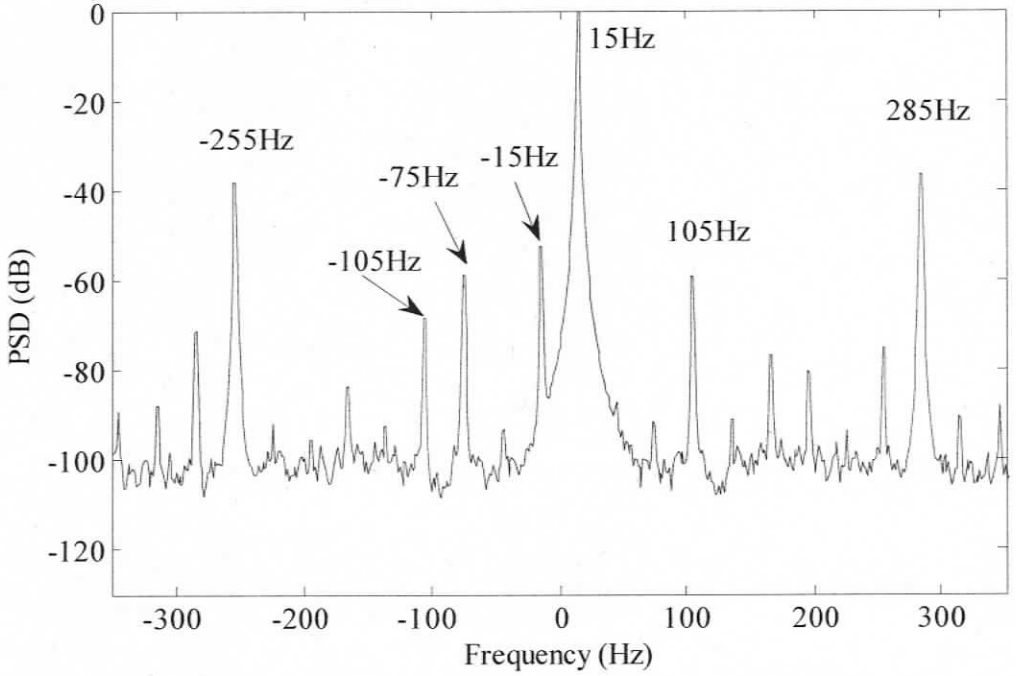

Figure 2.8 Complex PSD of rotor current vector, DFIG modelled with rotor asymmetry, connected to a balanced load, operating at slip = 0.25, full-load

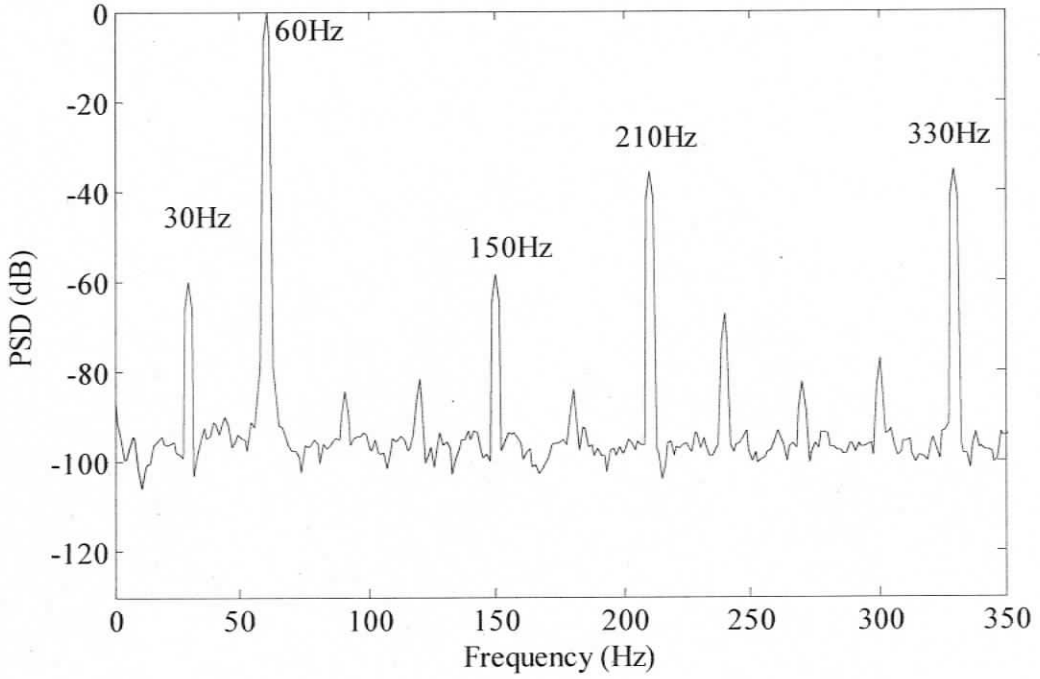

Figure 2.9 PSD of stator phase current, DFIG modelled with rotor asymmetry, connected to a balanced load, operating at slip = 0.25, full-load

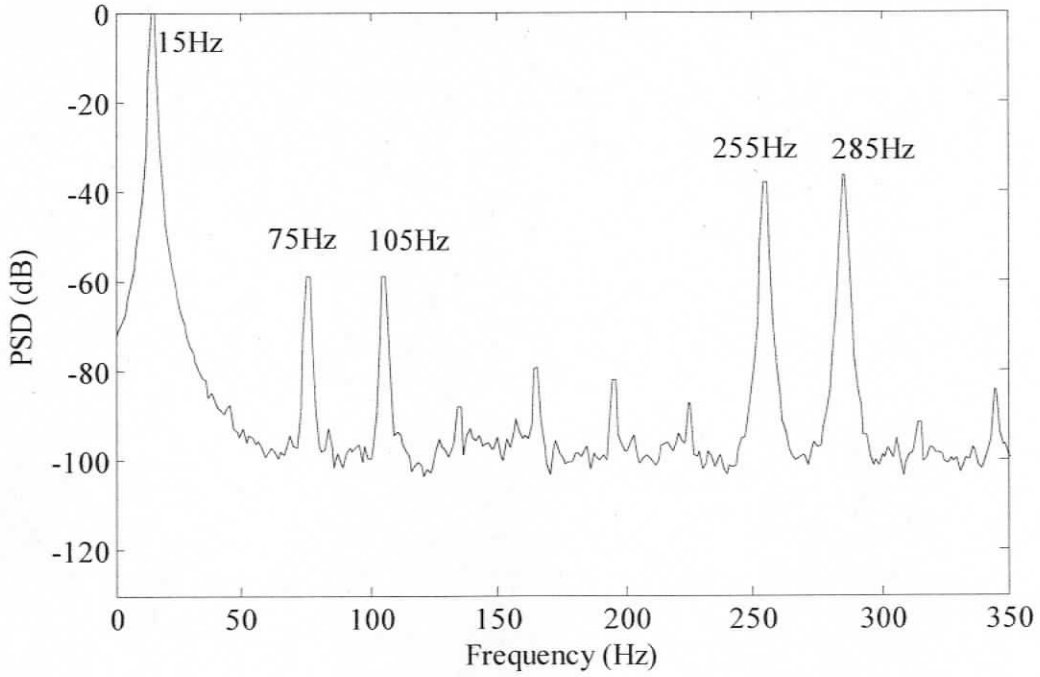

Figure 2.10 PSD of rotor phase current, DFIG modelled with rotor asymmetry, connected to a balanced load, operating at slip = 0.25, full-load

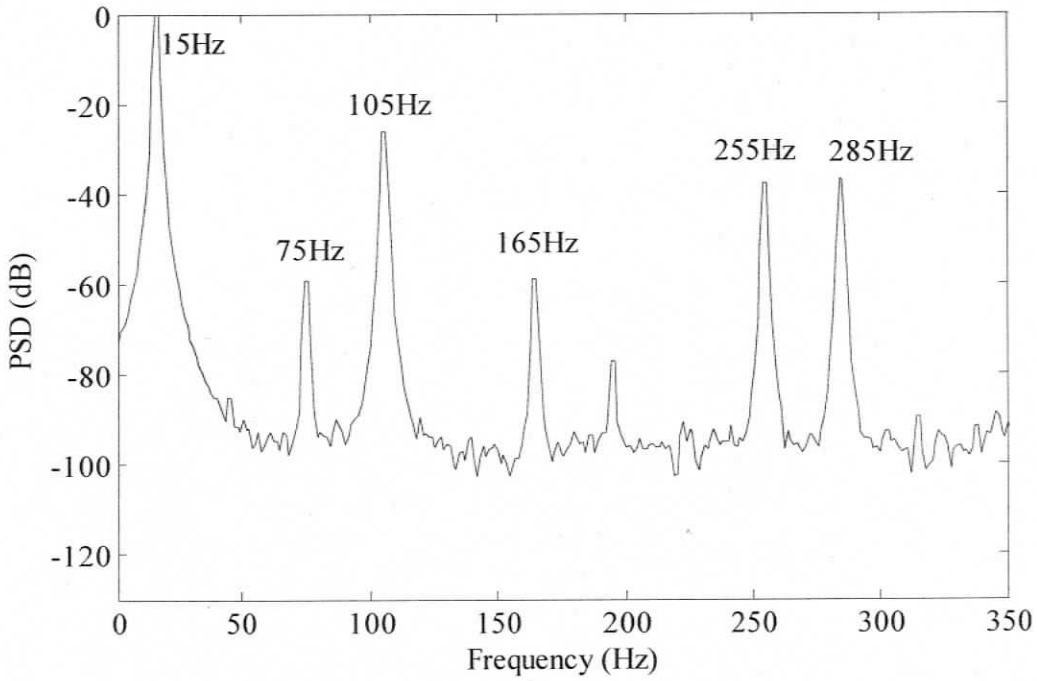

Figure 2.11 PSD of rotor phase current, DFIG modelled with rotor asymmetry, connected to an unbalanced load of 10% on phase-a, operating at slip = 0.25, full-load

Case D: DFIG is modelled with rotor asymmetry and connected to an un-balanced load of 10% on phase-a. Under this condition, the rotor current frequency spectrum shows the harmonics due to collective effect of rotor asymmetry and load unbalance discussed earlier. This can be inferred by comparing Figure 2.7, Figure 2.10 and 2.11. The frequency spectrum of rotor phase current shows a 75Hz component that is induced exclusively due to rotor asymmetry, a 165Hz component is induced exclusively due to the unbalanced load. However the 105Hz is influenced due to rotor asymmetry as well as load unbalance. The magnitude of the 105Hz component is observed to be larger due to this reason when comparing with the plots of Case B and Case C.

Case E: DFIG is modelled with symmetric rotor, connected to balanced load and subjected to a 4-turn fault in stator phase-a. Figure 2.12 shows the frequency spectrum of rotor phase current which consists of frequencies only associated with even values of k that are multiple of 1, 3, 5… in Table 2.1.

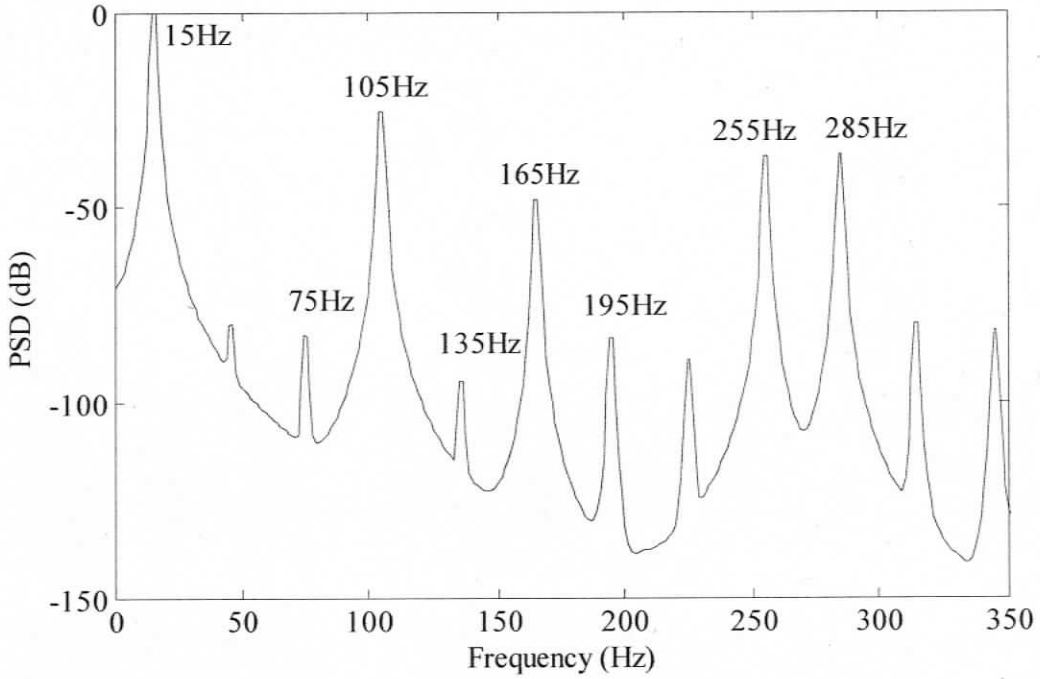

Figure 2.12 PSD of rotor phase current, DFIG modelled with symmetric rotor, connected to a balanced load with a 4-turn fault, operating at slip = 0.25 full-load

Case F: DFIG is modelled with rotor asymmetry, connected to balanced load and subjected to a 4-turn fault in stator phase-a. As discussed in section 2.2.3, under a stator inter-turn fault, all the frequencies listed in Table 2.1 are visible in the frequency spectrum of rotor current, shown in Figure 2.13. However PSD (dB) level of frequencies 82.5Hz ($k = 1$) and 127.5 Hz ($k = 3$) are observed to have increased the most under inter-turn fault. These components are observable only under fault conditions when asymmetry is present in the rotor circuit. Since such non-ideality exists in any machine, these components can be tracked for fault detection.

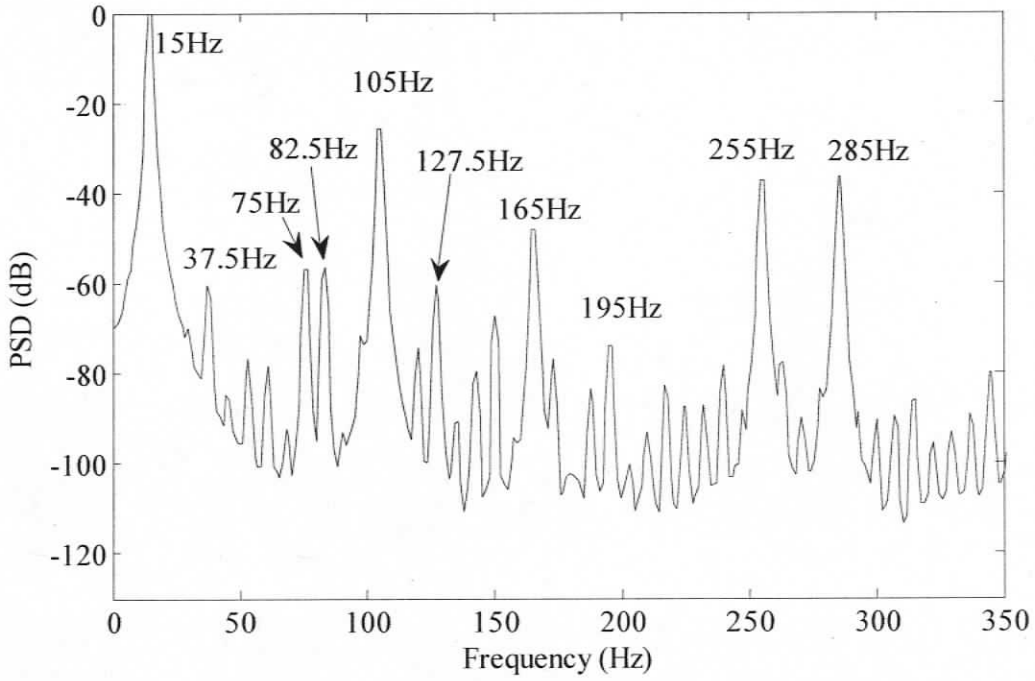

Figure 2.13 PSD of rotor phase current, DFIG modelled with rotor asymmetry, connected to a balanced load with a 4-turn fault, operating at slip = 0.25 full-load

2.5 Comparison of Rotor Current Spectrum under Different Operating Conditions

From observation of the frequency spectrum, it is clear that a number of frequencies are influenced due to unbalancing of the load or turn-faults. However from the simulation results and analysis of Section 2.2 and 2.3, for slip = 0.25, 82.5Hz ($k = 1$) and 127.5 Hz ($k = 3$) frequency components, based on Table 2.1, appear to be very promising as indicators of fault. It is later confirmed from the experimental results that change in the magnitude of the component at 127.5 Hz is a strong indicator of inter-turn stator fault. Simulations were conducted for DFIG operating at different load set-points for varying severity of fault levels, i.e. number of shorted turns and the PSD (dB) level rise of 127.5 Hz ($k = 3$) frequency component is compared with healthy balanced and

unbalanced load condition. The model with rotor asymmetry is used to test the PSD under different fault levels:

- Healthy balanced load (HB),
- Healthy unbalanced load of 10% on stator phase-a (UB),
- One-turn shorted of phase-a shorted, balanced load on 3 phases (1T),
- Two-turn shorted of phase-a shorted, balanced load on 3 phases (2T),
- Three-turn shorted of phase-a shorted, balanced load on 3 phases (3T),
- Four-turn shorted of phase-a shorted, balanced load on 3 phases (4T),

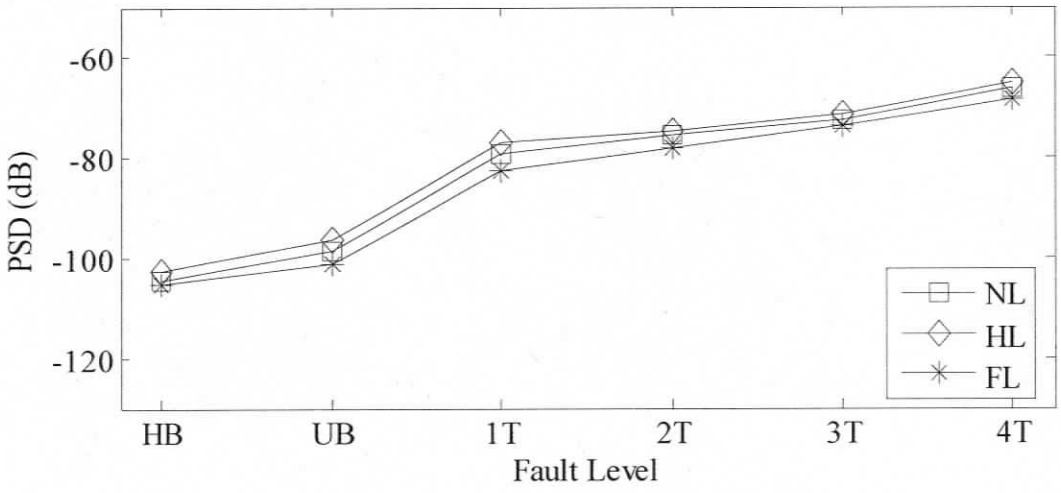

Figure 2.14 Simulation result, variation of fault spectra of rotor current frequency 127.5Hz (k=3) for slip 0.25 under no-load (NL), half-load(HL) and full-load(FL), with varying fault severity (Table B.1).

Change in magnitude of frequency 127.5Hz (k=3) for slip = 0.25 and varying load condition when subjected to different fault levels is compared in Figure 2.14. From the plot it can be observed that load unbalance does not increase the magnitude (dB) of the 127.5Hz (k=3) component as significantly compared to the rise caused by inter-turn faults. Further comparison of the rise of fault frequency power level for different slip, fault level and load conditions are done in Chapter 3 using experimental data.

Chapter 3

Experimental Results from Analysis of Rotor Phase Current, Rotor Current Vector and Search Coil Voltage to detect Inter-turn Fault in Stator of DFIG

In this chapter, the feasibility of detecting stator inter-turn fault for DFIG machines is verified through experiments, analyzing the component related to the k=3 harmonic in the rotor currents and in the rotor mounted search coil voltage. Owing to the structural asymmetries of the rotor, it has been found that the stator inter-turn faults clearly increase the magnitude of those frequency components in the rotor current and in the search coil voltage. These findings will now be validated using necessary experiments for different operating set-points of speed, load and inter-turn fault severity of DFIG. The fault diagnosis results obtained from using rotor-mounted search coil proved to be capable to detect even a single turn stator fault unambiguously under most load condition.

3.1 Description of Test-Setup and Hardware

A test arrangement as shown in Figure 3.1 (schematic) and Figure 3.2 (test-bench photo) are used to test the rotor currents and search coil voltage of DFIG under varying load, speed and fault condition.

The DFIG machine is a 3-phase, 1.5kVA 208V, 60Hz slip-ring induction generator which is mechanically coupled to a 2kW Synchronous motor. The stator of the synchronous motor is fed with a variable frequency voltage source through a Variable Frequency Drive-2 (VFD-2) (3-phase inverter with front end rectifier). The field winding on the rotor of the synchronous motor is provided with a dc excitation from a dc-power supply. By controlling the frequency of the voltage fed from VFD-2 to the stator of the synchronous motor, its rotor speed is controlled to different set-points.

The DFIG under test is run as a 60Hz stand alone generator connected to a 3-phase resistive load. The stator voltage and frequency of DFIG is controlled by feeding the rotor with slip frequency voltage using VFD-1. VFD-1 is a 3-phase Voltage Source Inverter (VSI) with a front-end diode bridge rectifier. A Digital Signal Processor (DSP) TMS320F2812 generates the gating signals for VSI. Figure 3.3 shows the schematic of the control scheme. The control of rotor voltage and frequency is done in an open loop. The control reference ω_r^* is changed manually to provide the slip frequency voltage and the modulation index such that the stator voltage is held constant at rated voltage and 60Hz even when load level is changed. This arrangement is used to simplify conducting the tests. In Chapter-4, the fault detection prototype is discussed for inductive and capacitive loads when the control of rotor frequency is done in closed loop.

The rotor currents of phase-u, v, search coil voltage, stator line voltage V_{ab}, current of phase-a and current in shorted turn are sampled using the data-acquisition system (NI DAQ-Pad6070E) using current probes and voltage probes. The sampled signals are fed to a computer for data logging and further analysis.

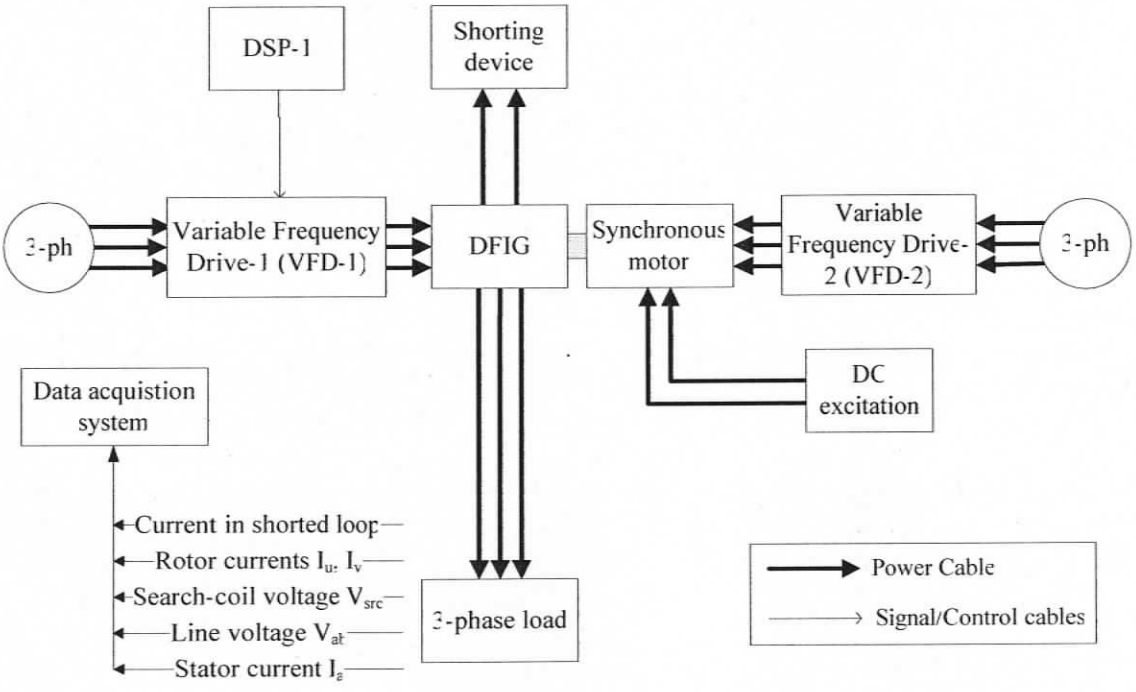

Figure 3.1 Schematic of experimental setup used to determine DFIG behaviour under varying load, speed and fault condition

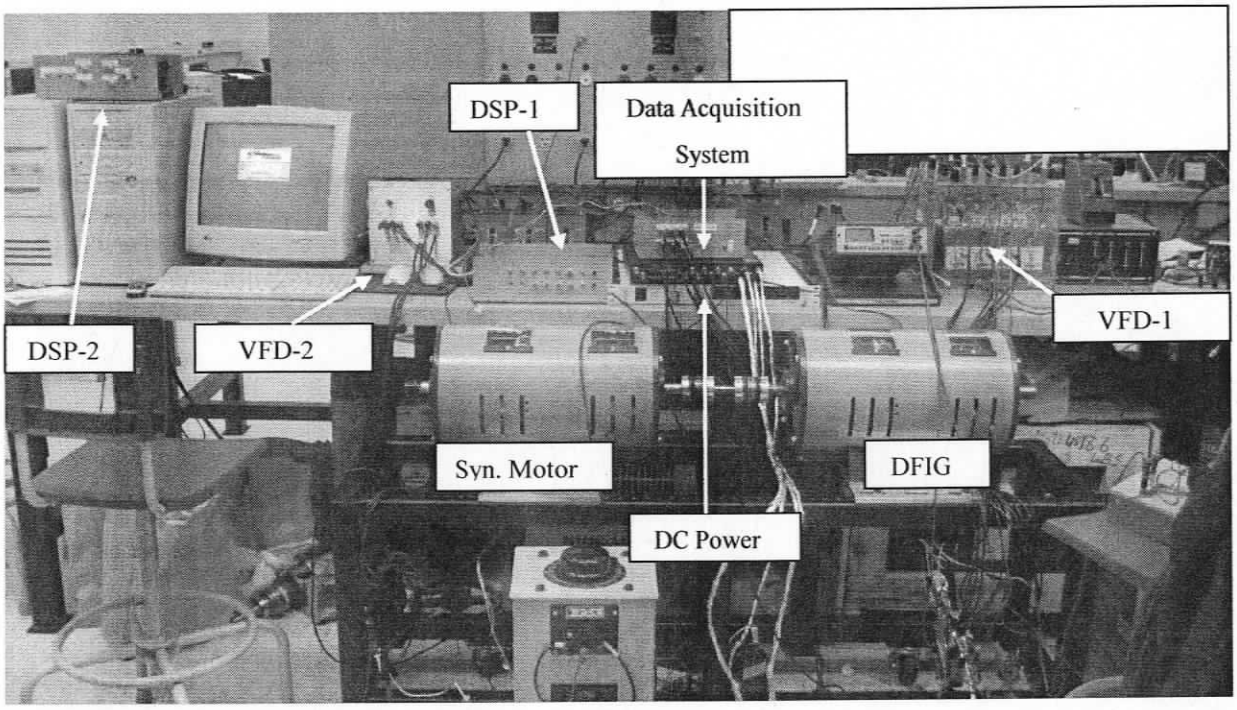

Figure 3.2 Photo of experimental setup for data acquisition

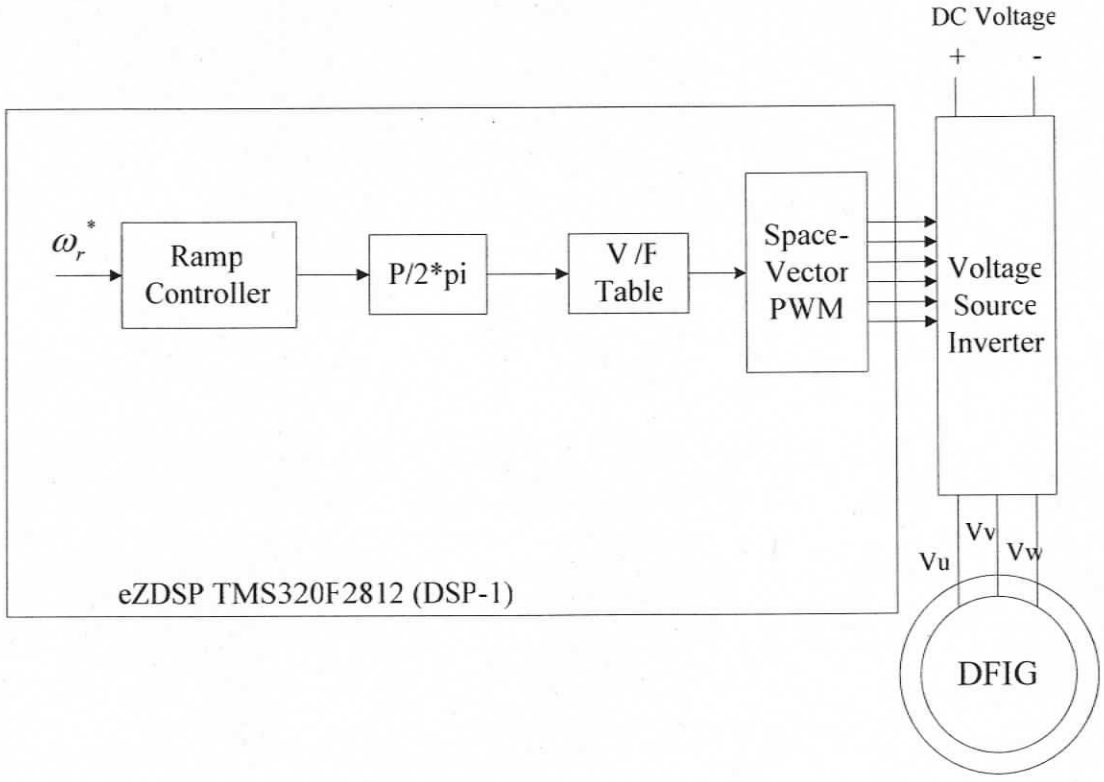

Figure 3.3 Scheme of constant V/F control of DFIG

3.2 Description of Test conditions

The DFIG is run at various sub-synchronous speeds, at 1000, 1350 and 1750 rpm each under no-load, half-load and full-load at varying fault conditions:

- Balanced load, no inter-turn fault
- Unbalanced load of 10% on stator phase-a
- 1-turn fault, balanced load
- 2-turn fault, balanced load
- 3-turn fault, balanced load
- 4-turn fault, balanced load

For analysis, six signals were sampled from the test-setup:

- Two rotor currents, I_u, I_v
- Rotor search coil voltage, V_{src}
- Stator current, I_a
- Current in fault circuit, I_f
- Stator line voltage, V_{ab}

The analysis of the fault condition is performed using Matlab to perform a PSD of the proper signal and monitoring the power level of the component related to the k=3 harmonic.

3.3 Description of Fault Simulation and Test Method

The DFIG machine used for testing has stator turn leads available at the motor terminals that can be shorted out. Out of 144 turns on stator phase-a, taps are available

at terminals to create 1, 2, 3 or 4 turn shorts. The construction and arrangement of the stator winding turns of the machine is detailed in [29]. Using a timer-relay and a contactor, the windings are shorted for a period of 2-10 seconds for testing. The device used for shorting the windings is shown in Figure 3.4. Shorting one of the leads of this turns, instantly emulates a shorted turn in one coil of the stator winding. During the shorted period, the data acquisition system samples the signals and feeds it to a computer for data logging and further analysis. Using this shorting device and the test conditions described in Section 3.2, the signals of rotor current were obtained. Figure 3.5 shows the current waveform of the rotor phase-u when the DFIG is operating at slip of 0.25, i.e. 1350 rpm at full-load under:

a) Balanced load,

b) Unbalanced load of 10% on phase-a,

c) 4-turn fault under balanced load

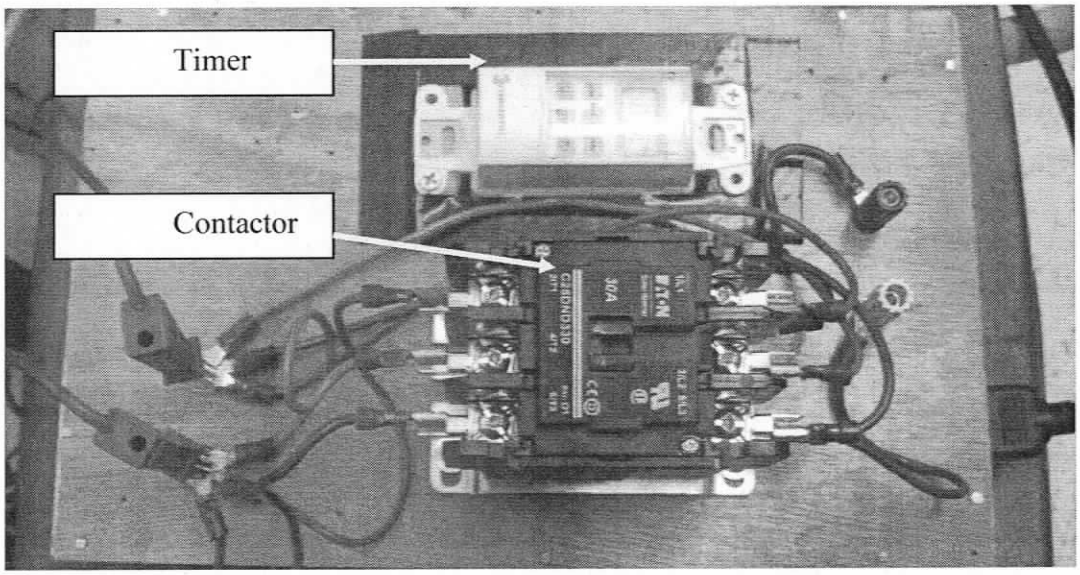

Figure 3.4 Photo of fault emulating stator inter-turn shorting device

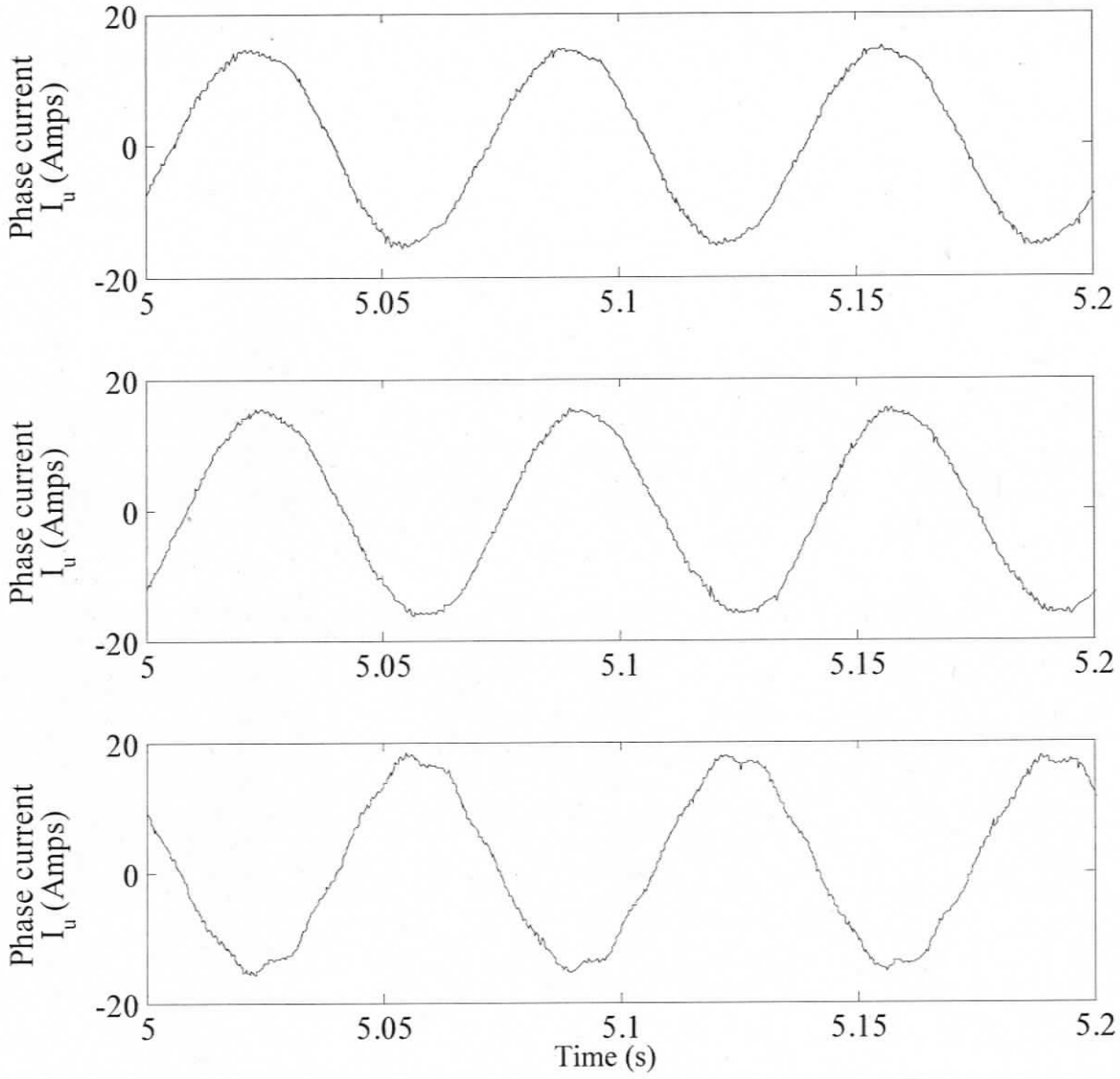

Figure 3.5 Experimental result, waveform of DFIG rotor current in phase-u when DFIG is operating at slip = 0.25 under full-load for (a) Healthy balanced load (b) Healthy unbalanced load of 10% on phase-a, (c) 4-turn fault, balanced load condition.

3.4 Comparison of Rotor Phase-u Current PSD under Different Operating Conditions

Figures 3.6, 3.7 and 3.8 show the spectrum of rotor current in phase-u under different fault conditions when DFIG is operating at full-load and slip of 0.25, i.e. DFIG rotor spinning at 1350 rpm. The PSD plots are obtained by analyzing 10 second of rotor current time signal in Matlab using the PSD function. The harmonic (127.5 Hz) related to fault frequency for s = 0.25, discussed previously, is highlighted. The peak at 127.5 Hz is observed to rise specifically only under the inter-turn fault condition and not when the DFIG is operating under balanced load or unbalanced load in a fault-free state.

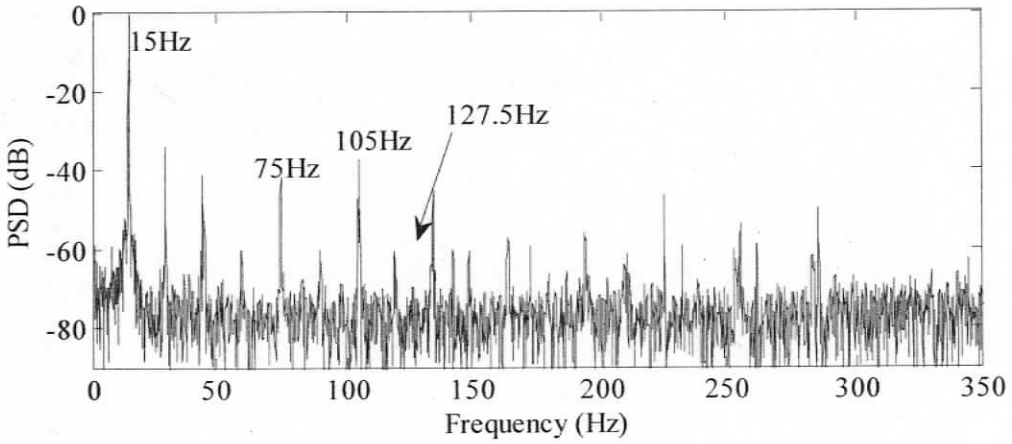

Figure 3.6 Spectrum of rotor phase-u current under balanced operating condition at full-load, s = 0.25

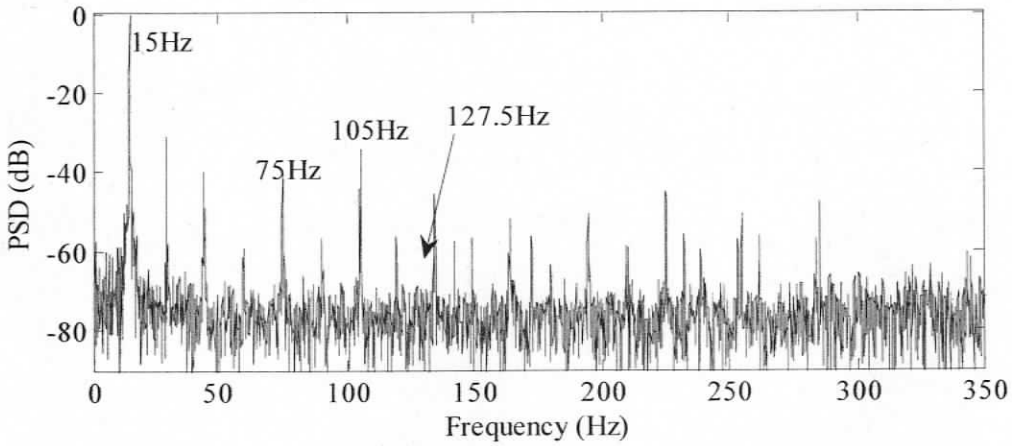

Figure 3.7 Spectrum of rotor phase-u current under unbalance operating condition at full-load, s = 0.25

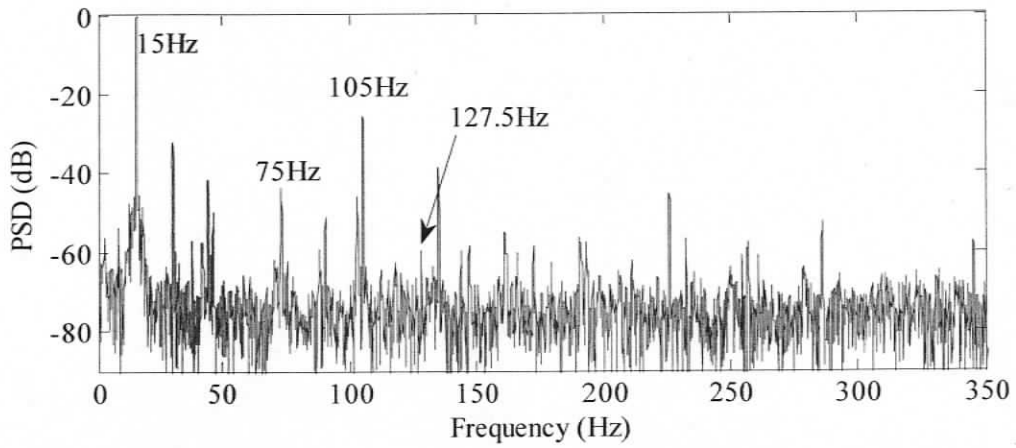

Figure 3.8 Spectrum of rotor phase-u current under 4-turn fault operating condition at full-load, s = 0.25

The rise in the fault frequency harmonic is monitored for various operating slip, load and fault conditions is graphically presented in Figure 3.9, 3.10 and 3.11 (actual values are available in Appendix-B, Tables B-2 to B-4). From the plots it is evident that the magnitude PSD (dB) level of fault frequency component rises with the severity of the faults. However, as the load is increased, the magnitude PSD (dB) of fault frequency component for 1-turn faults does not increase significantly to identify a fault. This can be attributed to the fact that, while shorting the turn, the lead impedance of wires add up with the impedance of the shorted turn. It was determined experimentally that the shorting lead impedance is equal to impedance of a 1-turn coil. Also as the load increases, the ratio of current in shorted coil to current in that phase winding decreases, which may worsen sensitivity. However in case of an actual dead-bolt fault, there will be no contact impedance and hence sensitivity will be much better. Improvement can also be achieved by applying a least square approximation method to compensate for the loading effect [29].

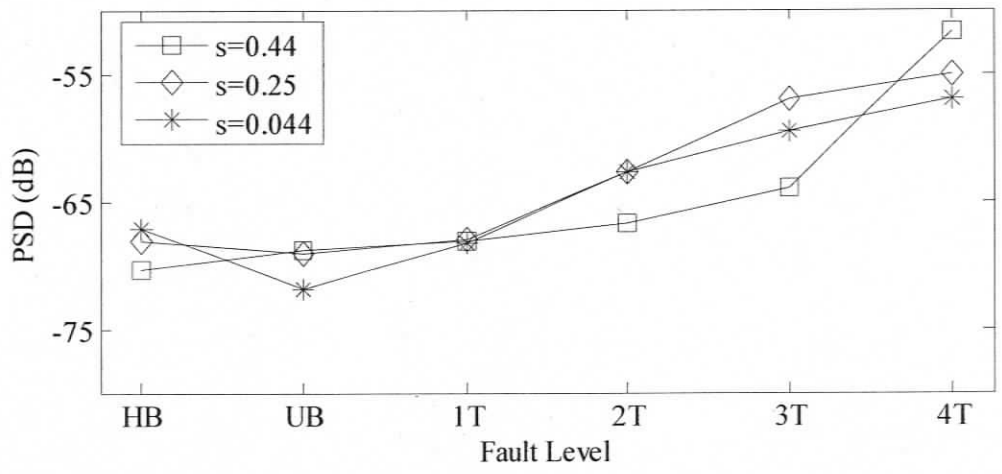

Figure 3.9 Variation of fault spectra under no load and various fault and slip conditions (Table B.2)

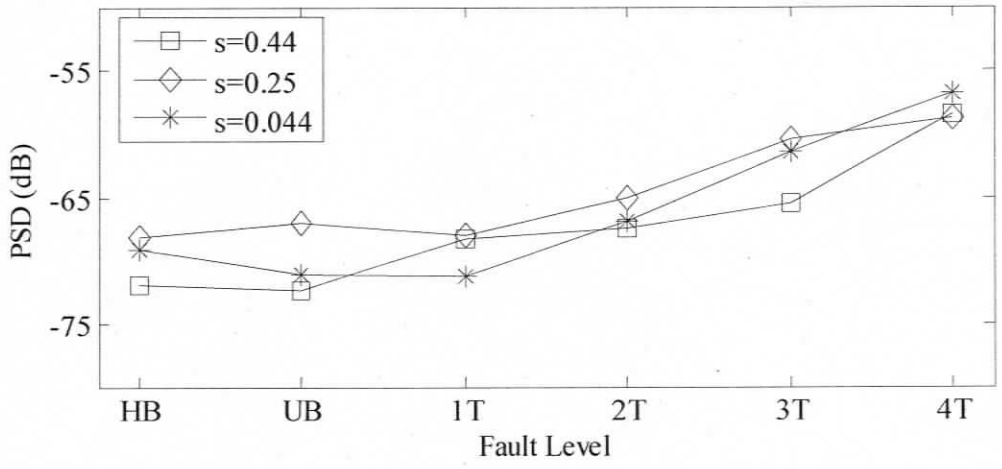

Figure 3.10 Variation of fault spectra under half load and various fault and slip conditions (TableB.3)

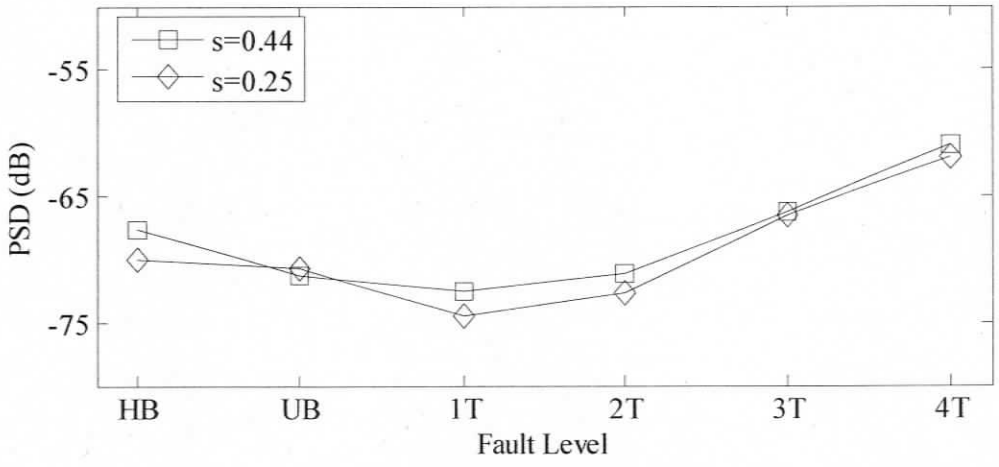

Figure 3.11 Variation of fault spectra under full load and various fault and slip conditions (Table B.4)

3.5 Comparison of PSD of Rotor Phase-u current with Vector sum of Rotor-Phase u, v, w currents

Further analysis was conducted to verify if PSD of vector sum of rotor-phase currents I_u, I_v, I_w can show better resolution in increase of the fault frequency component power level from the results obtained by PSD of phase current I_u described in Section 3.4. To compute the PSD of the vector sum of three rotor phase currents, complex PSD was used. Figure 3.12 shows the comparison of frequency spectrum of phase-current I_u with spectrum of current vector for $s = 0.25$ and full-load condition under a 4-turn fault.

The positive frequency components shown in Figure 3.12(b) does not show any indication of rise in the power level of fault frequency component at 127.5Hz, but it is visible in the power of the negative frequency component shown in Figure 3.12(c), which is measured as -59.74 dB. The PSD of the rotor phase current shows the power level of fault frequency component, measured to be -61.97dB which is comparatively less than power level of fault frequency observable by PSD of vector sums of rotor current. Figure 3.13 shows the relative increase of the power level for the fault frequency obtained from PSD of imaginary component of vector sum of three phase currents. Comparing this plot result with Figure 3.11 which shows increase of power level for fault frequency components obtained from PSD of phase current I_u, it is clear that spectral analysis of current vector seems to provide better indication of fault frequency component power increase compared to spectral analysis of phase-current, without any offset elimination required, as observed in [29].

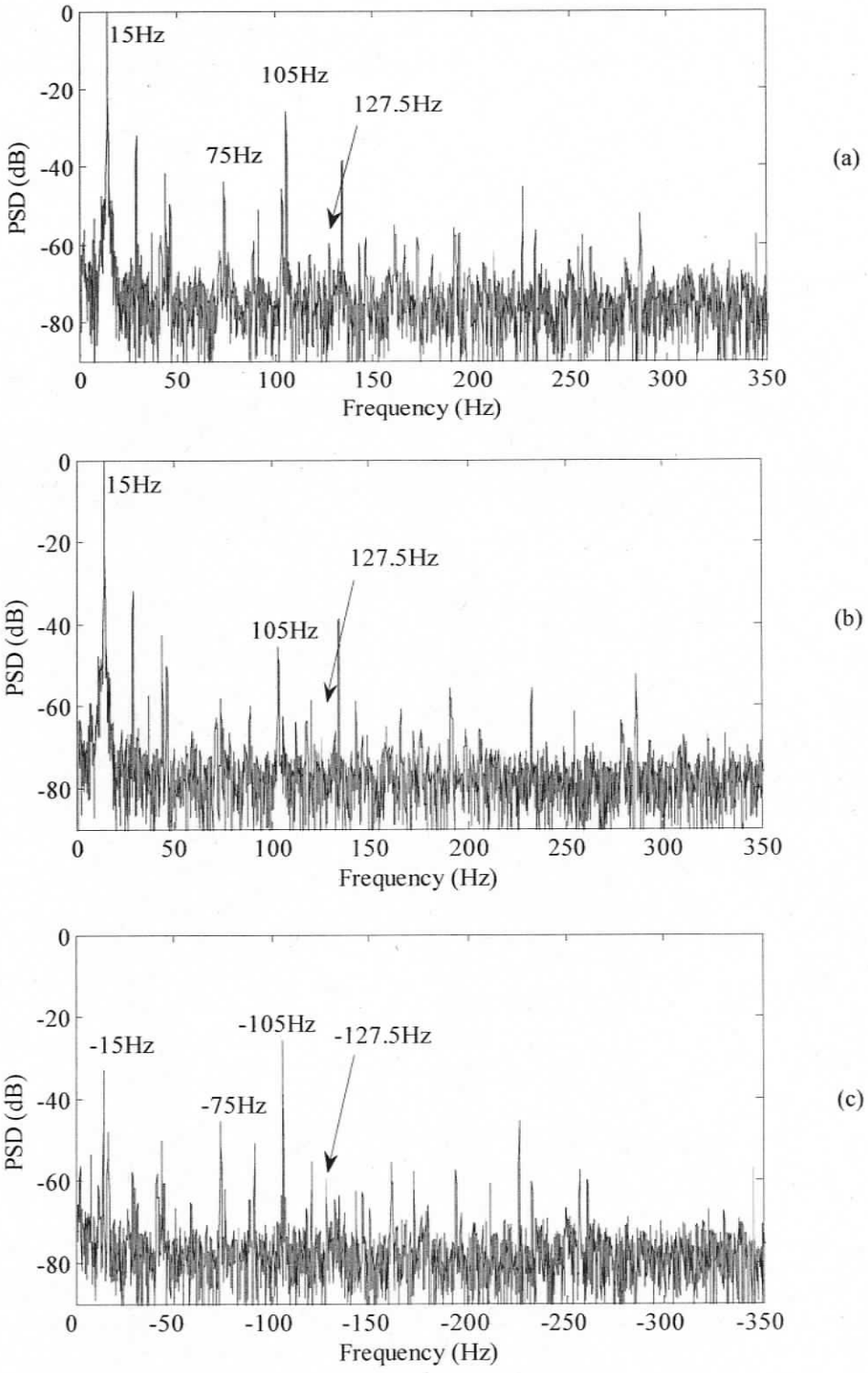

Figure 3.12 Comparison of PSD for rotor current of phase-u and current vector of three rotor phase currents when DFIG is operating at full-load and slip = 0.25 a) PSD of rotor curent of phase-a, b) PSD of current vector of three phases currents, positive frequency components, c) PSD of current vector of three phase currents, negative frequency components

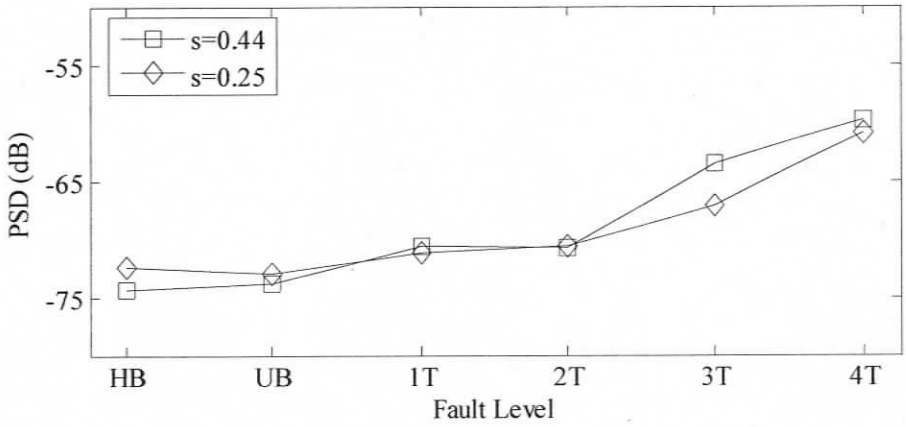

Figure 3.13 Variation of PSD of fault frequency obtained from complex PSD of rotor current vector under full-load and various fault and slip conditions (Table B.5)

3.6 Comparison of Search Coil Voltage PSD under Different Operating Conditions

To further validate the theory and simulation results, experiments were also conducted by analyzing the voltage induced in the rotor-mounted search coil. The search coil is wound on the rotor slots in which the voltage is induced due to the air-gap flux. The effect of any abnormality in this flux as a result of disturbance of flux linkage due to inter-turn fault is distinctly visible in frequency spectrum of search coil voltage. This is demonstrated in Figure 3.14, 3.15 and 3.16.

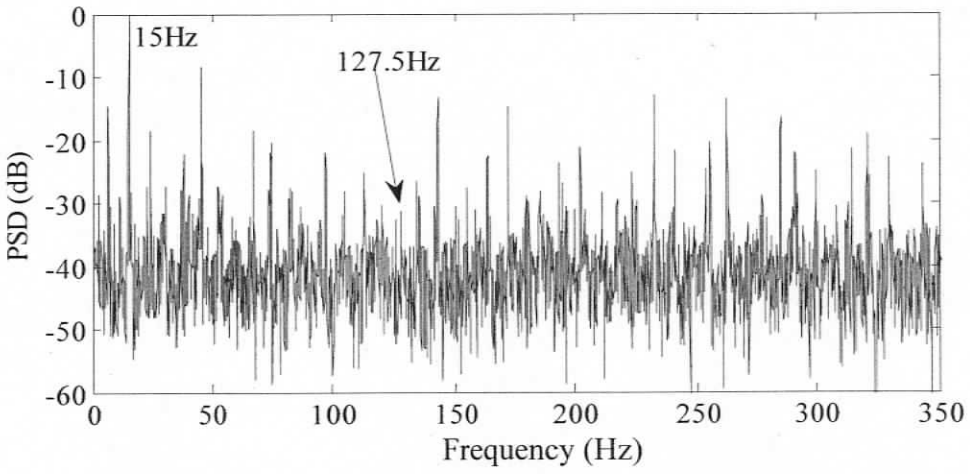

Figure 3.14 Spectrum of rotor search coil voltage under healthy operating condition at full-load, s = 0.25

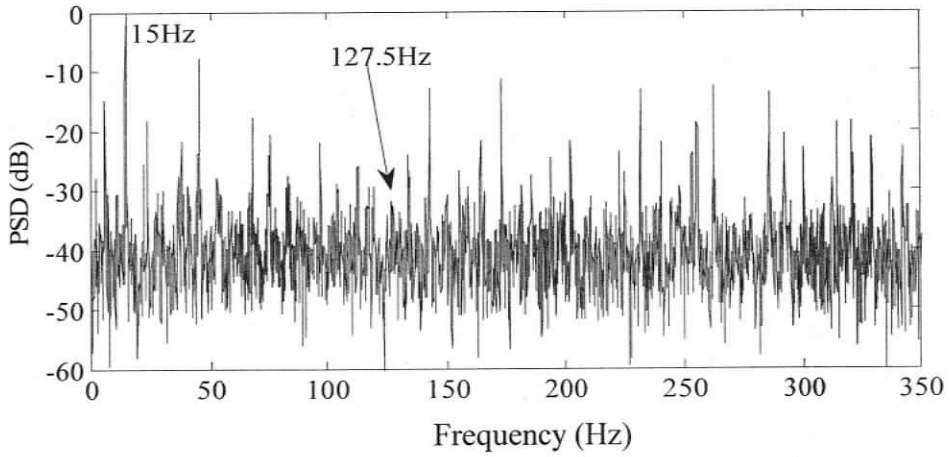

Figure 3.15 Spectrum of rotor search coil voltage under unbalance operating condition at full-load, s=0.25

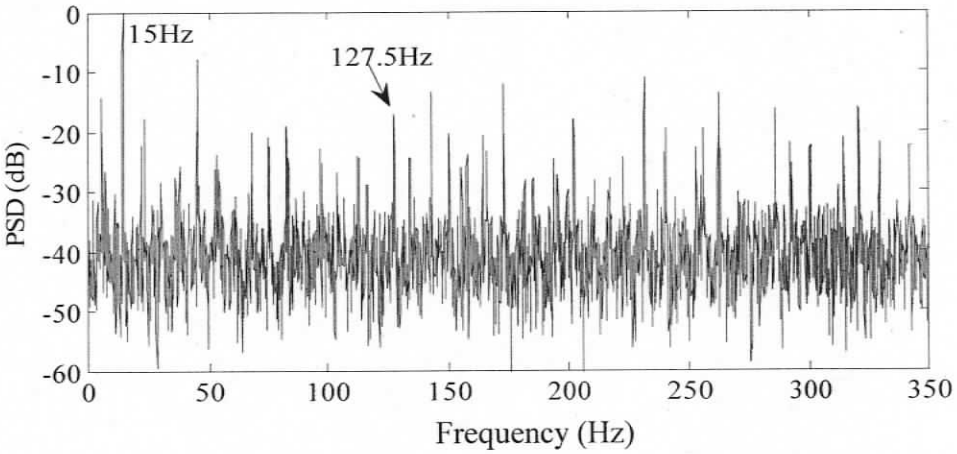

Figure 3.16 Spectrum of rotor search coil voltage under 4-turn fault operating condition at full-load, s = 0.25

The rise in the power of fault frequency component being monitored for various operating slip, load and fault condition is graphically presented in Figures 3.17, 3.18 and 3.19. From the plots it is very clear that 2-turn faults can be detected under all the test operating conditions. Even a 1-turn fault is detectable under some of the conditions. Comparing these results with results from spectrum of rotor phase current shows that the magnitude of the power rise of fault frequency components under inter-turn faults when observed in spectrum of search coil voltage is more distinct. Hence using search coil voltage to detect inter-turn faults seems to be more reliable method.

The use of search coil voltage measurements is invasive since it requires an extra winding to be wound on the rotor. Moreover slip rings with brushes are required to

acquire the voltage signal. However, this method appears to be more promising compared to monitoring the frequency spectrum of any other rotor circuit parameter. Also, by applying a least-square approximation technique, the effect due to loading of the generator is compensated for allowing even unambiguous single-turn fault detection [29].

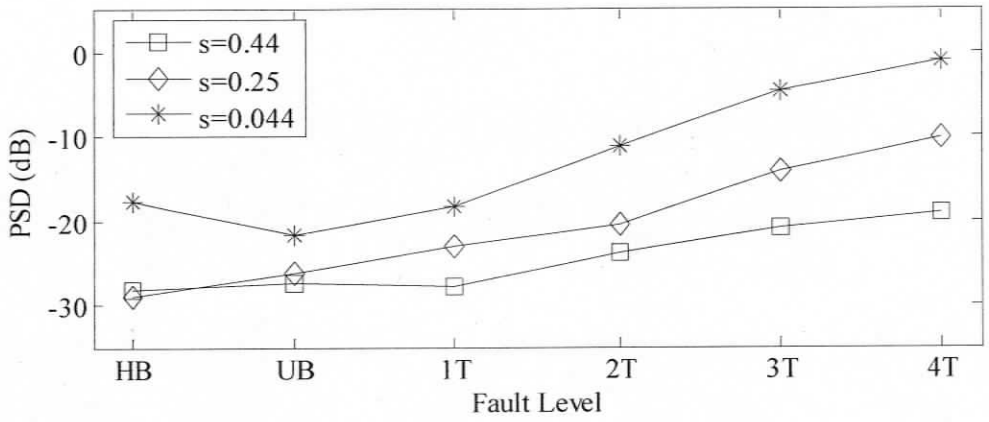

Figure 3.17 Variation of fault spectra obtained from search coil voltage signal, under no-load and various fault and slip conditions (Table B.6)

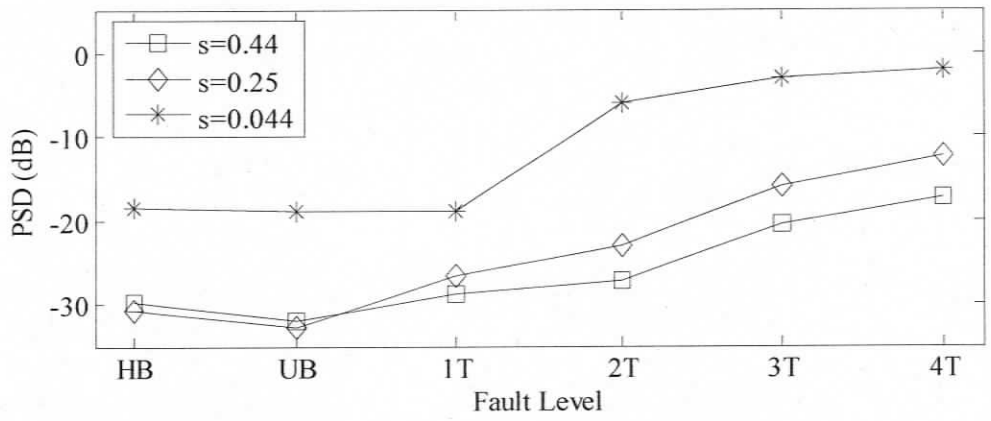

Figure 3.18 Variation of fault spectra obtained from search coil voltage signal, under half-load and various fault and slip conditions (Table B.7)

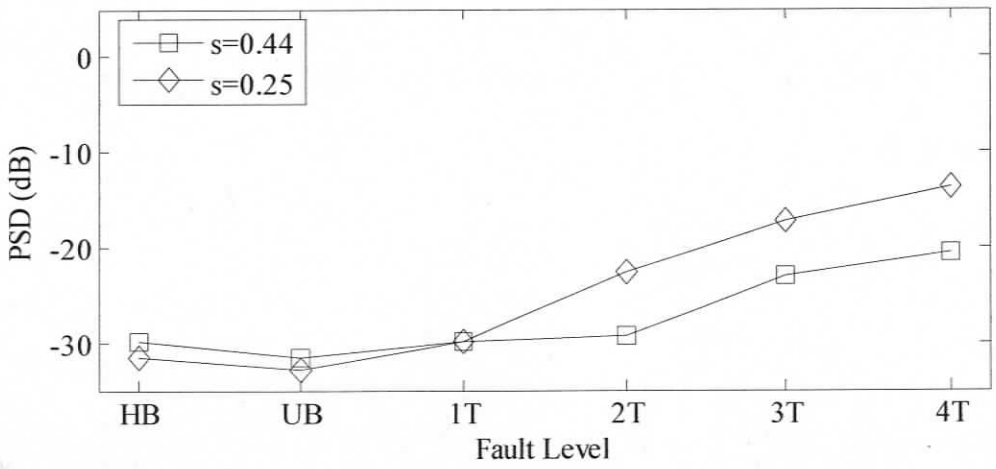

Figure 3.19 Variation of fault spectra obtained from search coil voltage signal, under full-load and various fault and slip conditions (Table B.8)

3.7 Signal to Noise Ration (SNR) comparison for various signals to detect fault.

From the experiment results it can be observed that, spectral analysis of all three signals; rotor phase current, rotor current vector and search-coil voltage show a rise in the power level of fault frequency component. However, the signal which will provide the best fault detection depends on SNR. Higher the SNR, better is the resolution of the fault signature. Table 3.1 describes the SNR for the three signal types under different slip conditions for various fault severity and full-load condition. The SNR values are obtained by calculating the difference in power level (in dB scale) between 4T and HB conditions from the experimental results tabulated in Appendix-B. This is equivalent to the ratio of signal to noise power in linear scale. From Table 3.1 it can be observed that SNR ratio for search-coil voltage is comparable to the SNR for fault frequency component obtained from rotor current vector. Both these signals have a much higher SNR compared to the rotor phase current signal. However it is computationally much simpler to work with the search-coil voltage signal compared to rotor current vector. Hence in the subsequent prototype development, search-coil voltage signal is used as a proof of principle for fault detection.

Table 3.1 Comparison of Signal to Noise Ratio for fault frequency component power level observed in search-coil voltage, rotor phase current and rotor current vector signals for different severity of fault under full-load condition at slip = 0.25 and slip = 0.44

Slip	0.25	0.25	0.25	0.25	0.44	0.44	0.44	0.44
No. of turn fault	1T	2T	3T	4T	1T	2T	3T	4T
Search-coil voltage	1.73	9.05	14.5	18.02	0.03	0.52	6.92	9.29
Rotor phase current	-4.47	-2.68	3.46	8.07	-4.93	-3.59	1.29	6.58
Rotor current vector	3.81	3.70	10.92	14.70	1.18	1.75	5.28	11.52

Chapter 4

DSP-based Online Stator Inter-turn Fault Detection System for DFIG

In this chapter, the prototype implementation of the proposed fault detection technique is presented and various practical implications of realizing it in the field are discussed. Through tests, it is proved that the fault detection system has the sensitivity and speed to detect the faults involving even one shorted turn within 2 seconds on average.

Rapid advancement of semiconductor technology and availability of digital signal processors (DSP) with micro-controller features has opened a new horizon in the area of electric drives. The recent trend has been to add fault diagnostic capability to drives [55]. Some researchers have attempted to use the computational capabilities of these processors to implement the fault diagnosis of machines. Hence, in this chapter, a scheme is proposed to detect stator inter-turn faults in a DFIG operating at sub-synchronous speeds using a DSP. An algorithm is presented that performs a Discrete Fourier Transform (DFT) using a DSP to monitor a particular harmonic component in the rotor search coil voltage while the rotor voltage frequency changes in the variable speed operation of the DFIG. Also, all the necessary hardware has been built to generate a trip signal and disconnect the machine in the event of a fault. Such a fault detector plays a very vital role in preventing fire hazards, explosion and potential loss of property and human life which is more important than saving the machine itself [19, 30].

4.1 Scheme of Online-Fault Diagnosis

A novel technique is used in order to avoid the long computation time involved with DFT. This method is very useful since the DSP has a limited memory and the processor operates in a time-shared mode. A schematic block-diagram of the fault detection scheme is shown below in Figure 4.1.

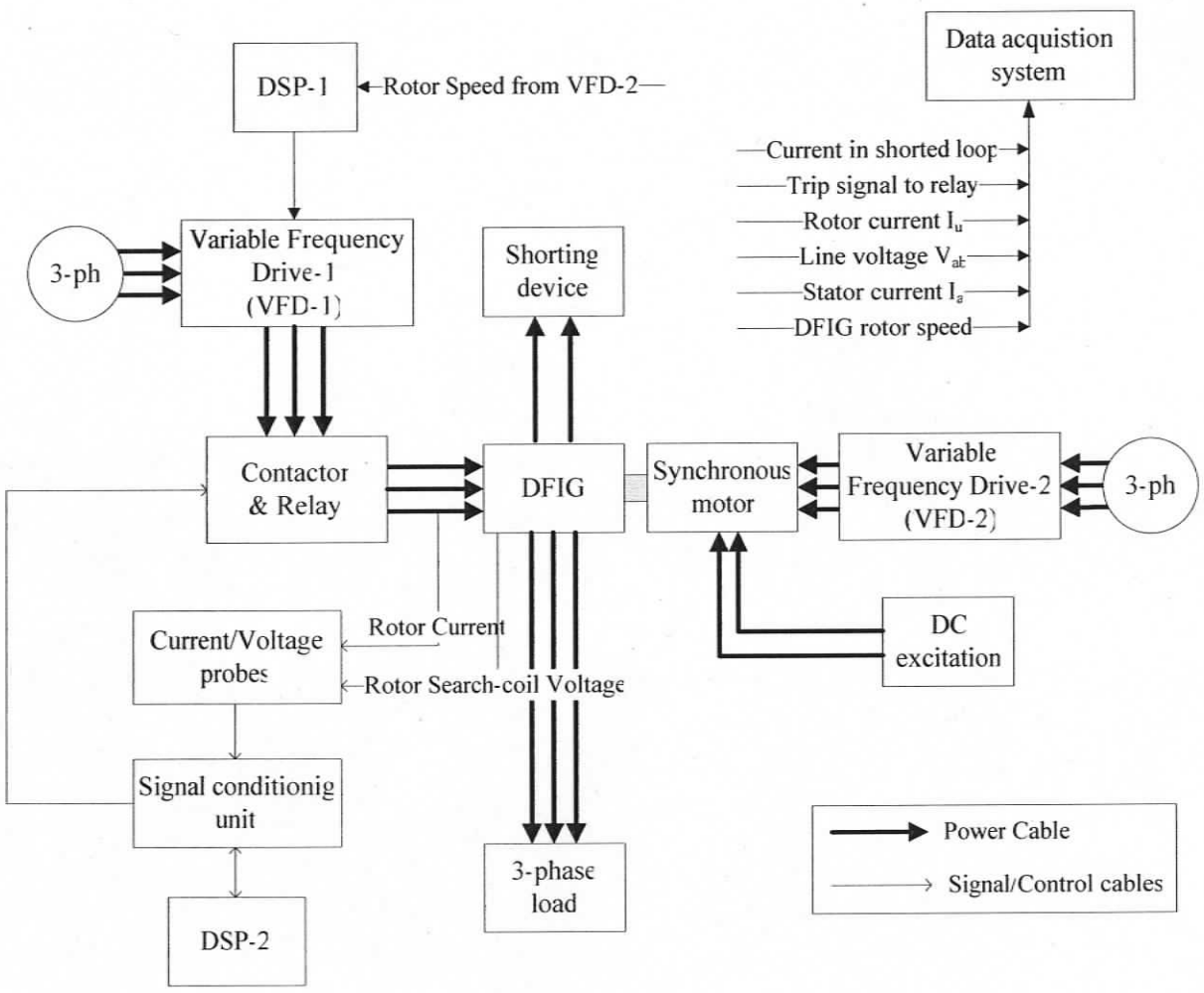

Figure 4.1 Schematic diagram of the fault detection scheme.

The purpose of DIFG, Synchronous motor, VFD-2, DC excitation, VFD-1, shorting device and data-acquisition unit is the same as explained in section 3.1. However the control of the rotor frequency is done by sensing speed. VFD-2 generates a voltage signal proportional to the speed of the Synchronous motor which is used by DSP-1 to adjust the slip frequency of the rotor voltage fed by VFD-1 to the rotor of DFIG. The search coil voltage signal is used for fault diagnosis in the proposed scheme. The on-line fault diagnosis system consists of three units; DSP-2, a signal conditioning unit and a contactor and relay assembly. The signal conditioning block contains three circuits with different purpose:

1) To add DC offset and change gain of the search coil voltage signal.

2) A zero-crossing detector (ZCD) circuit that generates pulses corresponding to frequency of rotor current.

3) An electronic relay driving circuit powering the relay that energizes the coil of normally closed contactor.

Signals from search coil voltage and rotor current are connected to the input of the on-board Analog to Digital Converter (ADC) of DSP-2 while the event manager module on the DSP-2 generates the trip signal for the tripping circuit. A detailed explanation of how DSP-2 uses these signals is explained in section 4.2.2. When a fault is detected, DSP-2 generates a trip signal which is used by the electronic relay driving circuit to open the normally closed contactor and cut-off power fed to the rotor of DFIG. Two separate DSPs have been used in presented scheme, to simplify the experiments. However the same computations can be performed by a single DSP. Three configurations of 3-phase load have been used, purely resistive, inductive and capacitive load (both 0.8 pf). The data acquisition system is used to capture the signals that relate to the operating condition of the system at the time of fault detection. The following section gives a detailed functional description of the scheme.

4.2 Hardware Setup and DSP logic

4.2.1 Circuits of Signal Conditioning Block

Either the rotor current or rotor search coil voltage can be used for fault detection. However search coil voltage is used in the presented scheme to prove sensitivity of the system to detect 1-turn fault. The signals from the current sensors connected to the rotor circuit or voltage sensors connected to the search coil voltage cannot be fed directly to the DSP. These signals are in range of +/-5V ac and need conditioning for gain and dc offset before they can be fed to the on-board ADC of the DSP which accepts 0-+3.3V dc. Figure 4.2 shows the schematic of the signal conditioning unit. Achieving high Signal to

Noise Ratio (SNR) and negligible distortion after amplification/attenuation and adding dc offset are very important for the DSP to function properly.

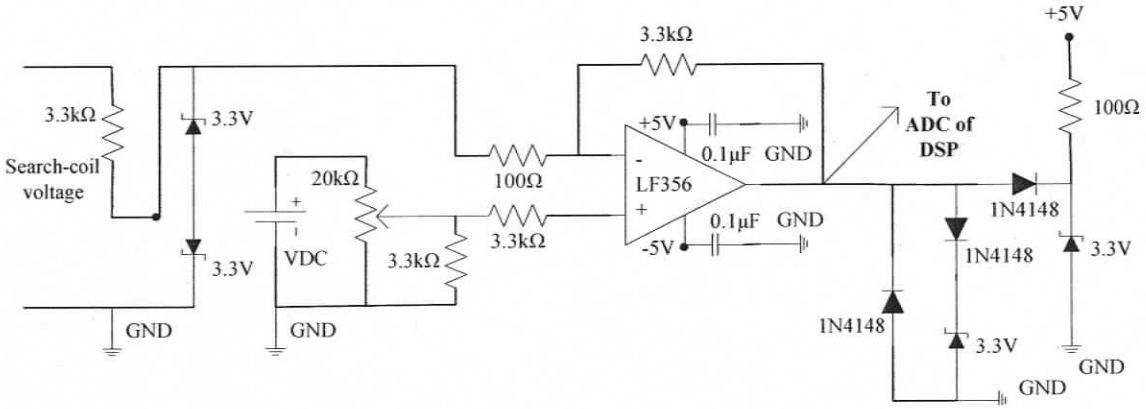

Figure 4.2 Circuit to DC offset and change gain of fault detecting signal

To measure the slip from frequency of rotor current, a ZCD circuit as shown in Figure 4.3 is used. The circuit generates a pulse of time period proportional to the positive cycle of rotor current. These pulses are fed to DSP-2 for calculating the time period and computation of the rotor current frequency and slip.

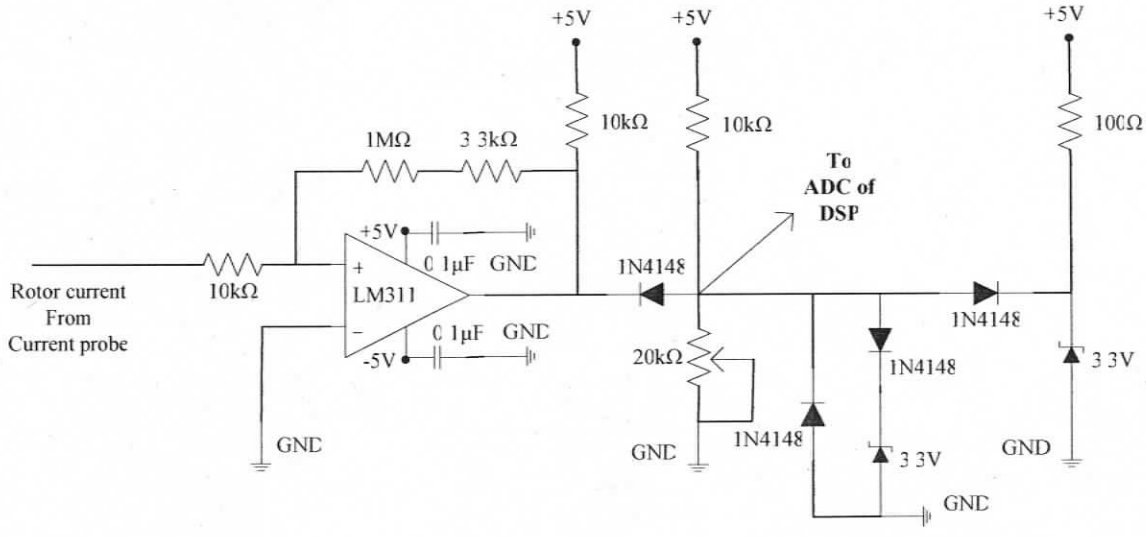

Figure 4.3 Circuit to detect slip frequency of DFIG using the rotor current signal.

Figure 4.4 shows the schematic for the circuit used to operate the relay in response to the trip signal from the DSP-2. The output of DSP is a maximum 3.3V signal that does not have the power to drive the relay for tripping the contactor. Hence a simple comparator-transistor circuit is used to amplify the signal. The contactor is required to be normally closed to allow power flow from VFD-1 to DFIG. When a fault is detected, DSP-2 drops the voltage from 3.3 to 0. This opens the contactor and cuts off the power to the rotor of DFIG.

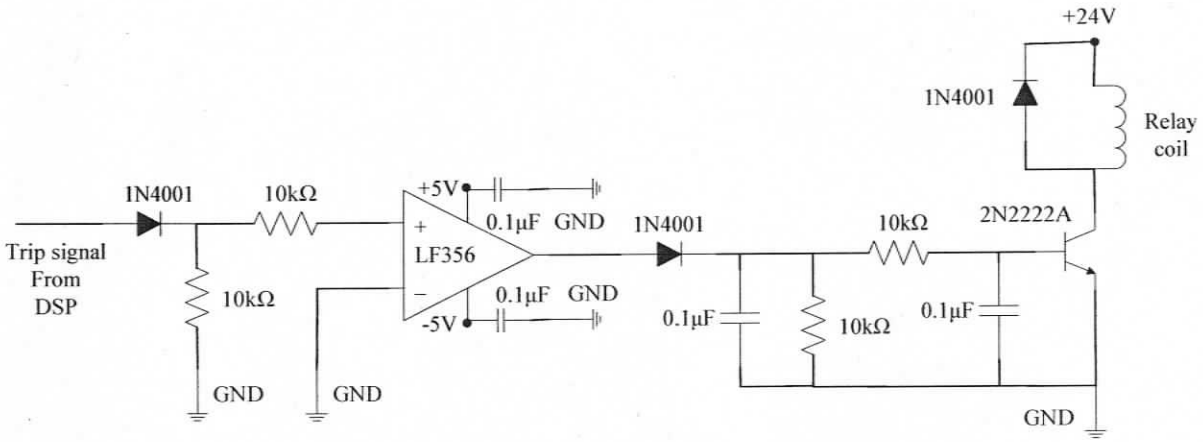

Figure 4.4 Circuit to operate relay using trip signal.

4.2.2 DSP-2 Online Fault Detection program

The flowchart of the program on DSP-2 that computes fault level from the signal being monitored is shown in Figure 4.5. The DSP-2 uses pulses from the ZCD circuit to calculate the fundamental frequency of the rotor current to derive the slip frequency and hence slip, since the stator frequency is constant at 60Hz. Based on the slip of the generator, the corresponding fault frequency is computed using (2.7) for k=3. Based on the slip frequency and fault frequency, the sampling frequency is selected such that it is a multiple of slip frequency and at least 10 times the fault frequency. Setting the sampling frequency in this manner has shown to give better results in the resolution of power level of fault frequency component. Samples of the search coil voltage are

collected for a one second interval and a Discrete Fourier Transform (DFT) is computed simultaneously with each sample acquired by ADC of DSP-2 both for the slip frequency and fault frequency bin. After the data block is sampled and processed using DFT, the fault frequency component power is normalized with respect to the slip frequency component power. Based on a table corresponding to the slip range and load range similar to Table B.6 or B.7 or B.8 (Appendix-B), the power level of fault frequency component is compared to the healthy balanced case. Any rise over this threshold value is considered a fault and a trip signal is generated to trigger the relay device which disables power to the rotor circuit of DFIG.

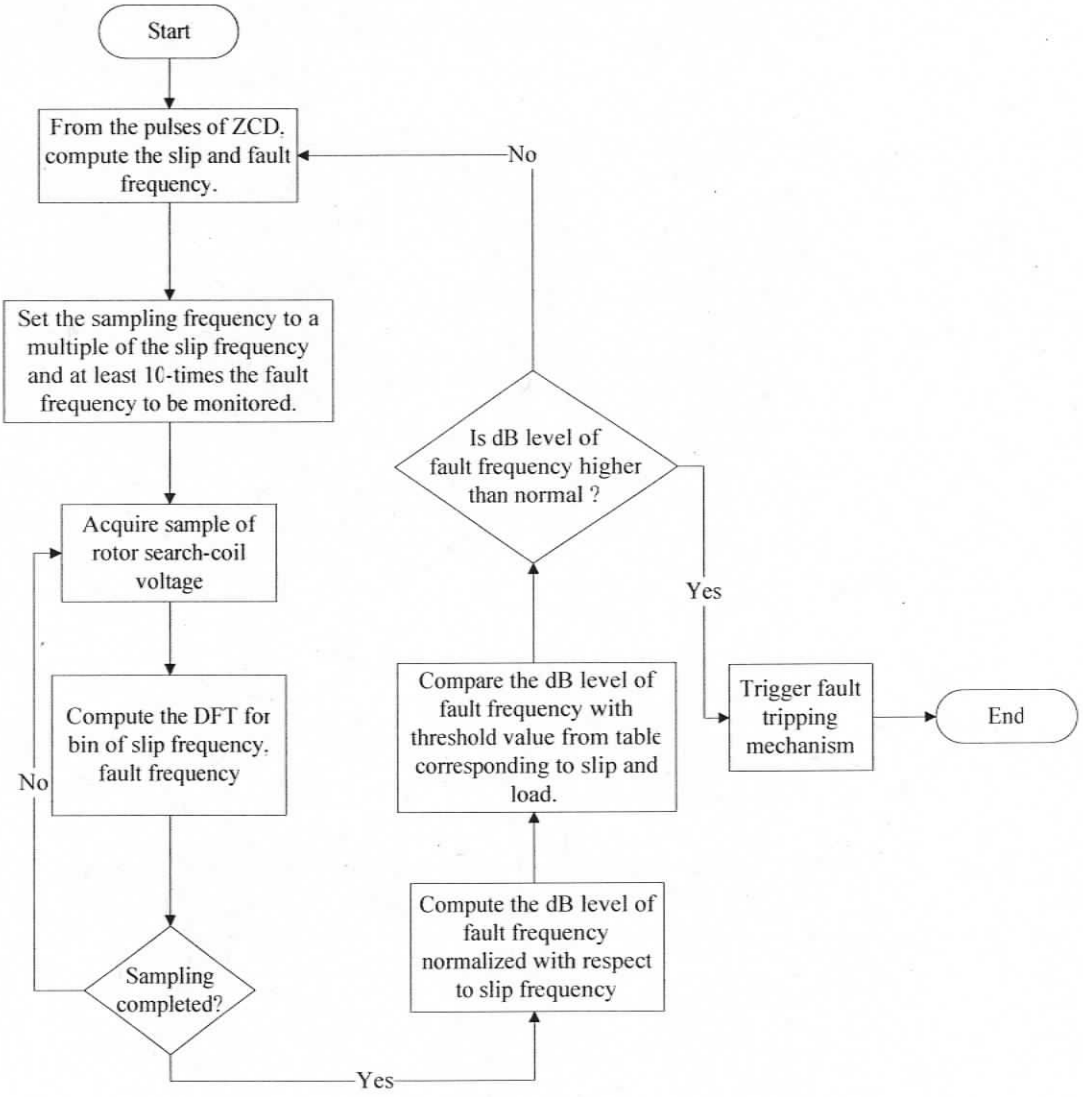

Figure 4.5 DSP-2 fault detection logic

4.3 Performance of the DSP-based Fault Detection Scheme

The performance of the fault detection scheme has been tested in the case of DFIG operating at s = 0.25, different load conditions and varying severity of fault. The DSP-based fault detection scheme detects the stator inter-turn faults and disconnects the machine from the service in a time period of less than 2 seconds on the average. The typical time of operation of the DSP-based fault detection scheme under different number of shorted turns (1T-4T) is shown for three different load levels in Figure 4.6. The variation in fault clearance time is due to the relative difference in rise of the power level of fault frequency component for varying fault severity.

The plots from Figure 4.7 to Figure 4.12 have been obtained using the data acquisition system described in Chapter 3. Various signals (line voltage, rotor phase currents, trip signal and the current in shorted loop) in each case have been shown for a 2-turn fault. The current in the shorted loop rises from zero at the instant of initiation of the fault. After detecting the fault, the trip signal is held low by the DSP-2 that opens the contactor and disconnects the rotor phases of the machine from VFD-1. In order to thoroughly validate the scheme, tests have been conducted at different operating conditions of DFIG. Figure 4.7, 4.8 and 4.9 show the average case, best case and worst case scenario respectively for tripping a 2-turn fault when DFIG is operating at slip = 0.25 and half-load (purely resistive). The variation is due to the randomness of the overlap between the fault duration and sampling duration. The diagnostic tool has been repeatedly tested under no-load, half-load and full-load condition. The maximum time taken to generate a trip signal under any severity of fault was found to be 2.01 seconds which was for a single-turn fault at full-load. Also, the performance of the fault detection system was tested for inductive and capacitive load with a power factor of 0.8 and found to satisfactorily detect a 2-turn fault. Figure 4.10, 4.11 show the best case results of test for 2-turn fault detection under capacitive and inductive load respectively. The diagnostic tool could successfully trip the machine for ten out of ten times in the event of 2-turn fault. Figure 4.12 shows various signals of fault detection, when the

DFIG is operated over a speed variation from 1250 rpm to 1550 rpm and 2-turn fault is induced. It is also to be noted that some of signals (in particular the 60Hz ones) in Figures 4.7-4.12 are compressed to fit the frame size. This gives and impression of under-sampling which is not the case as all the signals were sampled at the rate of 3600 Hz.

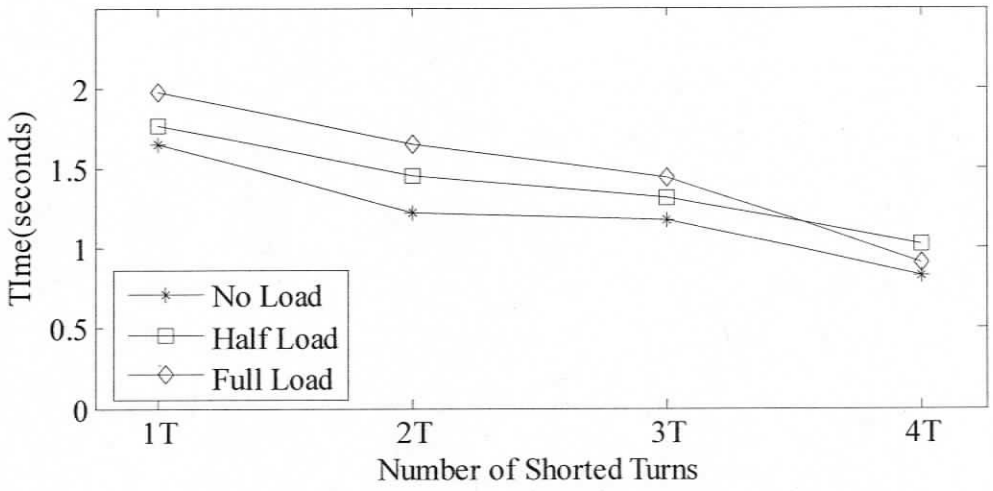

Figure 4.6 Typical time of operation of the DSP-based fault detection scheme when using search coil voltage signature analysis and DFIG operating at slip = 0.25 at different loads

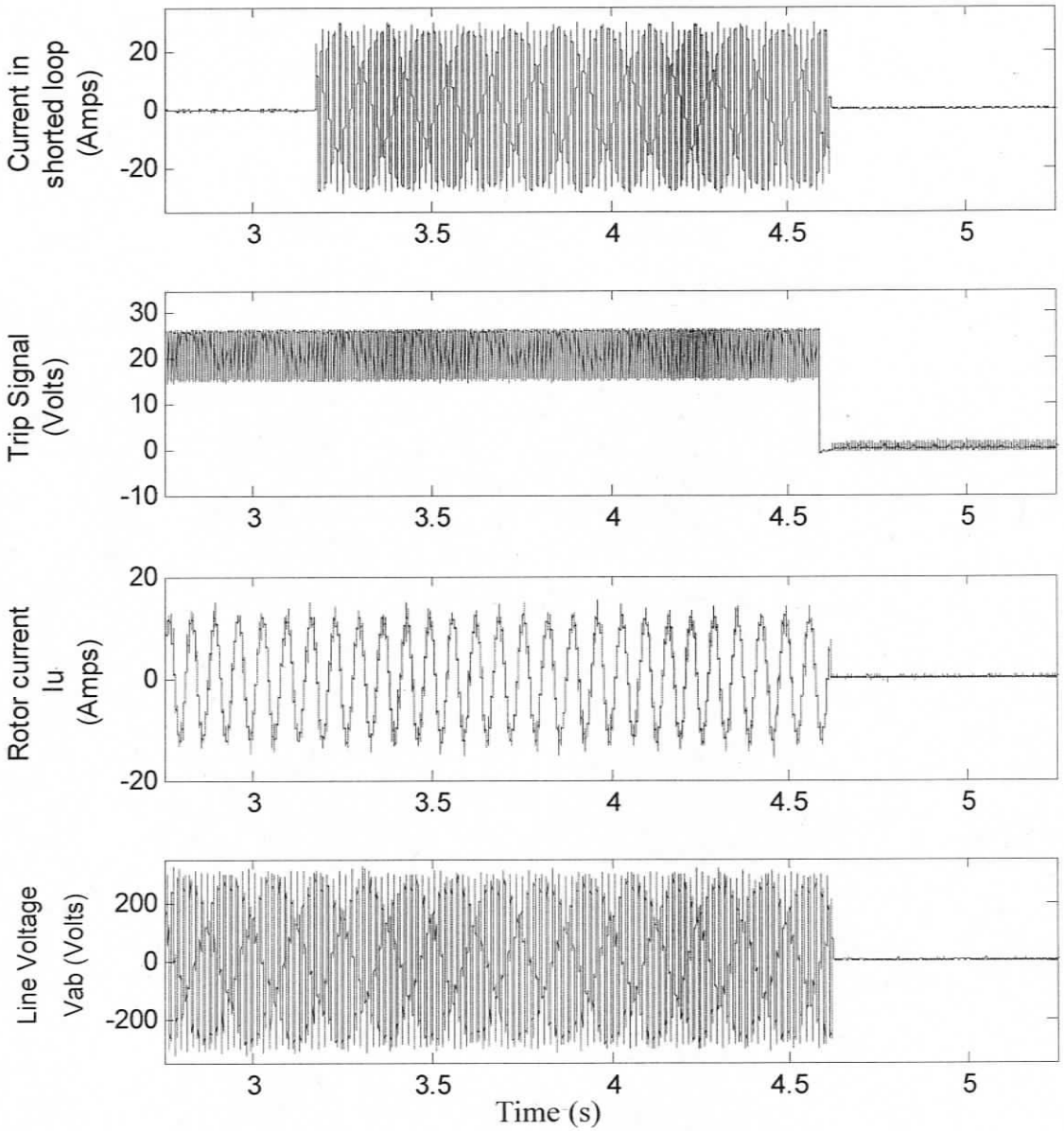

Figure 4.7 Various signals of the fault detection scheme, DFIG operating at half-load, slip = 0.25, fault severity is 2-turn, fault detection time is 1400 msec

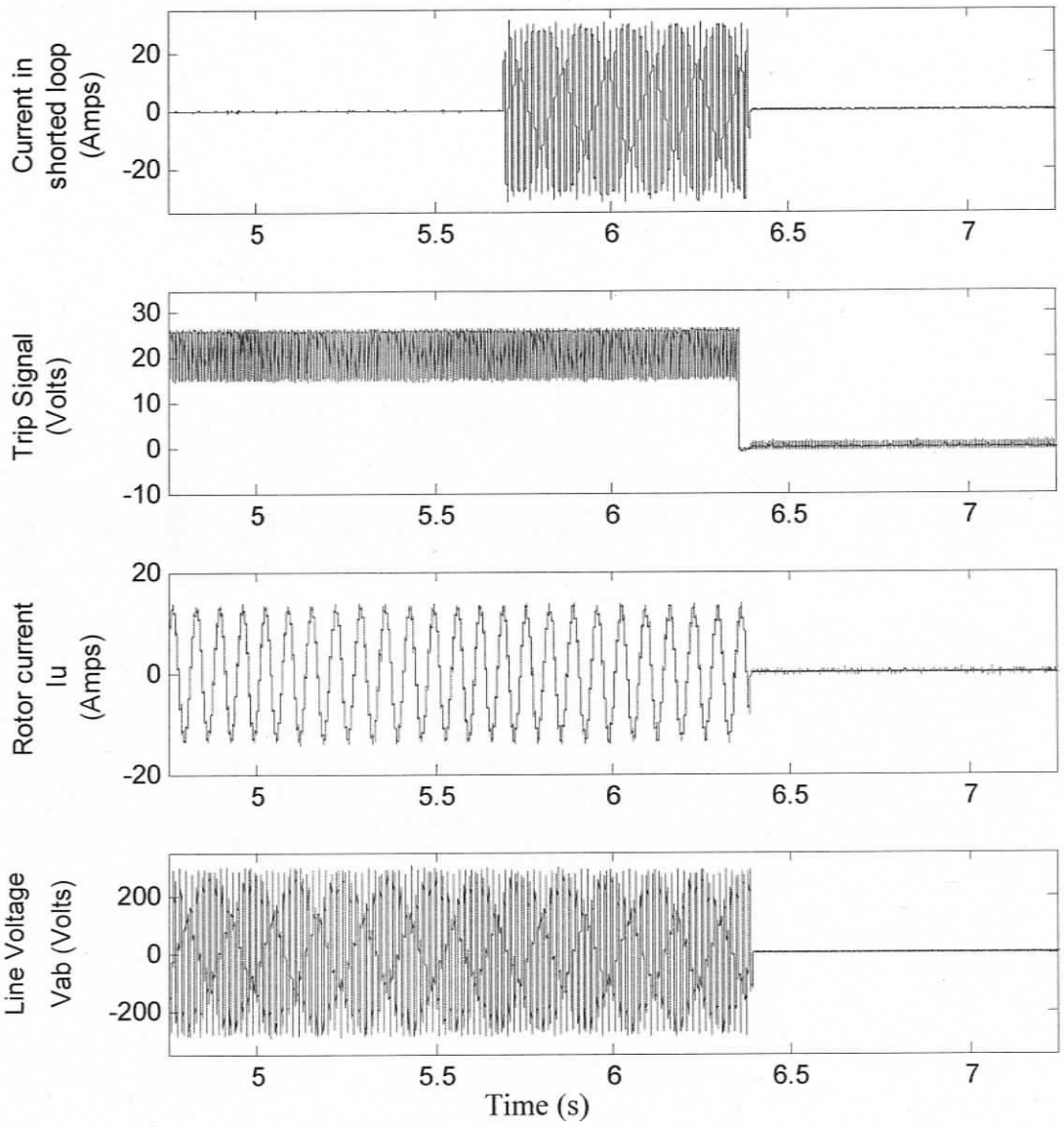

Figure 4.8 Various signals of the fault detection scheme, DFIG operating at half-load, slip = 0.25, fault severity is 2-turn, fault detection time is 700 msec

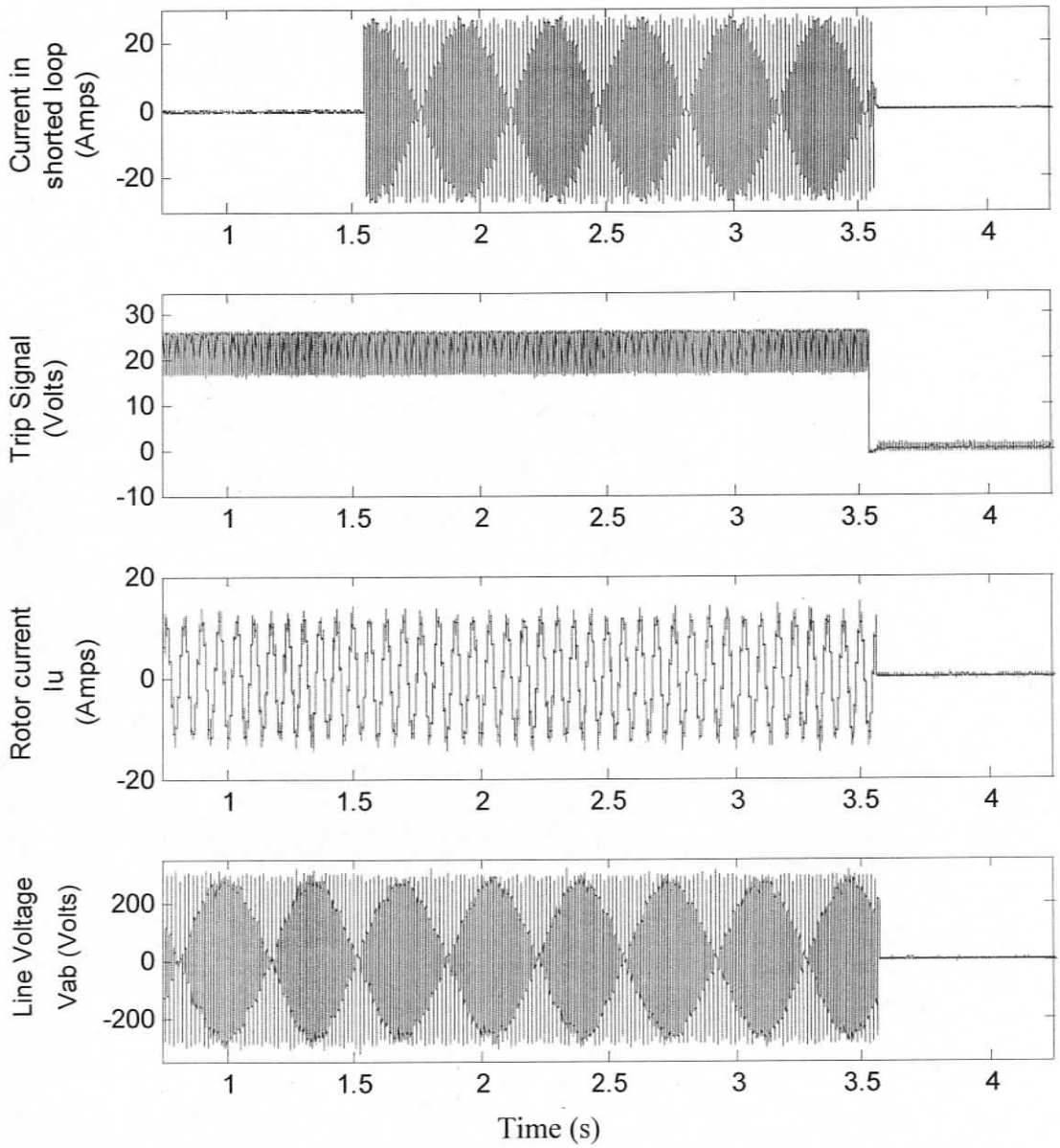

Figure 4.9 Various signals of the fault detection scheme, DFIG operating at half-load, slip = 0.25, fault severity is 2-turn, fault detection time is 2000 msec

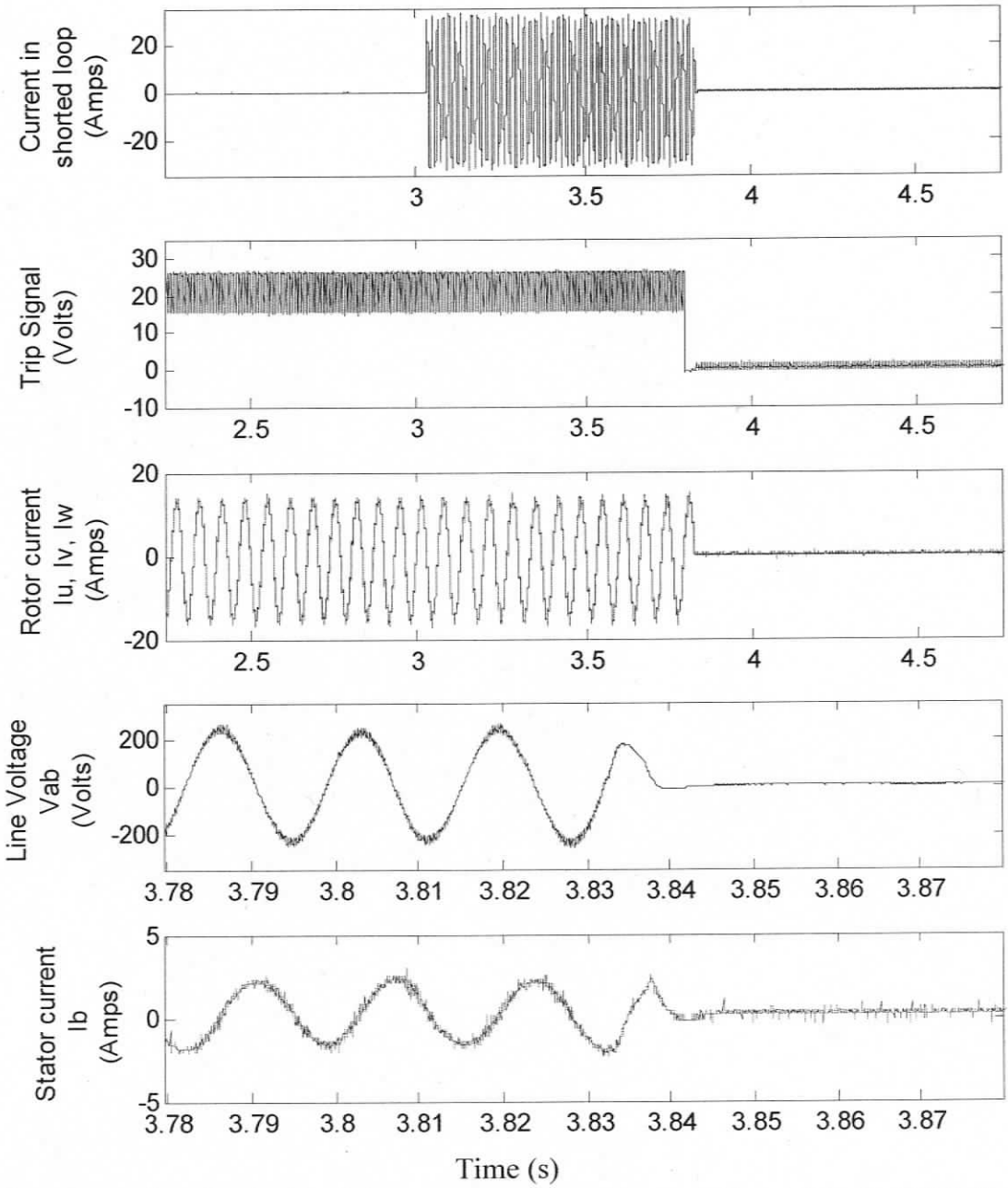

Figure 4.10 Various signals of the fault detection scheme, DFIG connected to an RC load of 0.8pf, slip = 0.25, fault severity is 2-turn, fault detection time is 700 msec.

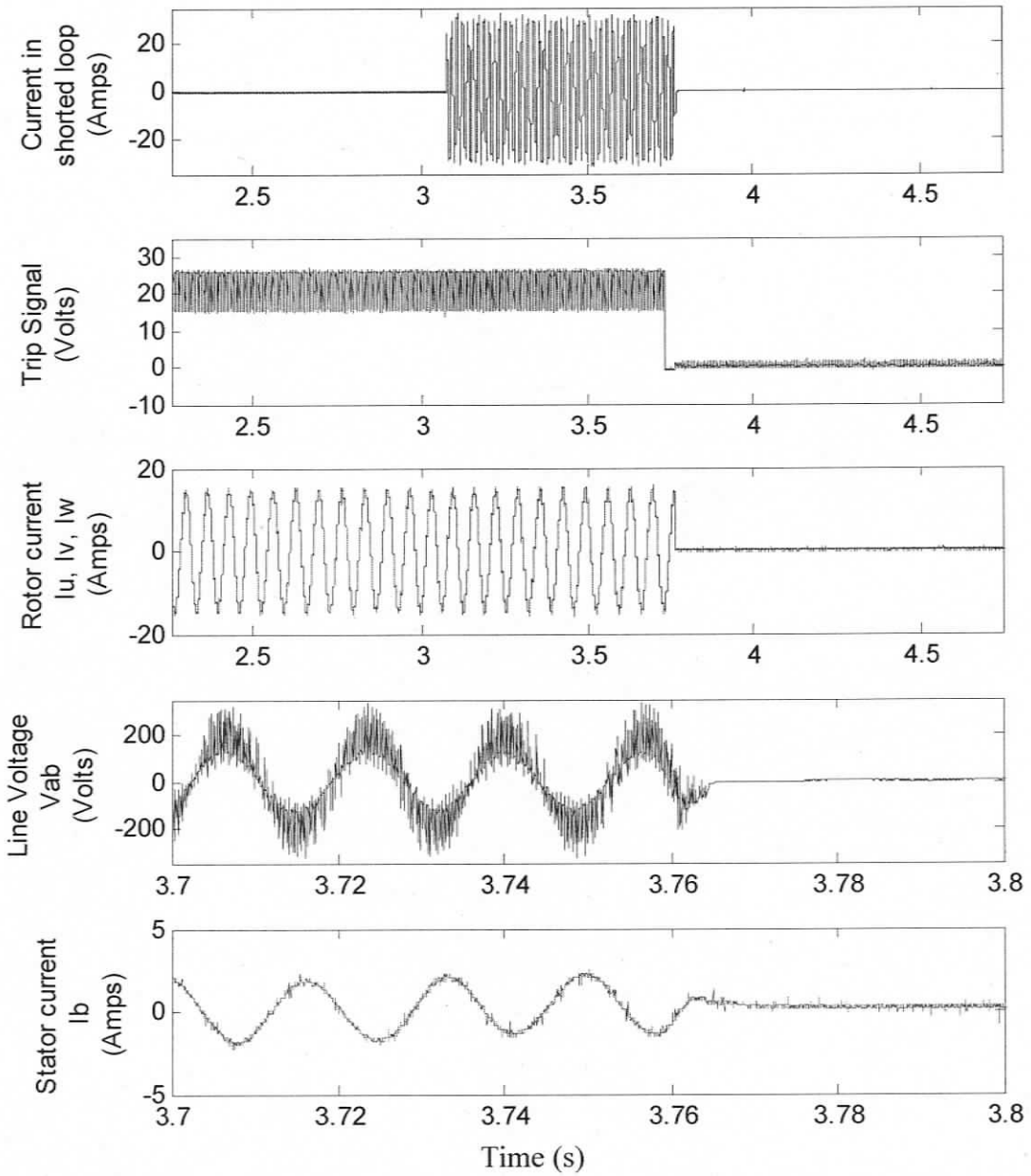

Figure 4.11 Various signals of the fault detection scheme, DFIG connected to an RL load of 0.8pf, slip = 0.25, fault severity is 2-turn, fault detection time is 700 msec.

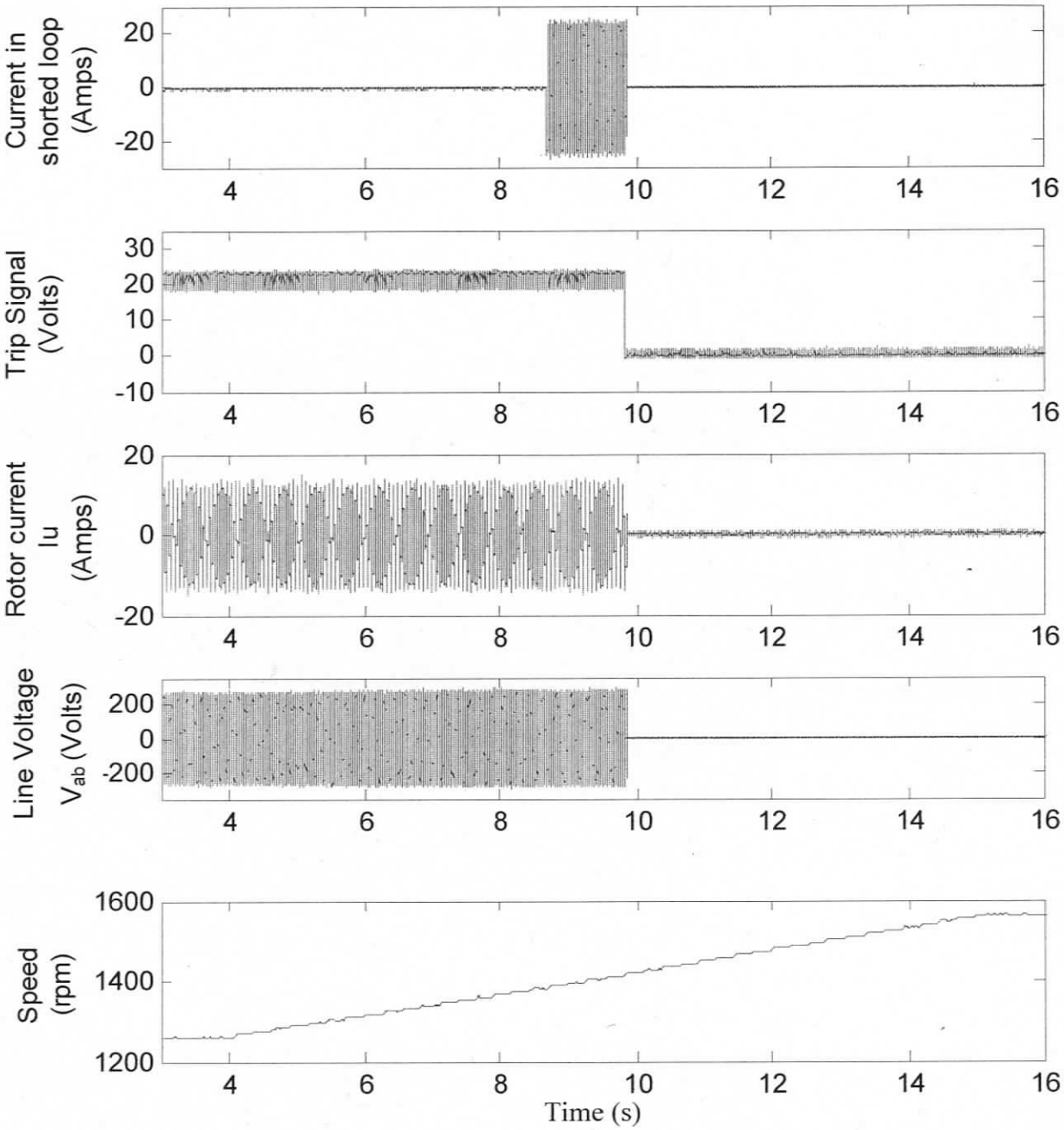

Figure 4.12 Various signals of the fault detection scheme, DFIG operating at half-load during a speed change, fault severity is 2-turn, fault detection time is 1300 msec.

4.4 Discussions on Results and Feasibility of industrial Implementation

As discussed in Section 1.2, an online fault diagnosis or condition monitoring system renders several benefits. However, the installation of such system is likely to be considered only when the benefits from fault detection at incipient stage or condition monitoring of the generator is more than the cost of implementing and maintaining that system or if safety issues are a major concern.

This chapter describes a fast and effective instrument to detect stator inter-turn faults in the DFIG. Predicted harmonic components in the rotor search coil voltage have been shown to work very well for detecting these faults using a DSP. With this instrument, the harmonic components are tracked even under changing speed condition in the case of variable speed generators.

In industry, there are several challenges to meet before the fault-diagnostic system can be implemented. There are serious concerns relating to:

- Unambiguous fault detection
- Scalability and generality of the system
- Repeatability
- Cost of implementation
- Response time

Amongst the above five factors, scalability and generality are of crucial importance. Since, any fault diagnostic technique is based on continuous monitoring of a signal and detecting deviation from a preset value, finding the ideal preset value is very important. The procedure required to find this series of preset values for varying operating conditions could greatly vary based on the Fault Diagnostic System (FDS). In the present case, the FDS requires the collection of fault frequency component power level at different load conditions and slip. This could be challenging; the preset-value

table will have to be created based on the generator rating; the type of sensors used in the system and the operating range. This can be done during the commissioning process of the DFIG, which is analogous to the process followed in industry these days while commissioning high power motor drives, like an identification (ID) run conducted on all ABB drives using DriveWindow [56]. The purpose of such application software is to collect machine parameter values such as inductances and resistances of stator and rotor, moment of inertia, which could be used to tune the control system and achieve optimum efficiency and performance.

Cost of implementing an FDS in an existing system would be far more than implementing it in a new system. This is because an operational system will have to go for an upgrade and a temporary shutdown is required to collect machine dependent data for the FDS. Also, most existing system do not have search coils wound on the rotor of the DFIG machine. Hence, addressing the repeatability and unambiguous fault detection is compromised to a certain degree if rotor current is used. However in case of new systems, to implement the proposed FDS, would have a relatively small cost since all the preset-value data can be collected during commissioning and ID run process. Search coils can be wound around the rotor for a DFIG machine. The cost of FDS would constitute cost incurred due to the addition of the search coils on rotor, the cost of the additional DSP (if required) to perform fault computations, the cost of electronics for signal conditioning and tripping in the event of a fault. For installations with power level 500KW to 2MW, the cost of such a FDS is expected to be less than 0.5% of the total cost of wind power energy conversion system's installation. The benefit of reducing the downtime in the event of a fault and other safety issues can further prove its viability [7, 57, 58].

Chapter 5

Conclusion and Future Scope

5.1 Conclusion

In this work, the condition monitoring of DFIG machines is addressed for stator inter-turn faults. A feasibility study for unambiguous detection of stator inter-turn faults in DFIG is conducted by analyzing rotor phase currents and search coil voltage under varying operating conditions of speed and load. To justify the proposed diagnostic scheme, the necessary theory is developed such as an explanation of the origin of various spectral components in the rotor current signals and criteria for selecting those harmonics for detecting faults are developed.

A coupled circuit approach is adopted for the modeling of DFIG machines under healthy, unbalanced asymmetric and stator inter-turn fault conditions. Various inductances of the machines have been computed using WFA. A rigorous experimental study has been carried out which involves testing the machines under healthy, unbalanced load operation and different stator inter-turn fault levels. In order to test the machine under faulty conditions, a customized DFIG machine with different taps has been used to emulate inter-turn fault of stator windings. Experiments were conducted for DFIG operating at different slips, load condition and on-line data was collected for different signals for varying fault severities. An off-line spectral analysis was conducted on rotor phase current, vector sum of rotor phase currents and search coil voltage signals and the results were compiled. Search coil voltage signal and vector sum of rotor phase currents are shown to provide a better fault detection indication compared to rotor phase current signals.

Also, an instrument that uses a DSP board to generate a trip signal in the event of a stator inter-turn fault was built. The necessary control software as well as hardware has been developed and tested. The fault detector has good sensitivity and speed to

detect the faults involving even one shorted turn within two seconds under most operating conditions.

However, the fault detection ability of these diagnostic schemes has not been tested by changing the location of the fault inside the machine.

5.2 Contributions

- A new technique of detecting stator inter-turn faults in DFIG by analyzing the rotor phase current and validated by rotor search coil voltage has been obtained.
- A detailed theoretical proof for the induction of various frequency components induced in the rotor circuit due to stator inter-turn fault has been completed.
- Simulation study and detailed experimental results have been presented showing the influence of load and slip of the machine on the fault diagnosis results. Through monitoring a suitable component in the rotor circuit phase current and rotor search coil voltage, a definite indication of inter-turn fault in the stator winding is obtained even for a very small numbers of turns.
- A prototype based on DSP has been constructed to demonstrate the timely detection of stator inter-turn faults unambiguously in approximately two seconds for two-turn faults in all cases.

5.3 Future Scope

On-line fault diagnosis has the potential to become an integral part of any converter/drive that runs the electric machine. Selection of such a diagnostic method will be based on:

- cost

- unambiguity
- response time
- sensitivity
- generality.

The proposed FDS method has the potential to meet all the above five primary goals if the work is conducted further to improve its performance. Following are the approaches and avenue to improve the performance:

- This method requires a threshold value table of a fault frequency for a slip and load. DFIG operates over a wide range of slip and load condition and hence, acquiring such tables for each generator is a time consuming and expensive. Extrapolation techniques can be used for intermediate loads and slip to derive the threshold levels for various operating conditions. An efficient method would be to use least-square technique to compute the coefficients to map the effect of slip and load change on rotor current.
- High signal to noise ratio is the basic premises of effective fault diagnostic system. However the inverter switching is a major cause of high frequency harmonics injected into rotor. Using adequate signal conditioning and filtering circuit can assist to provide better sensitivity in detection of fault frequency.

References

1. Global Wind Energy Council Reports, 2007 http://www.nawindpower.com/naw/e107_plugins/content/content.php?content.1700

2. Wind turbine manufacturers datasheets for 5MW and 2MW turbines http://www.repower.de/fileadmin/download/produkte/5m_uk.pdf http://www.repower.de/fileadmin/download/produkte/PP_MM92_uk.pdf http://www.nordex-online.com/fileadmin/MEDIA/Produktinfos/EN/Nordex_N80-N90_GB.pdf

3. C.B. Hasager; A. Peña; T. Mikkelsen; M. Courtney; I. Antoniou; S.E. Gryning; P. Hansen; P.B. Sørensen, "12MW Horns Rev experiment". *Risø-R-1506(EN) (2007) 83 p.*

4. S. Muller; M. Deicke; R. W. De Doncker., "Doubly fed induction generator systems for wind turbines," *Industry Applications Magazine, IEEE* , vol.8, no.3, pp.26-33, May/Jun 2002.

5. T.W. Verbruggen, "Wind Turbine Operation & Maintenance based on Condition Monitoring," WT-Ω Final report, April 2003

6. M. Durstewitz Ed. "Windenergie report Deutschland 2004–2005," , ser. Institut für Solare Energieversorgungstechnik (ISET) Kassel, Germany, Institut für Solare Energieversorgungstechnik (ISET).

7. L.H. Hansen; L. Helle; F. Blaabjerg; E. Ritchie; S. Munk-Nielsen; H. Bindner; P. Sørensen; B. Bak-Jensen, "Conceptual survey of generators and power electronics for wind turbines", Risø-R-1205(EN) (2001).

8. Thomas Ackermann, "Wind Power in Power Systems" John Wiley & Sons. Inc., New York, 2005, 1st Edition.

9. Y. Amirat; M.E.H. Benbouzid; B. Bensaker; R. Wamkeue, "Condition Monitoring and Fault Diagnosis in Wind Energy Conversion Systems: A Review," *IEEE International Electric Machines & Drives Conference, 2007. IEMDC '07.*, vol.2, no., pp.1434-1439, 3-5 May 2007.

10. Theodore Wildi, "Electrical Machines, Drives, And Power Systems", Prentice Hall, 2005, 6th edition.

11. J.A. Baroudi; V. Dinavahi; A.M. Knight, "A review of power converter topologies for wind generators," *IEEE International Conference on Electric Machines and Drives,* vol. 1, pp. 458-465, 15-18 May 2005.

12. R. Datta; V.T. Ranganathan, "Variable-speed wind power generation using doubly fed wound rotor induction machine-a comparison with alternative schemes," *IEEE Transaction on Energy Conversion*, vol.17, no.3, pp. 414-421, Sep 2002

13. W.T. Thomson : "A Review of On-Line Condition Monitoring Techniques for Three-Phase Squirrel-Cage Induction Motors -Past Present and Future" *Keynote address at IEEE Symposium on Diagnostics for Electrical Machines, Power Electronics and Drives, Gijon, Spain,* pp 3-18, *Sept. 1999.*

14. S. Nandi; H.A. Toliyat, "Condition monitoring and fault diagnosis of electrical machines-a review," *IEEE Conference Record of the Industry Applications Conference, Thirty-Fourth IAS Annual Meeting*, vol.1, pp.197-204, 1999.

15. A.H. Bonnett; G.C. Soukup, "Cause and analysis of stator and rotor failures in three-phase squirrel-cage induction motors," *IEEE Transactions on Industry Applications,* vol.28, no.4, pp.921-937, Jul/Aug 1992.

16. W.T. Thomson, "On-line MCSA to diagnose shorted turns in low voltage stator windings of 3-phase induction motors prior to failure," *IEEE*

International Electric Machines and Drives Conference. IEMDC 2001, pp.891-898, 2001.

17. G. B. Kliman, W.J. Premerlani, R.A. Koegl, and D. Hoeweler, "A new approach to on-line turn fault detection in ac motors," *IEEE Conference of Industry Applications Society, Annual Meeting* San Diego, CA, pp. 687–693, Oct. 1996.

18. S. Nandi and H.A. Toliyat, "Novel frequency domain based technique to detect stator inter-turn faults in induction machines using stator induced voltage after switch-off," *IEEE Transaction on Industrial Applications*, Vol. 38, No. 1, pp. 101–109, Jan./Feb. 2002.

19. S. Nandi, "Detection of Stator Faults in Induction Machines Using Residual Saturation Harmonics," *IEEE Transactions on Industry Applications,* Vol. 42, Issue 5, Sep. – Oct. pp. 1201– 1208, 2006.

20. Wind turbine burning at the Nissan Motor Manufacturing (UK) Ltd (Sunderland, UK) after an oil leak. http://rawdenbydale.co.uk/sunderland%20fire.htm

21. J. Ribrant; L.M. Bertling, "Survey of Failures in Wind Power Systems With Focus on Swedish Wind Power Plants During 1997–2005," *IEEE Transactions on Energy Conversion,* , vol.22, no.1, pp.167-173, March 2007.

22. P. Tavner; J. Xiang; F. Spinato, "Reliability analysis for wind turbines" *Journal of Wind Energy*, vol 10; no. 1, pages 1-18, 2007.

23. S.C. Stone; B.K. Gupta; M. Kurtz; D.K. Sharma., "Investigation of Turn Insulation Failure Mechanisms in Large AC Motors," *IEEE Transactions on Power Apparatus and Systems*, vol.PAS-103, no.9, pp.2588-2595, Sept. 1984.

24. T.G. Habetler; R.G. Harley; R.M. Tallam; Sang.-Bin Lee; R. Obaid; J. Stack, "Complete current-based induction motor condition monitoring: stator, rotor, bearings, and load," *Technical Proceedings of VIII IEEE International Power Electronics Congress, CIEP 2002*, pp. 3-8, 20-24 Oct. 2002.

25. T.G. Habetler.; L. Youngkook, "Current-based condition monitoring and fault tolerant operation for electric machines in automotive applications," *International Conference on Electrical Machines and Systems, 2007. ICEMS,* pp.2011-2016, 8-11 Oct. 2007.

26. G. Stone and J. Kapler, "Stator winding monitoring," *IEEE Industry Applications Magazine*, Vol. 4, No. 5, pp. 15–20, Sep./Oct. 1998.

27. P.C Sen, "Principles of Electrical Machines and Power Electronics", John Wiley & Sons Inc., 1996.

28. A. K. Sawhney, "Electrical Machine Design", Dhanpat Rai and Sons, Delhi, 1984.

29. Q. Wu, "Single-turn Sensitive Stator Inter-turn Fault Detection of Induction Machines", M. A. Sc. thesis, University of Victoria, Canada, 2008.

30. P. Neti, "Stator Fault Analysis of Synchronous Machines", Ph. D. thesis, University of Victoria, Canada, 2007.

31. S. Nandi, "A Detailed Model of Induction Machines With Saturation Extendable for Fault Analysis," *IEEE Transaction on Industry Applications*, Vol. 40, No. 5, Sep/Oct. 2004.

32. H. Douglas; P. Pillay; P. Barendse, "The detection of inter-turn stator faults in doubly-fed induction generators," *Conference Record of the Industry Applications Conference, 2005. Fourtieth IAS Annual Meeting*, vol.2, pp. 1097-1102, 2-6 Oct. 2005.

33. I. Albizu; A. Tapia; J.R. Saenz; A.J. Mazon; I. Zamora, "On-line stator winding fault diagnosis in induction generators for renewable generation," *Proceedings of the 12th IEEE Mediterranean Electro-technical Conference, MELECON 2004.* vol.3, pp. 1017-1020, 12-15 May 2004.

34. S. Williamson; K. Mirzoian, "Analysis of Cage Induction Motors with Stator Winding Faults", *IEEE Transactions on Power Apparatus and Systems*, vol-104, no.7, pp.1838-1842, July 1985.

35. J.L. Kohler, J. Sottile and F. C. Trutt, "Alternatives for assessing the electrical integrity of induction motors", *IEEE Transactions on Industry Applications*, vol. 28, no. 5, pp.1109-1117, Sept./Oct. 1992.

36. J.L. Kohler, J. Sottile and F. C. Trutt, "Condition monitoring of stator windings in induction motors. I. Experimental investigation of the effective negative-sequence impedance detector", *IEEE Transactions on Industry Applications*, vol. 38, no. 5, pp. 1447-1453, Sept./Oct. 2002.

37. J. Sottile F.C. Trutt and J.L. Kohler, "Condition monitoring of stator windings in induction motors. II. Experimental investigation of voltage mismatch detectors," *IEEE Transactions on Industry Applications*, Vol. 38, no. 5, pp. 1454-1459, Sept./Oct. 2002.

38. F. Filippetti; G. Franceschini; C. Tassoni; P. Vas, "Recent developments of induction motor drives fault diagnosis using AI techniques," *IEEE Transactions on Industrial Electronics,* vol.47, no.5, pp.994-1004, Oct. 2000.

39. R.M. Tallam; T.G. Habetler; R.G. Harley; D.J. Gritter; B.H. Burton, "Neural network based on-line stator winding turn fault detection for induction motors," *Conference Record of the 2000 IEEE Industry Applications Conference*, vol.1, pp.375-380, vol.1, 2000.

40. R.M. Tallam; T.G. Habetler; R.G. Harley, "Self-commissioning training algorithms for neural networks with applications to electric machine fault diagnostics," *IEEE Transactions on Power Electronics,* vol.17, no.6, pp. 1089-1095, Nov 2002.

41. M.G. Melero; M.F. Cabanas; C.H. Rojas; G.A. Orcajo; J.M. Cano, J. Solares, "Study of an induction motor working under stator winding inter-turn short circuit condition", *IEEE Symposium on Diagnostics for Electrical Machines, Power Electronics and Drives SDEMPED'03,* Atlanta, *2003.*

42. H. Henao: C. Demian; G.A. Capolino, "A frequency-domain detection of stator winding faults in induction machines using an external flux sensor", *IEEE Transactions on Industry Applications,* vol. 39, no. 5, pp. 1272-1279, 2003.

43. J. Penman; H.G. Sedding; B.A. Lloyd; W.T. Fink, "Detection and location of interturn short circuits in the stator windings of operating motors," *IEEE Transaction on Energy Conversion*, vol.9, no.4, pp.652-658, Dec 1994.

44. S.M.A. Cruz; A.J.M. Cardoso, "Stator winding fault diagnosis in three-phase synchronous and asynchronous motors, by the extended Park's vector approach," *IEEE Transactions on Industry Applications,* vol.37, no.5, pp.1227-1233, Sep/Oct 2001.

45. M. El Hachemi Benbouzid, "A review of induction motors signature analysis as a medium for faults detection," *IEEE Transactions on Industrial Electronics,* vol.47, no.5, pp.984-993, Oct 2000.

46. I. Tsoumas; E. Mitronikas; A. Safacas, "Induction motor mixed fault diagnosis based on wavelet analysis of the current space vector," *Proceedings of the Eighth International Conference on Electrical*

Machines and Systems. ICEMS 2005. vol.3, pp. 2186-2191, 27-29 Sept. 2005.

47. O. Touhami; M. Fadel, "Detection of Broken Rotor Bars and Stator Faults in Squirrel-Cage Induction Machine by Spectral Analysis," *Thirty-Ninth Southeastern Symposium on System Theory, 2007. SSST '07.*, pp.274-278, 4-6 March 2007.

48. X. Li, "Performance Analysis of a 3-Phase Induction Machine with Inclined Static Eccentricity", M. A. Sc. thesis, University of Victoria, Canada, 2004.

49. Y. Zhongming; W. Bin, "A review on induction motor online fault diagnosis," Proceedings of The Third International Power Electronics and Motion Control Conference, 2000. IPEMC 2000., vol.3, pp.1353-1358, 2000.

50. W.T. Thomson; M. Fenger, "Current signature analysis to detect induction motor faults," *Industry Applications Magazine, IEEE* , vol.7, no.4, pp.26-34, Jul/Aug 2001.

51. D. Casadei; F. Filippetti; C. Rossi; A. Stefani; A. Yazidi; G.A. Capolino, "Diagnostic Technique based on Rotor Modulating Signals Signature Analysis for Doubly Fed Induction Machines in Wind Generator Systems," *Conference Record of the 2006 IEEE Industry Applications Conference, 2006. 41st IAS Annual Meeting.* vol.3, pp.1525-1532, 8-12 Oct. 2006.

52. P. Neti; S. Nandi, "Stator Inter-turn Fault Detection of Synchronous Machines Using Field Current Signature Analysis," *Conference Record of the 2006 IEEE Industry Applications Conference. 41st IAS Annual Meeting*, vol.5, pp.2360-2367, 8-12 Oct. 2006.

53. S. Nandi, "Space and time harmonics related problems and their mitigation for position and speed sensor-less slip-ring induction motor

drives applications", *National Power Electronics Conference, 17-19 Dec, 2007.*

54. H.A. Toliyat and T.A. Lipo, "Transient analysis of cage induction machines under stator, rotor bar and end ring faults", *IEEE Transactions on Energy Conversion*, vol.10, no.2, pp.241-247, June, 1995

55. B. Akin; H.A. Toliyat; U. Orguner; M. Rayner; "Low-Cost Motor Drive-Embedded Fault Diagnosis - A Simple Harmonic Analyzer," *IEEE Applied Power Electronics Conference, APEC 2007 - Twenty Second Annual*, pp.243-249, Feb. 25 -March 1 2007.

56. ABB, DriveWindow software, datasheet

    http://library.abb.com/global/scot/scot201.nsf/veritydisplay/a5ae37d539433eacc2256eed00217b2e/$File/DriveWindow_2_Leaflet.pdf

57. J. Nilsson; L. Bertling, "Maintenance Management of Wind Power Systems Using Condition Monitoring Systems—Life Cycle Cost Analysis for Two Case Studies," *IEEE Transaction on Energy Conversion* , vol.22, no.1, pp.223-229, March 2007.

58. GE W650, Wind Generation Protection System, http://www.geindustrial.com/products/presentations/w650/w650pres.pdf http://www.gepower.com/prod_serv/products/oc/en/orbit/downloads/2q04windpower.pdf

Appendix A: Modeling of the DFIG [18, 19, 54]

The stator and rotor winding diagram of the DFIG machine are shown in Figures A.1, A.2 & A.3.

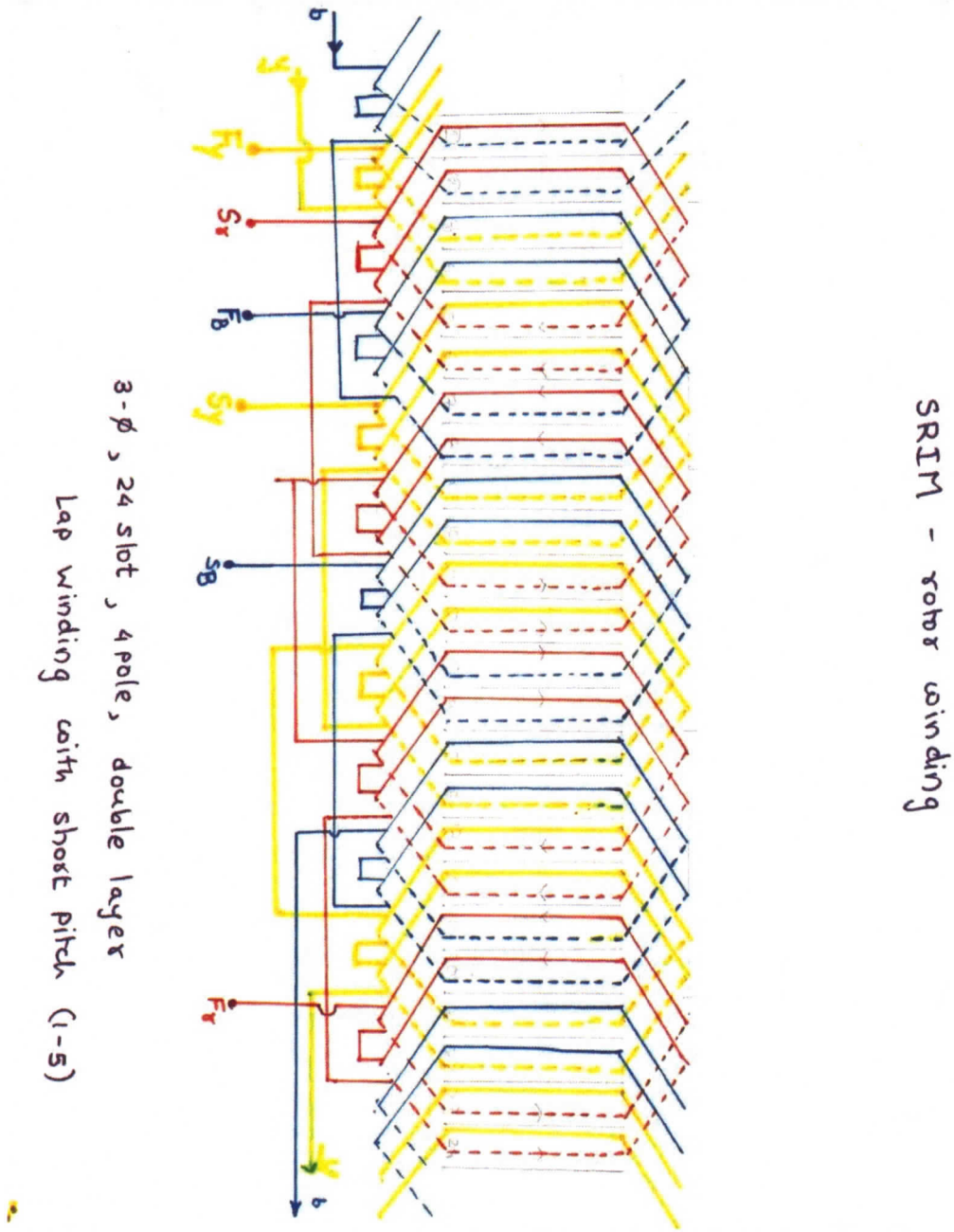

Figure A.1 Winding diagram of DFIG rotor

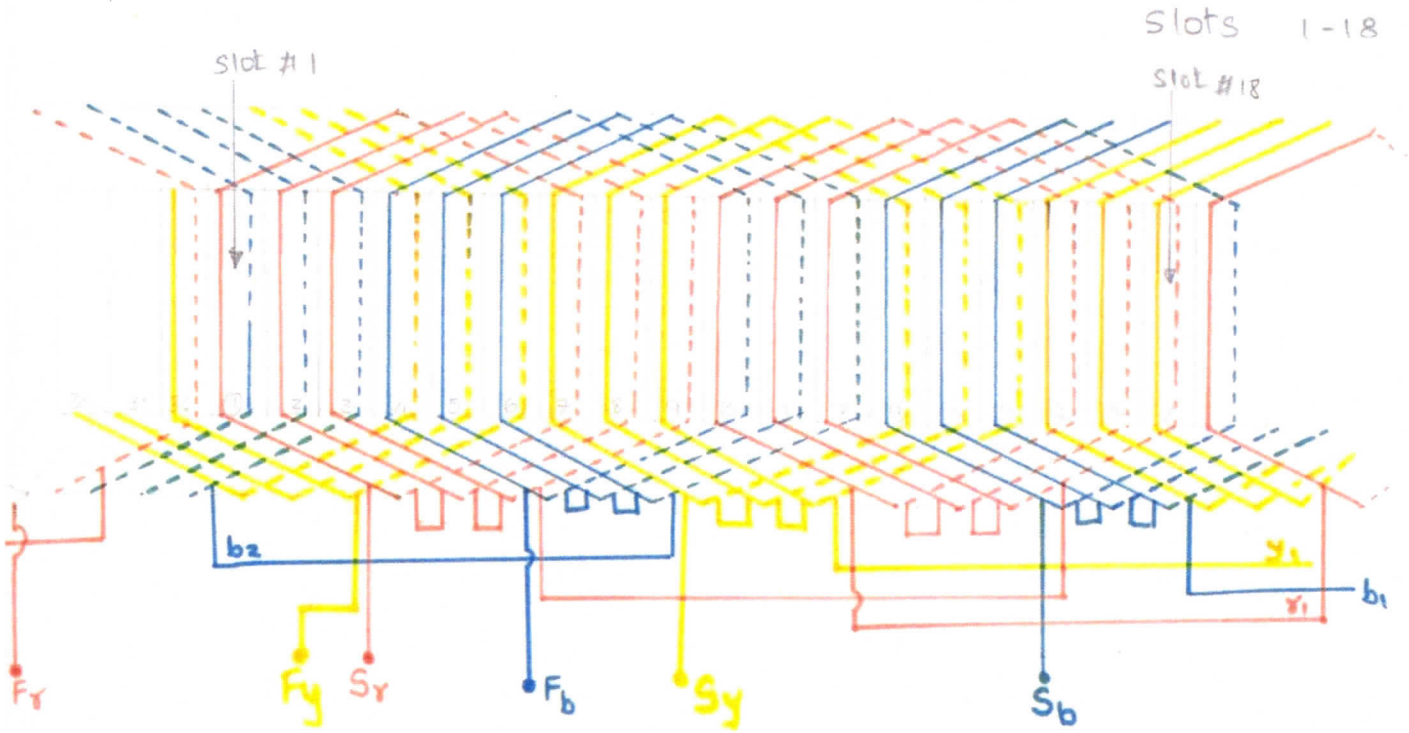

3-ϕ, 36 slot, 4 pole, double layer
Lap winding with short pitch (1-7)

Figure A.2 Winding diagram of DFIG stator, part-1

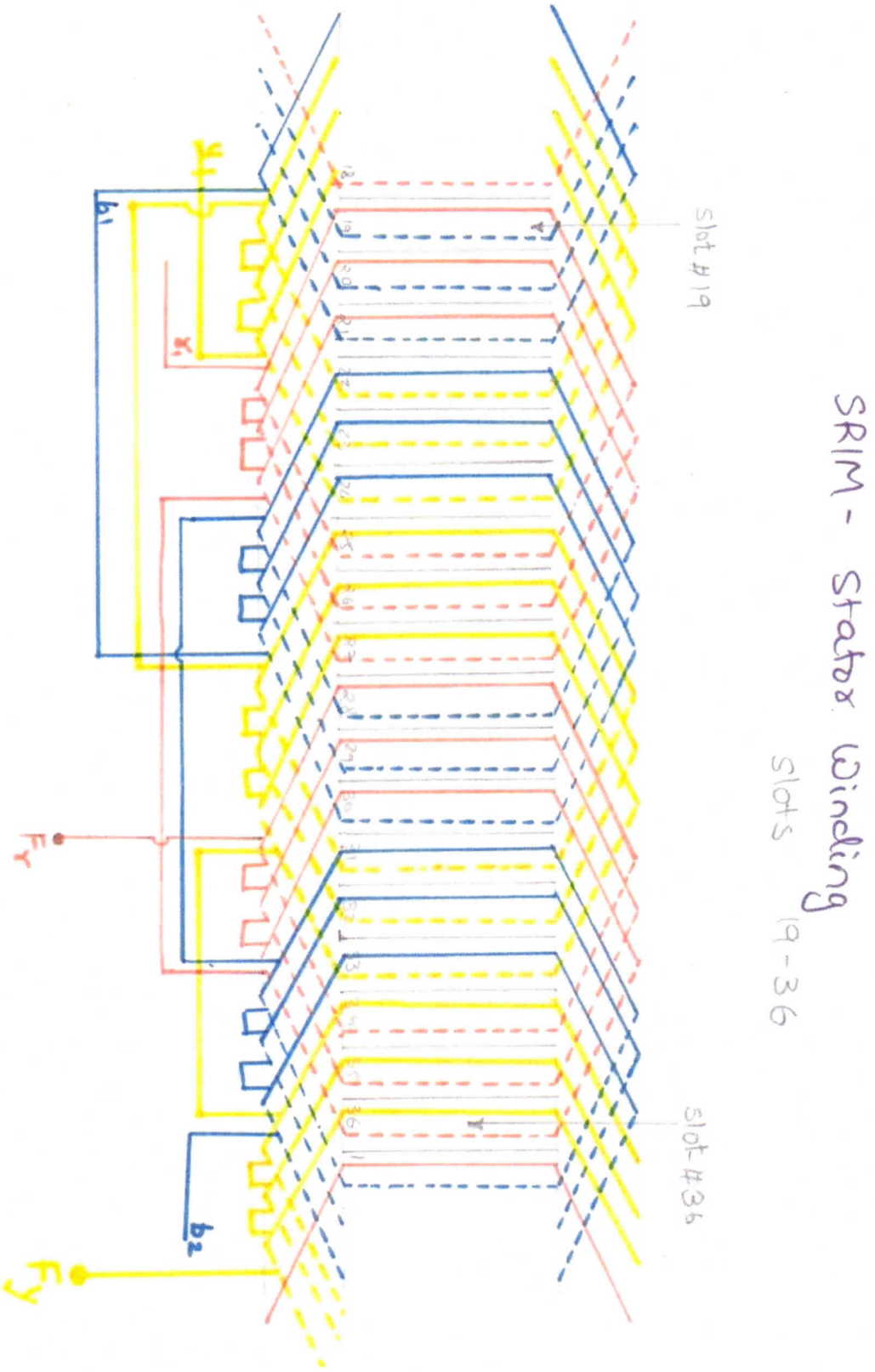

Figure A.3 Winding diagram of DFIG stator, part-2

In the above figures, S_r, S_y, S_b and F_r, F_y, F_b refer to the terminals of windings of three phases which on the actual motor are connected in a star-star configuration. The suffixes a, b, c refer to stator phases, u, v, w refer to rotor phases, a_2 refers to the shorted turn in phase-a of stator, while u_2 refers to turn in rotor winding phase-u that have been removed to generate asymmetry. a_1 and u_1 refer to the remainder of phases a and u respectively after removing a_2 and u_2.

Based on the winding diagrams, the turns functions for the stator winding of phase 'a' can be given by:

$$n_a(\phi) = \sum_{p=1,3,5...}^{\infty} \left(\frac{4N_s}{\pi p} sin\frac{\pi p}{3} \right) \cdot \left(1 + 2cos\frac{\pi p}{9} \right) \cdot cos(2p\phi) + 3N_s \qquad (A.1)$$

Where, ϕ is the stator position measured from phase 'a' axis. Ns = 12, the number of series connected stator turns per coil. Turns function for phase b and c are shifted by $\frac{\pi}{3}$ and $\frac{2\pi}{3}$ respectively. Figure A.4 shows the turns function for stator phase 'a'.

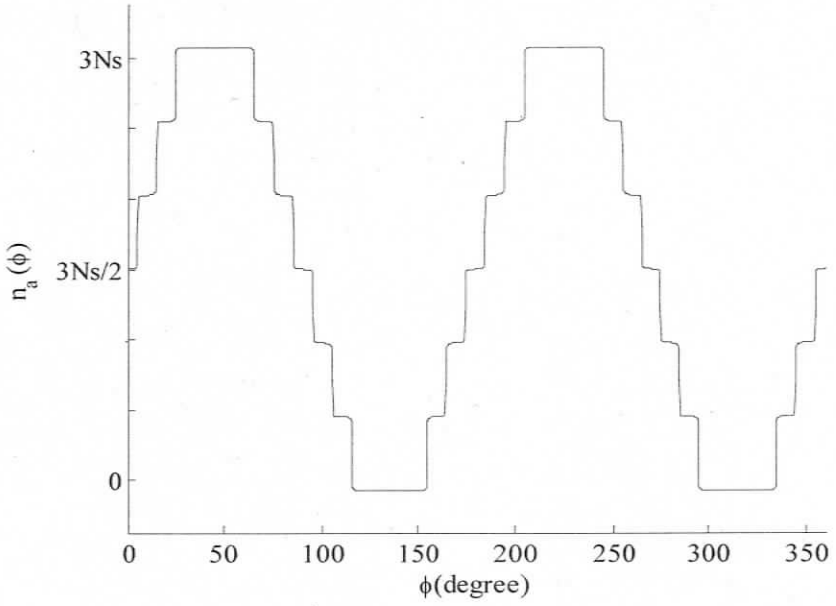

Figure A.4 Turns function for stator phase 'a'

Similarly, based on the rotor winding diagram, the turns functions for the rotor winding of phase 'u' can be given by:

$$n_u(\phi') = \sum_{p=1,3,5...}^{\infty} \left(\frac{4N_r}{\pi p}\right) \cdot \left(sin\frac{\pi p}{4} + sin\frac{5\pi p}{12}\right) \cdot cos(2p\phi') + 2N_r \qquad (A.2)$$

Where $\phi' = \phi - \theta_r$ is the rotor position measured from phase 'u', Nr = 18, the number of series connected rotor turns per phase. The turns function for phase v and w are shifted by $\frac{\pi}{3}$ and $\frac{2\pi}{3}$ respectively. Figure A.5 shows the turns function for rotor phase 'u'.

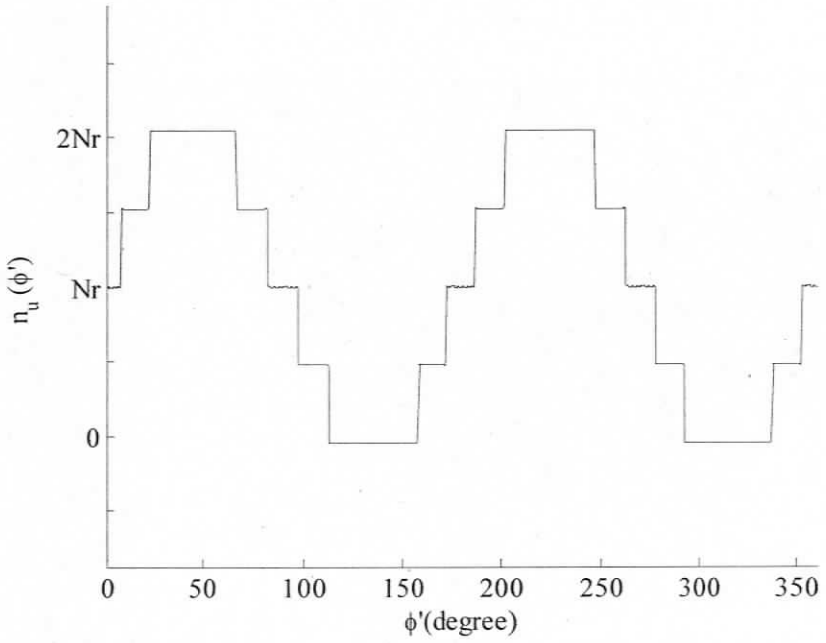

Figure A.5 Turns function for rotor phase 'u'

The turns function for the shorted turn in phase-a is given by:

$$n_{a2}(\phi) = \sum_{p=1,2,3...}^{\infty} \left(\frac{2N_d}{\pi p} sin\frac{\pi p}{6}\right) \cdot cos\left(p\left(\phi + \frac{\pi}{18}\right)\right) + \frac{N_d}{6} \qquad (A.3)$$

Where N_d is the number of shorted turns

The turns function of the section removed to create asymmetry in the rotor phase-u winding is given by:

$$n_{u2}(\phi') = \sum_{p=1,3,5...}^{\infty} \left(\frac{2N_e}{\pi p} sin\frac{\pi p}{6} \right) \cdot cos\left(p\left(\phi' + \frac{\pi}{24} \right) \right) + \frac{N_e}{6} \tag{A.4}$$

Where N_e is the number of turns removed from phase-u to create asymmetry. The asymmetric rotor u-phase winding turns function is given by:

$$n_{ueff}(\phi') = n_u(\phi') - n_{u2}(\phi') \tag{A.5}$$

Using the turns functions, the magnetizing and mutual inductances of Stator and Rotor can be calculated by:

$$L_{xy} = \mu_0 rl \int_0^{2\pi} \left[n_x(\phi) \cdot n_y(\phi,\theta) \cdot g_s^{-1}(\phi,\theta) \right] \cdot d\phi \tag{A.6}$$

Calculation of stator phase-a leakage inductance L_{ls1} and shorted winding inductance L_{ls2}

$$L_{ls1} = L_{ls} \cdot \left(\frac{N_s^2 - N_d^2}{N_s^2} \right) \tag{A.7}$$

$$L_{ls2} = L_{ls} \cdot \left(\frac{N_d^2}{N_s^2} \right) \tag{A.8}$$

Similarly the leakage inductance for rotor phase winding with asymmetry L_{lr1} can be found.

Calculation of mutual inductance for shorted turn in phase-a and stator phase-a, b, c [19]

$$L_{a1a1} = L_{aa} - 2 \cdot L_{aa2} + L_{a2a2} - L_{ls2} \tag{A.9}$$

$$L_{a1a2} = L_{aa2} - L_{a2a2} - L_{ls2} \tag{A.10}$$

$$L_{a1b} = L_{ba1} = L_{ab} - L_{a2b} \tag{A.11}$$

$$L_{a1c} = L_{ca1} = L_{ac} - L_{a2c} \tag{A.12}$$

Similarly the mutual inductances for asymmetry turn in phase-u and rotor phase-u,v,w can be calculated.

Calculation of equivalent fault inductances arising only due to stator phase-a

$$L_{a2a1ceq} = L_{a2a1} - L_{a2c} \tag{A.13}$$

$$L_{a2beq} = L_{a2b} - L_{a2c} \tag{A.14}$$

Similarly calculation for equivalent fault inductances arising due to rotor phases, can be calculated

Calculation of equivalent fault inductance arising only due to fault phase

$$L_{a1a2beq} = L_{a1a2} - L_{ba2} \tag{A.15}$$

Similarly calculation for equivalent rotor inductances arising due to rotor phases, can be calculated

Calculation of equivalent stator inductance for phase-a arising only due to stator phase-b

$$L_{a1a1eq} = L_{a1a1} - L_{a1c} - L_{ba1} + L_{bc} \tag{A.16}$$

$$L_{a1beq} = L_{a1b} - L_{a1c} - L_{bb} + L_{bc} \tag{A.17}$$

Similarly calculation for equivalent stator inductances arising due to rotor phases, rotor inductances arising due to stator phases can be calculated.

Calculation of equivalent rotor inductances arising only due to fault phase

$$L_{u1a2veq} = L_{u1a2} - L_{va2} \tag{A.18}$$

$$L_{va2eq} = L_{va2} - L_{wa2} \tag{A.19}$$

Based on the computation of equivalent inductances, the stator flux linkages $\lambda_a, \lambda_b, \lambda_c$ rotor flux linkages $\lambda_u, \lambda_v, \lambda_w$ and stator shorted turns flux linkage λ_{a2} can be given by:

$$\begin{aligned}
\lambda_{a1} &= L_{a1a1eq} i_a + L_{a1beq} i_b + L_{a1ceq} i_c + L_{a1u1eq} i_u + L_{a1veq} i_v + L_{a1weq} i_w + L_{a1a2eq} i_{a2} \\
\lambda_b &= L_{ba1eq} i_a + L_{bbeq} i_b + L_{bceq} i_c + L_{bu1eq} i_u + L_{bveq} i_v + L_{bweq} i_w + L_{ba2} i_{a2} \\
\lambda_c &= L_{ca1eq} i_a + L_{cbeq} i_b + L_{cceq} i_c + L_{cu1eq} i_u + L_{cveq} i_v + L_{cweq} i_w + L_{ca2eq} i_{a2} \\
\lambda_{a2} &= L_{a2a1eq} i_a + L_{a2beq} i_b + L_{a2ceq} i_c + L_{a2u1eq} i_u + L_{a2veq} i_v + L_{a2weq} i_w + L_{a2a2eq} i_{a2} \\
\lambda_{u1} &= L_{u1a1eq} i_a + L_{u1beq} i_b + L_{u1ceq} i_c + L_{u1ueq} i_u + L_{u1veq} i_v + L_{u1weq} i_w + L_{u1a2eq} i_{a2} \\
\lambda_v &= L_{va1eq} i_a + L_{vbeq} i_b + L_{vceq} i_c + L_{vu1eq} i_u + L_{vveq} i_v + L_{vweq} i_w + L_{va2eq} i_{a2} \\
\lambda_w &= L_{wa1eq} i_a + L_{wbeq} i_b + L_{wceq} i_c + L_{wu1eq} i_u + L_{wveq} i_v + L_{wweq} i_w + L_{wa2eq} i_{a2}
\end{aligned} \tag{A.20}$$

During the simulation the DFIG is run at constant speed, hence, $T_m = T_l$, and $\frac{Jd\omega}{dt}$ term can be neglected. The position is found by integrating speed. This gives the stator and rotor voltage equations as:

$$\begin{aligned}
i_a Z_L + i_a R_{a1} + \frac{d\lambda_{a1}}{dt} + v_{gs} &= 0 \\
i_b Z_L + i_b R_b + \frac{d\lambda_b}{dt} + v_{gs} &= 0 \\
i_c Z_L + i_c R_c + \frac{d\lambda_c}{dt} + v_{gs} &= 0 \\
i_{a2} R_{a2} + \frac{d\lambda_{a2}}{dt} &= 0 \\
v_{u1} = i_u R_{u1} + \frac{d\lambda_{u1}}{dt} + v_{gr} \\
v_v = i_v R_v + \frac{d\lambda_v}{dt} + v_{gr} \\
v_w = i_w R_w + \frac{d\lambda_w}{dt} + v_{gr}
\end{aligned} \tag{A.21}$$

Where, v_{gs} is the voltage between load and stator phase neutrals, and v_{gr} is the voltage between the rotor phase and neutral. Use of v_{gs} and v_{gr} can be eliminated by using line-to-line quantities as

$$\begin{aligned}
&(i_a - i_b)Z_L + i_a R_{a1} - i_b R_b + \frac{d(\lambda_{a1} - \lambda_b)}{dt} = 0 \\
&(i_b - i_c)Z_L + i_b R_b - i_c R_c + \frac{d(\lambda_b - \lambda_c)}{dt} = 0 \\
&(i_c - i_a)Z_L + i_c R_c - i_a R_{a1} + \frac{d(\lambda_c - \lambda_{a1})}{dt} = 0 \\
&v_{u1} - v_v = i_u R_{u1} - i_v R_v + \frac{d(\lambda_{u1} - \lambda_v)}{dt} \\
&v_v - v_w = i_v R_v - i_w R_w + \frac{d(\lambda_v - \lambda_w)}{dt} \\
&v_w - v_u = i_w R_w - i_u R_{u1} + \frac{d(\lambda_w - \lambda_{u1})}{dt}
\end{aligned} \tag{A.22}$$

(A.22) can further be reduced to a system of four equations by using,

$$\begin{aligned}
&i_a + i_b + i_c = 0 \\
&i_u + i_v + i_w = 0
\end{aligned} \tag{A.23}$$

Appendix B: Fault Diagnostic Results in Tabular form.

Table B.1 Simulation result, PSD (dB) level of rotor phase-u current frequency 127.5Hz (k=3), DFIG modeled with rotor asymmetry operating at slip = 0.25 and varying load level

Load	Freq	HB	HU	T1	T2	T3	T4
No Load	110	-104.51	-98.53	-79.22	-75.31	-72.49	-66.35
Half Load	127.5	-102.74	-96.42	-77.06	-74.69	-71.33	-65.12
Full Load	146	-105.09	-101.21	-82.52	-78.27	-73.71	-68.55

Table B.2 PSD (dB) level of rotor phase-u current frequency 127.5Hz (k=3), DFIG operating at no-load, for varying slip

Slip	Freq.	HB	HU	T1	T2	T3	T4
0.44	110	-70.32	-68.83	-68.08	-66.70	-63.95	-51.69
0.25	127.5	-68.19	-67.06	-62.98	-62.68	-57.03	-55.02
0.044	146	-67.1	-71.81	-68.28	-62.67	-59.52	-56.96

TableB.3 PSD (dB) level of rotor phase-u current frequency 127.5Hz (k=3), DFIG operating at half-load, for varying slip

Slip	Freq.	HB	HU	T1	T2	T3	T4
0.44	110	-71.94	-71.33	-68.29	-69.52	-65.47	-58.51
0.25	127.5	-68.12	-66.97	-67.97	-65.02	-60.49	-58.82

0.044	146	-69.09	-71.15	-71.22	-66.94	-61.4	-56.79

Table B.4 PSD (dB) level of rotor phase-u current frequency 127.5Hz (k=3), DFIG operating at full-load, for varying slip

Slip	Freq.	HB	HU	T1	T2	T3	T4
0.44	110	-67.6	-71.26	-72.53	-71.19	-66.31	-61.02
0.25	127.5	-70.04	-70.67	-74.51	-72.72	-66.58	-61.97

Table B.5 PSD (dB) level of complex part of vector sum of rotor current frequency 127.5Hz (k=3), at full-load, for varying slip

Slip	Freq.	HB	HU	T1	T2	T3	T4
0.44	110	-72.40	-73.04	-71.22	-70.65	-67.12	-60.88
0.25	127.5	-74.44	-73.88	-70.63	-70.74	-63.52	-59.74

Table B.6 PSD (dB) level of rotor search coil voltage frequency 127.5Hz (k=3), DFIG operating at no-load, for varying slip

Slip	Freq	HB	HU	T1	T2	T3	T4
0.44	110	-28.19	-27.35	-27.79	-23.85	-20.93	-19.02
0.25	127.5	-28.93	-26.25	-23.06	-20.51	-14.05	-10.18
0.044	146	-17.76	-21.67	-18.36	-11.1	-4.57	-1.1

Table B.7 PSD (dB) level of rotor search coil voltage frequency 127.5Hz (k=3), DFIG operating at half-load, for varying slip

Slip	Freq	HB	HU	T1	T2	T3	T4
0.44	110	-29.67	-31.89	-28.81	-27.18	-20.35	-17.21
0.25	127.5	-30.68	-32.67	-26.62	-23.09	-15.92	-12.36
0.044	146	-18.56	-18.85	-18.95	-5.96	-3.114	-2.05

Table B.8 PSD (dB) level of rotor search coil voltage frequency 127.5Hz (k=3), DFIG operating at full-load, for varying slip

Slip	Freq	HB	HU	T1	T2	T3	T4
0.44	110	-29.91	-31.51	-29.88	-29.39	-22.99	-20.62
0.25	127.5	-31.64	-32.77	-29.91	-22.59	-17.14	-13.62

Table B.9 Average tripping time for 2-turn fault when DFIG opearting under steady state at slip=0.25, for varying load level

Load level	T1	T2	T3	T4
No-load	1.65	1.22	1.77	0.83
Half-load	1.77	1.45	1.31	1.025
Full-load	1.97	1.65	1.44	0.91